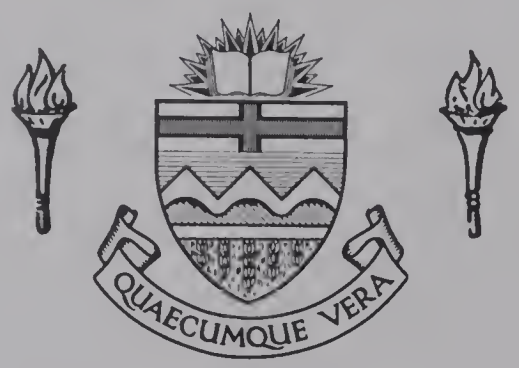

The University of Alberta
Printing Department
Edmonton, Alberta

THE UNIVERSITY OF ALBERTA

UNSTEADY STATE GAS FLOW IN THE PRESENCE OF A LIQUID SATURATION

BY

MICHAEL N. KINAKIN

A THESIS

SUBMITTED TO THE FACULTY OF GRADUATE STUDIES

IN PARTIAL FULFILLMENT OF THE REQUIREMENTS FOR THE

DEGREE OF MASTER OF SCIENCE

IN

PETROLEUM ENGINEERING

FACULTY OF ENGINEERING

DEPARTMENT OF CHEMICAL AND PETROLEUM ENGINEERING

EDMONTON, ALBERTA

APRIL, 1968

UNIVERSITY OF ALBERTA

FACULTY OF GRADUATE STUDIES

The undersigned certify that they have read, and recommend to the Faculty of Graduate Studies for acceptance a thesis entitled UNSTEADY STATE GAS FLOW IN THE PRESENCE OF A LIQUID SATURATION submitted by Michael N. Kinakin in partial fulfillment of the requirements for the degree of Master of Science in Petroleum Engineering.

ABSTRACT

Although the progress made in the past thirty years to describe the transient nature of gas flow through porous media has been somewhat staggering, very little experimental data exist to substantiate the validity of the results obtained. Tests were performed on a number of different cores in the presence of a residual fluid saturation and the results analyzed on the basis of an effective porosity and permeability to gas. Originally it was intended that the presence of the immobile fluid would simulate a connate water saturation. Kerosene, nonetheless, was chosen for this second phase in order to prevent damaging the core by the expansion of inherent clay materials on contact with water[20,33]. The theory, however, shows that the method of analysis for a residual oil phase is also applicable to the presence of a residual water saturation.

The validity of the dimensionless cumulative production function and the radius of drainage equation derived for the constant terminal pressure case was tested by comparison with experimental data obtained for heterogeneous porous systems. It was found that the presence of heterogeneities seriously limited the applicability of the common dimensionless parameters used in normal reservoir calculations. A numerical solution was also effected and the results compared

to experimental data. The large discrepancies obtained were attributed mainly to limitations in the experimental apparatus. The presence of the fluid saturation further accentuated these limitations by increasing the reaction time of the equipment to changes in pressure.

ACKNOWLEDGEMENTS

The author wishes to express his appreciation to Dr. D.L. Flock, Department of Chemical and Petroleum Engineering, University of Alberta, under whose guidance and supervision this project was completed, and to the Alberta and Southern Gas Co. Ltd., the National Research Council, and the University of Alberta for providing the required financial assistance.

Appreciation is also extended to my colleague, Mr. C.C. Fortems, for his assistance and helpful suggestions throughout the course of this work. A debt of gratitude is certainly due my wife, Hilda, for her assistance with the more tedious computations and for typing the original manuscript.

TABLE OF CONTENTS

LIST OF TABLES

LIST OF FIGURES

INTRODUCTION

Because of the complexity of fluid flow through consolidated porous media, original investigations into the transient phenomena yielded results purely of an academic interest. It was not until 1949, when Van Everdingen and Hurst[43] published their classical solutions for slightly compressible fluids, that a practical method was available to analyze common reservoir engineering problems. Their presentation of the dimensionless cumulative production and pressure functions greatly facilitated the prediction of reservoir histories. Later other investigators extended this work to include the flow of gases. However, even before these solutions are applied to a practical problem, further simplifying assumptions must be made with regard to the physical properties of the porous medium. Heterogeneities are usually combined into single effective values of porosity and permeability. For gas reservoirs connate water saturations are considered only to reduce the effective porosity available to the gaseous phase, and the effects of solubility are completely neglected.

The advent of high speed electronic computers facilitated a numerical approach for a direct solution to the nonlinear gas flow equation. The introduction of finite difference approximations for the derivatives enabled the analysis of more sophisticated problems. It now became possible to

incorporate such pressure dependent terms as gas viscosity and gas compressibility factors into the final solution. The phenomenon of slip and its influence on the transient response was analyzed. Heterogeneities in the form of permeability distributions were introduced and the range of analyses extended to two and three dimensions.

Although these concepts have been the basis for numerous engineering studies, to date very little experimental data have been provided to substantiate the application of the developed theory to practical situations. Thus, the prime objective of this investigation was to obtain transient data on a number of different reservoir cores, and to determine how well the theory would describe the experimental results obtained. A second immobile phase was introduced to simulate a connate water saturation, and attempts were made to analyze the theory proposed to describe the constant terminal pressure case. In particular, emphasis was placed on the dimensionless cumulative production function and the radius of drainage equation derived for an infinite linear system.

LITERATURE REVIEW

A review of the literature was conducted in order to determine the extent of the theoretical and experimental techniques available to describe the transient phenomenon. The survey revealed that the entire analysis of transient isothermal flow of gas through porous media is based on the solution of the general diffusivity equation and its inherent assumptions

$$\nabla\left(\frac{k}{\mu Z} P \nabla P\right) = \phi \frac{\partial}{\partial t}\left(\frac{P}{Z}\right) \qquad (1)$$

where

k = effective permeability of the porous media, darcies

μ = viscosity of the gas, centipoises

Z = compressibility factor of the gas

ϕ = effective porosity of the porous media, fraction

P = pressure, atmospheres

t = time, seconds

with all lengths measured in centimeters.

A historical review of the solution to this problem may be divided into two parts, the point of separation roughly occurring with the advent of high speed electronic computers.

Early Empirical and Analytical Investigations

Assuming that the properties of the porous media and flowing gas are constant, equation (1) may be simplified to

$$\nabla^2 p^2 = C \frac{\partial P}{\partial t} \qquad (2)$$

where C is a constant dependent upon the properties of the gas and the porous media. Because of the non-linear characteristics of equations (1) and (2), analytical solutions to these relationships have not yet been obtained.

Muskat and Botset[34] in 1931 made one of the first attempts at solving this transient behavior of gases in porous media. By way of a dimensional analysis of the problem, they obtained the general law for the flow of gas through a sand as

$$\delta P^2 = k(\rho v)^n \qquad (3)$$

where ρv is the mass velocity, ρ being the density, and v the effective velocity. The left hand side of the equation is equivalent to the difference in pressures squared $(P_1^2 - P_2^2)$ and n is an empirical constant determining the nature of flow, varying between the limits 1 and 2, and corresponding to completely viscous and completely turbulent flow respectively. The final solution for a radial system was obtained by applying a continuous succession of

steady states, each governed by the equation

$$\text{div}\left[\left(\frac{\partial P^2}{\partial S}\right)^{1/n}\right] = 0 \qquad (4)$$

where S represents the space variable, the time being introduced as a parameter through the boundary conditions. This approximation is equivalent to assuming that the velocity of flow is negligible when compared to the propagation of disturbances through the porous material. In a later analysis Muskat[35] introduced the concept of a "radius of drainage", which is considered to recede to the boundary of the reservoir as the steady state condition is established. In this instance no gas is removed from any point within the system until the radius of drainage has passed through that point. Similar attempts were made to apply these concepts to two phase flow[36] with a minor degree of success.

Hetherington et al[19] developed empirical equations relating cumulative production and future production rates from gas reservoirs as a function of time for a linear system with a sealed external boundary. Again the approximation of a continuous succession of steady states was employed, with further assumptions being that the average pressure over the entire system is negligibly different from the pressure at the external boundary, and the downstream pressure is small. However, unlike the work of their predeces-

sors, the equations advanced by Hetherington et al are based mainly on the characteristic back-pressure equation.

$$\frac{Q}{t} = a(P_e^2 - P_f^2)^N \qquad (5)$$

Q = total volume of gas produced at time t

P_e = pressure at the external boundary of the system

P_f = pressure at the outlet side of the system

a = experimental constant describing the geometry of the system

N = experimental exponent describing the nature of the flow

and as a consequence are void of any complicated integration or series terms. The validity of these equations was favorably tested by comparison with experimental results and the concept of a "steady state decline" introduced. That is to say, upon the inception of production there would initially exist a period of transient conditions referred to as "the recession of the radius of drainage", followed by a longer period of steady decline in which the rate of change of pressure with respect to time would be independent of position in the system.

The classical solutions of Van Everdingen and Hurst[8,25,43] for equation (6),

$$\frac{\partial^2 P}{\partial r^2} + \frac{1}{r}\frac{\partial P}{\partial r} = \frac{\phi \mu c}{k}\frac{\partial P}{\partial t} \qquad (6)$$

which describes the transient radial flow of a slightly compressible fluid through porous media, have been the foundation for the analysis of many reservoir engineering problems concerning water influx and fluid flow (both oil and gas) into a well bore. A slightly compressible fluid has been defined as that which is governed by the equation

$$\rho = \rho_o \left[1 + c(P - P_o)\right] \qquad (7)$$

where c is the compressibility of the fluid and the subscript, o, refers to some standard condition.

Upon further examination it is noted that equation (6) is linear and as such is amenable to analytic treatment. Although explicit solutions for equation (6) had been obtained in prior investigations[22,35], these were much too involved and cumbersome to be of any value in handling practical engineering problems. Basically the approach of Van Everdingen and Hurst consisted of converting equation (6) and the prescribed boundary conditions into an ordinary differential equation by applying the Laplace transformation. The transformed equation was then solved analytically and the result converted to "real" time by way of Mellin's inversion formula. This analysis involved the introduction of two dimensionless parameters as functions of dimensionless time: Q_{t_D}, the dimensionless cumulative influx term; and P_{t_D}, the dimensionless pressure term, where

$$Q_{t_D} = \frac{\int_0^{t_D} \left[\frac{\partial P}{\partial \left(\frac{r}{r_w}\right)} \right]_{r=r_w} dt_D}{(P_f - P_e)} \qquad (8)$$

r = radial distance

r_w = inner radius

t_D = dimensionless time

P_f = constant flowing pressure at the inner radius

P_e = the initial reservoir pressure

and

$$P_{t_D} = f(t_D) \qquad (9)$$

the exact nature of the function on the right hand side of equation (9) being dependent upon the value of t_D itself and the boundary conditions applied. The final results were presented as working tables and charts of dimensionless parameters, thus eliminating the time consuming process of evaluating complicated series solutions involving Bessel functions.

It was soon discovered that the Van Everdingen and Hurst solutions could be applied to gas flow through porous media if equation (2) is linearized in pressure squared by introducing an average constant reservoir pressure for the time interval considered[12,13,25]. Rewriting equation (2) provides

$$\nabla^2 P^2 = C' \frac{\partial P^2}{\partial t} \qquad (10)$$

where C' incorporates the assumed average pressure, $\bar{P}$. The net effect is to replace the pressure, P, by P^2 and the fluid compressibility, c, by the inverse of $\bar{P}$ in all the relationships developed for a slightly compressible fluid. The method of solution now lends itself to a trial and error procedure in an attempt to choose an appropriate value for $\bar{P}$.

Finite Difference Approximations and Numerical Solutions

Aronofsky and Jenkins[1] obtained numerical solutions to equation (2) for linear systems of infinite and finite length, in which the initial and terminal pressures and/or rates were specified. The non-linear gas flow equation was expressed in finite difference form, and the pressure at time t + Δt determined explicitly. In order to insure numerical stability it was necessary to limit the size of the time increment as determined by equation (11).

$$\Delta t \leq \frac{\alpha}{4} (\Delta x)^2 \qquad (11)$$

$\alpha = \frac{2\phi\mu}{P_i k}$, where P_i is the initial pressure in the system. A comparison of the results obtained with an analytical relationship for transient fluid flow revealed the necessity for specifying the pressures involved in order to uniquely define the solution for the flow of gases. The basis of this

work was later extended to include transient radial flow through porous media[2,23]. However, in this instance the restrictions imposed on Δt for a predictive solution were partially overcome by the introduction of a fictitious well bore radius. Steady state conditions were assumed to exist within the bounds of this radius and it was necessary to correct the final numerical solutions to account for the gas produced from this region.

The work of Roberts[40] is significant in that he showed that $\partial P^2/\partial x$ is a measure of the flux, and the non-linear effect of the gas flow equation acts in such a way as to retard the rate at which the pressure drops within the system. A solution was accomplished by applying a step by step linearization process to the diffusivity equation and integrating the result numerically. Green and Wilts[18] solved the transient problem for gas flow by satisfying the finite difference equation with an electrical analogy. The limitations of this approach are obvious.

The classical numerical analysis of equation (2) for both the linear and radial systems was performed by Bruce, Peaceman, Rachford, and Rice[6] in 1953. An implicit procedure was proposed which greatly relaxes the stringent control on the maximum size of Δt. This, however, necessitates the solution of a tri-diagonal matrix with each iteration of the numerical procedure.

Cornell and Katz[11] developed a graphical method of solution in an endeavor to account for turbulence[10] in the vicinity of the well bore. It was assumed that steady state turbulent flow exists in the region near the well bore and that laminar transient flow prevails at some larger distance away from the well. The procedure consists of first solving for the unsteady state case and then correcting the result for turbulence.

Aronofsky[3] extended the scope of his earlier numerical approach to include the effects of molecular streaming or slip. It had been shown in a prior investigation by Klinkenberg[27] that the effective permeability to gas is a linear function of the mean pressure in the system and is dependent on the nature of the flowing gas.

$$k_g = K\left(1 + \frac{b}{\overline{P}}\right) \qquad (12)$$

k_g = effective permeability to gas

K = absolute (liquid) permeability and is dependent on the geometry of the porous media only

b = a constant dependent on the nature of the gas and the porous material

$\overline{P}$ = mean pressure

The modus operandi consisted of incorporating equation (12) in the finite difference approximations and solving the

resultant expression. It was shown from the results, and later by experimentation[45], that the slip effect is negligible for pressures normally encountered in gas reservoirs even though deviations in the laboratory may be significant. Kolada[28] combined the effects of molecular streaming and turbulence in his steady state analysis of the viscous and visco-inertial regions of flow. Chwyl[9] then extended this concept to the transient case by combining equation (12) with the well-known Forchheimer equation. His numerical solution showed that the effects of turbulence tend to counteract the effects of slip.

A similar technique to account for pressure dependent variables was employed by Aronofsky and co-authors to determine the non-ideal behavior of real gases in linear[4] and radial[5] systems. Both the compressibility factor Z and the viscosity μ were assumed to be simple functions of pressure, and in particular

$$Z = 1 - mP \tag{13}$$

$$\mu = d + nP \tag{14}$$

where m, d, and n are constants dependent on the nature of the gas.

Eilerts[16] in 1964 combined the major contributions of previous investigators,in particular Bruce et al, and developed a numerical method for the solution of

equation (1) for a linear system. Effect was given to the pressure dependency of the compressibility factor, the viscosity, and the effective gas permeability, and to the change of absolute permeability with position. The pressure dependent properties were combined into one simple function of pressure before expressing the differential equation in finite difference form. Carter[7] extended this analysis to two-dimensional steady state flow and effected a solution by the method of Saul'ev, commonly referred to as ADEP (Alternating Direction Explicit Procedure). Like Eilerts, Carter combined the pressure dependent properties into one term, which he defined as

$$\Phi(P) = \int_{P_c}^{P} \frac{\lambda d\lambda}{\mu(\lambda) Z(\lambda)} \qquad (15)$$

P_c in equation (15) is any fixed value of pressure.

Although the above review is by no means complete, it, nonetheless, serves to indicate the degree of sophistication to which the transient analysis of gas flow has progressed. Of major concern, however, is the apparent lack of experimental evidence to support many of the concepts proposed.

THEORY

Basic Diffusivity Equation for Gas Flow

Before an analysis of the basic diffusivity equation for gas flow can be effected, it is imperative to examine the limitations imposed on this relationship by way of its derivation. A review of the basic laws describing the flow of fluids reveals that equation (1) is derived by combining the equation of continuity governing the flow of fluids through porous media of constant porosity,

$$\nabla \cdot (\rho \vec{v}) = -\phi \frac{\partial \rho}{\partial t} \tag{16}$$

the equation of state for a gas,

$$\rho = \frac{MP}{ZRT} \tag{17}$$

and Darcy's Law neglecting gravitational effects.

$$\vec{v} = -\frac{k}{\mu} \nabla P \tag{18}$$

R, in equation (17), is the universal gas constant. M, the molecular weight of the gas, and T, the temperature, are assumed to be constant.

To be strictly correct the empirical relationship expressed by equation (18) should be replaced by the classical hydrodynamic equations of Navier-Stokes. However, the solution of this system of equations for a geometry as complex as a porous medium would prove to be insurmountable.

If the permeability, the viscosity, and the compressibility factor are assumed to be constant, equation (1) can be re-written as

$$\nabla \cdot (P \nabla P) = \frac{\phi \mu}{k} \frac{\partial P}{\partial t} \tag{19}$$

Applying the mathematical relationship expressed by

$$\nabla P^2 = 2P \nabla P \tag{20}$$

equation (19) can be simplified to

$$\nabla^2 P^2 = \frac{2\phi \mu}{k} \frac{\partial P}{\partial t} \tag{21}$$

Finally, multiplying the right hand side of equation (21) by P/P and assuming an average pressure, $\bar{P}$ in the denominator, yields an equation linear in P^2.

$$\nabla^2 P^2 = \frac{\phi \mu}{k \bar{P}} \frac{\partial P^2}{\partial t} \tag{22}$$

It can now be shown that the study of transient gas flow in the presence of a residual fluid saturation is theoretically substantiated by the expressions describing multiphase flow (Appendix I). The method of obtaining a solution is the same as for a single phase system. However, now the compressibility of the single phase is replaced by the total compressibility of the system, and the mobility is replaced by the total mobility of the flowing fluids. For the case of gas flowing in the presence of a residual

fluid saturation, only the mobility and compressibility of the gaseous phase need be considered. The latter approximation is attributed to the small values of liquid compressibilities when compared to the compressibilities of gases.

Dimensionless Cumulative Production

Following the procedure outlined by Van Everdingen and Hurst[43] for the constant terminal pressure case, it can be shown that for linear gas flow

$$n_c = \frac{\phi LA}{\overline{P}} \cdot \frac{P_f}{Z_f RT} \cdot (P_f - P_e) Q_{t_D} \qquad (23)$$

where Q_{t_D} is the dimensionless cumulative production defined by

$$Q_{t_D} = \int_o^{t_D} \frac{\left(\frac{\partial P}{\partial (x/L)}\right)_{x=0}}{(P_f - P_e)} \, dt_D \qquad (24)$$

n_c = cumulative production in moles

L = length in inches

$\overline{P}$ = average pressure from the dimensionless time expression in psia

A = area in inches

P_f = constant flowing pressure at the downstream end in psia

P_e = constant pressure at the external boundary in psia

R = universal gas constant

T = temperature in ^{o}R

ϕ = porosity, fraction

Z_f = compressibility factor at P_f

Radius of Drainage

Van Poolen's[44] investigation of the various equations describing the radius of drainage and stabilization time reveals that the final expressions obtained are dependent upon the criteria used to define both the radius of drainage and stabilization time. Consider the solution for the constant terminal pressure case governing the linear flow of gas in an infinite porous system.

$$\frac{P^2(x,t) - P_e^2}{P_f^2 - P_e^2} = \text{erfc}\,\frac{1}{2t_D^{\frac{1}{2}}} \qquad (25)$$

where

$$t_D = \frac{k\bar{P}t}{\mu\phi x^2} \qquad (26)$$

Defining the radius of drainage as the point where

$$\frac{P^2(x,t) - P_e^2}{P_f^2 - P_e^2} = 0.01 \qquad (27)$$

and following a procedure similar to Jones[24], the final equation for the radius of drainage becomes

$$x_d = 4\sqrt{kt\bar{P}/\mu\phi} \qquad (28)$$

and upon re-arranging and solving for t, the stabilization time becomes

$$t_s = \frac{\mu\phi x_d^2}{16k\bar{P}} \qquad (29)$$

The units of equations (28) and (29) are in the c-g-s system. It should be noted that the derivation of equation (28) involves making the assumption

$$1.82 \simeq 2.0 \qquad (30)$$

Consequently, a more accurate solution to the radius of drainage would be

$$x_d = 3.64\sqrt{kt\bar{P}/\mu\phi} \qquad (31)$$

Numerical Solution

Assuming a constant compressibility factor and defining the compressibility of the gas as $1/\bar{P}$, equation (1) for a linear system becomes

$$\frac{\partial}{\partial x}\left(\frac{k(x)}{\mu(P)} \cdot \frac{\partial P^2}{\partial x}\right) = \frac{\phi}{\bar{P}} \frac{\partial P^2}{\partial t} \qquad (32)$$

where the permeability is now a function of position and the viscosity a function of pressure. A finite difference approximation was obtained for equation (32) by a method similar to Eilerts[16] (Appendix II), and a computer program written to numerically solve the result (Appendix III) for a number of boundary conditions.

EXPERIMENTAL APPARATUS

Description of Cores

Tests were performed on a total of four different cores, an Indiana limestone, two Berea sandstones,and a "Series" core composed of a Berea sandstone and a section of Alundum. Excluding the Series core for the moment, the remaining cores were set in 5-inch I.D. oil well production casing, using an epoxy resin to fill the annular space. The method for pouring the resin is described in detail by Mackett[30]. Once a permanent set had been achieved, five 1/4-inch diameter pressure taps were machined at convenient intervals along the length of the core. The depths of these pressure taps extended through the casing and epoxy resin, and approximately 1/4 inch into the core material itself. The ends of the core samples were fractured, as opposed to machining, to prevent damage to the core faces.

The core holder consisted of two heavy duty mild steel flanges, specially designed to accommodate a metal insert at the inner faces. These flanges were held together on either side of the core by eight 3/4-inch diameter mild steel rods threaded at both ends. For instances where the core face protruded past the length of the casing, spacer rings were inserted between the flange and the casing. Metal to metal contact was avoided by using Garlock rubber gaskets,

which provided an excellent seal to pressures as high as 900 psig. Centrally located pressure taps permitted the flow of gas through the flanges, and a second pressure tap provided a direct means of measuring the pressure at the core faces.

A Series core, shown in Figure 1, was assembled to study the effects of heterogeneities on the transient behavior of a porous system. The Berea sandstone was introduced in two distinct sections in an attempt to determine the influence, if any, of the Berea-Alundum interface. The three sections of core were assembled to simulate two different permeabilities in series and set in 4-inch I.D. production casing. Five 3/8-inch diameter pressure taps were then drilled along the length of the core to facilitate the measuring of pressure distributions. Unlike the previous arrangements, two inches of thread were machined at both ends of the casing to accommodate metal caps. These provided the final seal for the core faces. It should be noted that each of these metal caps contained only a single centrally located pressure tap to allow for communication between the core and the remaining portion of the experimental apparatus. Consequently it was necessary to install a "T" at both ends of the Series core arrangement to provide a means for obtaining the absolute pressures at these points. Two complete sets of experimental data were obtained for

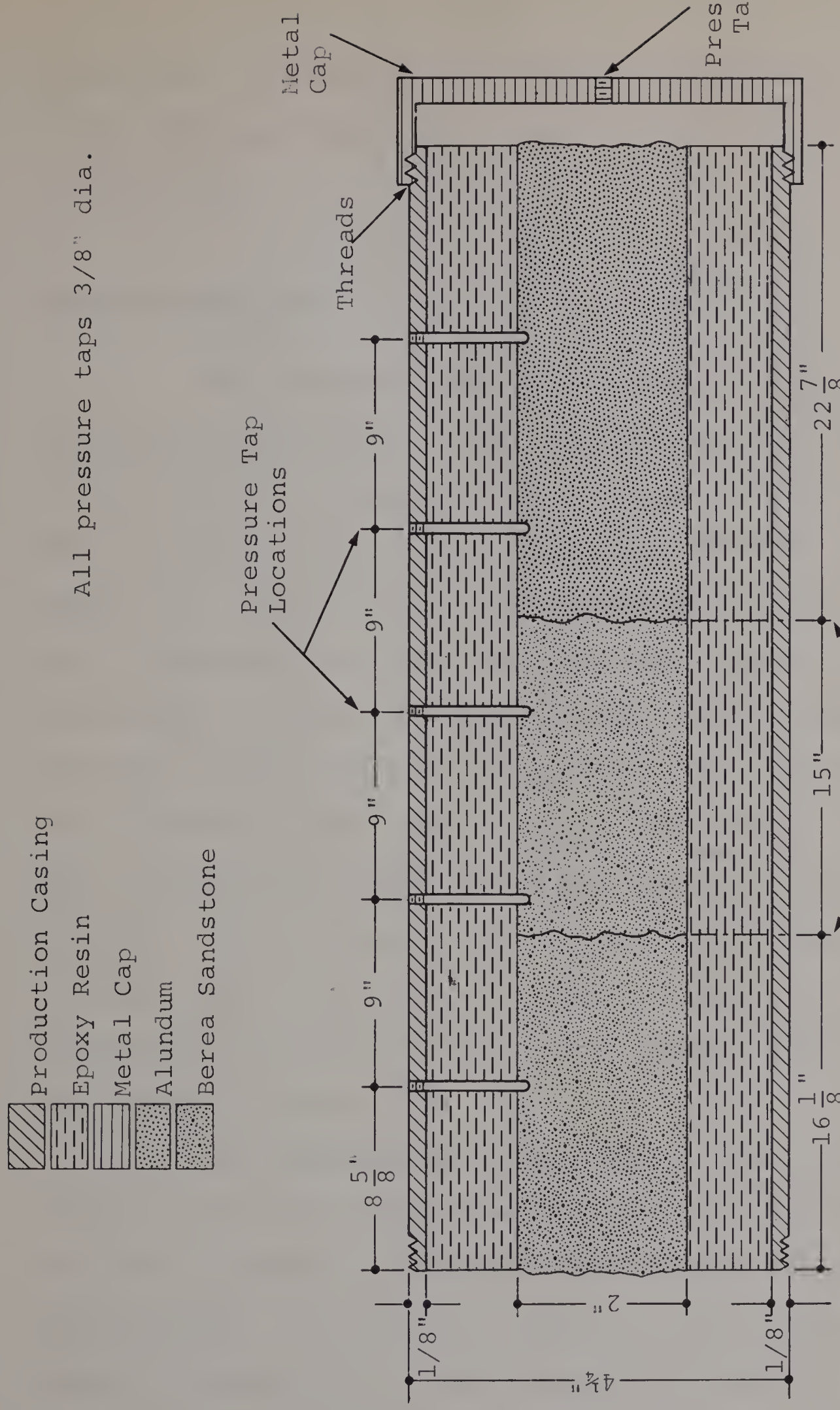

Figure 1 Cross Section of Series Core Assembly

this core; one with the Alundum section upstream of the Berea sandstone (AUS), and a second with the core positions reversed (ADS).

Measuring Devices

The transient behavior of commercially pure nitrogen gas was measured on a model 906C Honeywell "Visicorder", which provided a permanent record of the pressure drop across each section of the core as a function of time (refer to Figure 2). Five ±15 psid Statham PM80TC differential pressure transducers provided the electrical input into the Visicorder. A sixth ±50 psid Statham PM60TC transducer was required at the producing end of the core, because of the large pressure drops experienced in this region. A 0-18v Kepco Laboratories power supply provided the electrical input into a central panel, which in turn controlled the individual inputs into each transducer. Inputs into the transducers were monitored on a Non-Linear Systems Model 481 digital voltmeter.

The temperature of the flowing gas stream was sensed by two iron-constantan thermocouples and the electrical output measured on a Leeds and Northrup millivolt potentiometer. As shown in Figure 2, the upstream and downstream pressures at the core faces were measured with bourdon tube pressure gauges. A 0-1500 psig pressure regulator

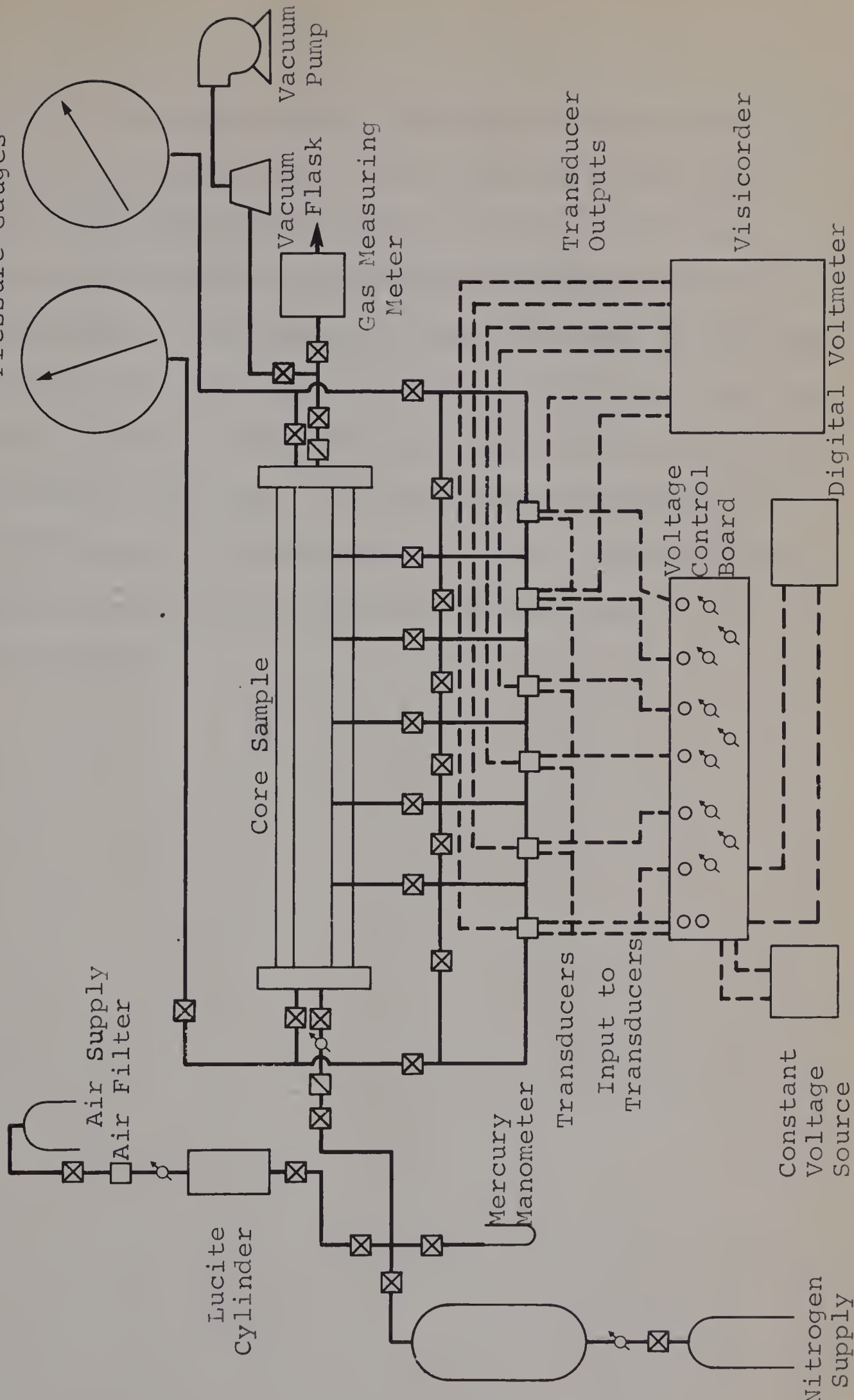

Figure 2 Schematic Diagram of Experimental Apparatus

inserted at the nitrogen supply permitted direct control of the flowing upstream pressure. More precise control was effected by means of a continuously bleeding 0-50 psig Moore "Nullmatic" pressure regulator installed downstream of the surge tank. All pressure lines consisted of 1/8-inch O.D. Autoclave stainless steel tubing and fittings, rated at 10,000 psig. Finally, a Toggle valve was introduced on the producing side of the core. The snap-open characteristics of this valve enabled the simulation of the boundary condition prescribing the sudden decrease in pressure at the downstream location.

EXPERIMENTAL PROCEDURE

Effective Porosity

The effective porosity of each core sample was determined directly by expanding a gas isothermally into a known volume. This necessitated the construction of a special porosimeter which is shown in Figure 3. The extraneous pressure taps in each core were sealed by utilizing a combination of steel ball bearings and female fittings. The procedure consisted of closing valve A and introducing a controlled amount of nitrogen into the system by means of a pressure regulator. Several minutes were usually required to attain stabilized conditions, and the equilibrium pressure was read from a bourdon tube pressure gauge. A vacuum was simultaneously drawn on the expansion chamber and the result measured on a mercury manometer. Valve A was then opened allowing direct communication between the core sample and expansion chamber. Once equilibrium conditions had been achieved, the final pressure was measured on the manometer and the porosity calculated from

$$\phi = \frac{100}{V_b}\left[\frac{V_t(P_f - P_a) + P_f V_e}{(P_N - P_f)} - V_{SL}\right] \qquad (33)$$

where

ϕ = porosity in percent

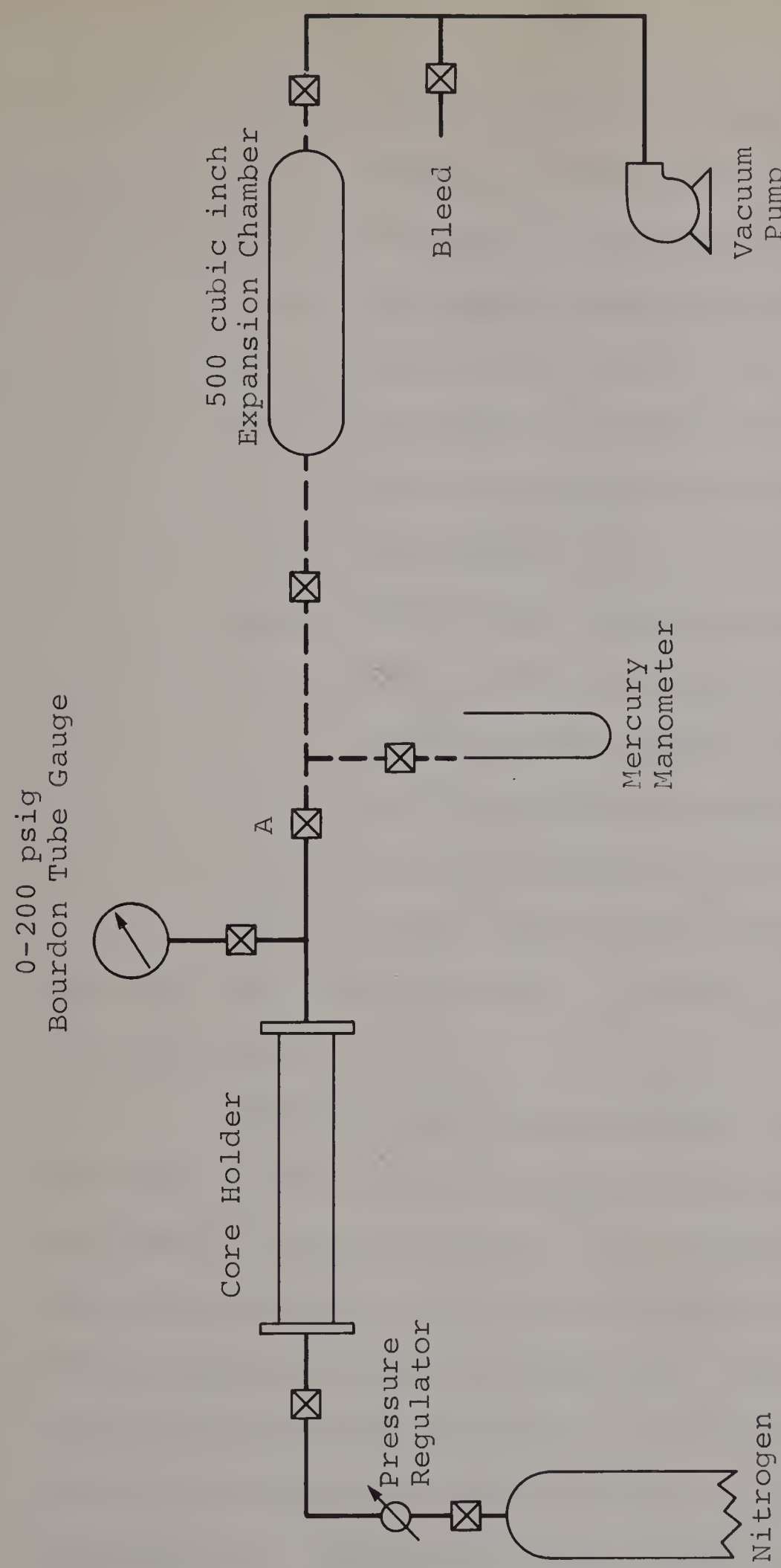

Figure 3 Schematic Diagram of Porosimeter

V_b = bulk volume of the core obtained from caliper measurements

V_t = volume of the expansion chamber and interconnecting pressure lines, including the manometer

V_e = increase in volume of the total system due to the change in the level of mercury in the manometer

V_{SL} = additional apparent void volume of the core due to the nitrogen source lines, core holder spacer rings, etc.

P_N = initial pressure in the core sample

P_a = initial pressure in the expansion chamber

P_f = final equilibrium pressure in the system

Equation (33), as presented, is valid for any system of consistent units.

Several runs were performed on each core at various pressure levels and the results from equation (33) averaged to obtain a final porosity. All barometric pressure readings were corrected for latitude and temperature throughout the entire course of the investigation. It was noted that by following the above procedure, initial nitrogen pressures of less than 170 psig provided final equilibrium pressures below atmospheric. Consequently no vacuums were drawn on the expansion chamber for these runs in order to prevent damage from occurring to the pressure gauge. Equation (33), however,

is still valid.

Saturating the Core

In order to obtain the liquid or absolute permeability of each core, it was first necessary to saturate the entire porous network with kerosene. This was accomplished by completely evacuating the core with a vacuum pump; then opening a valve to allow the kerosene to naturally imbibe into the pore spaces, all the while continuously drawing a vacuum at the opposite end of the sample. The extent of the vacuum drawn was measured on a mercury manometer as shown in Figure 2. The above procedure was continued until breakthrough of kerosene was detected in the vacuum flask. Approximately 40-50 psig pressure was externally applied to the surface of the kerosene in the lucite container to aid in the imbibition process of the tighter cores. A simple before-and-after weighing of the lucite container and vacuum flask permitted a material balance to be performed. This, along with a knowledge of the density of kerosene, provided a means for calculating the volume of fluid imbibed. Next the line was broken downstream of the lucite cylinder and a WII Ruska Proportionating Pump introduced. The core was then flushed with approximately 450 cc of kerosene, the efflux discharged into the vacuum flask, and a second material balance performed to account for any volumetric discrepancies.

Finally kerosene was "squeezed" into the core at 150 psig. The difference between the initial and final pump readings at 0 psig represented a further fluid loss to the core. By combining the results of the above procedure and accounting for the presence of kerosene in the flow lines, etc., it was possible to obtain a check on the effective porosity previously determined. In all cases agreement was obtained to within 1.2 percent of the total porosity.

Absolute Permeability

To determine the absolute permeability, kerosene was injected into the respective cores at some known preset rate utilizing the Ruska pump. The upstream and downstream temperatures and pressures at the steady state were recorded by means of the thermocouples and pressure gauges shown in Figure 2, and the permeability calculated from the integrated form of Darcy's Law

$$K = \frac{q\mu L}{A\Delta P} \qquad (34)$$

where ΔP is the pressure drop equal to $(P_2 - P_1)$. A periodic check of P_2 was sufficient to determine as to when steady state conditions had been attained. Several runs were performed at different injection rates, and the results of equation (34) averaged to obtain a final value for the absolute permeability. An experimentally determined correla-

tion provided a means for obtaining the viscosity of kerosene at the measured temperatures. The length and cross-sectional area of each core were determined by direct measurement. In cases where P_2 exceeded 250 psig, the upstream gauge was replaced by a 0-1500 psig Heise pressure gauge.

Relative Permeability Ratio and Residual Fluid Saturation

The composite relative permeability ratio of each core was determined by the familiar "modified external gas drive technique", and the results interpreted according to the procedure outlined by Welge[46], and based on his classical relationship

$$S_{av} - S_2 = (f_{oil})_2 Q_i \qquad (35)$$

where

S_{av} = average gas saturation in the core

S_2 = gas saturation at the producing end of the core

$(f_{oil})_2$ = fraction of oil flowing at the producing end of the core

Q_i = cumulative gas injected in pore volumes at the mean pressure in the core

A typical set of results are shown in Figure 32, Appendix IV. Nitrogen gas was used to displace the kerosene from the core, and a gravitational separation of the two phases

effected by means of the apparatus shown in Figure 4. The oil production was determined directly from the scale readings on the inverted burettes and the cumulative gas injected measured on a calibrated Sargent Wet Test Meter. The process was continued until the liquid phase completely ceased to flow. Because of the large volumes of nitrogen injected, it was necessary to saturate the gas by bubbling through water in order to preserve the calibration of the wet test meter. Finally a volumetric balance on the kerosene, accounting for liquid within the lines, etc., provided a means for determining the residual fluid saturation. In all cases attempts were made to use pressures higher than those expected in ensuing tests, in order to eliminate the possibility of additional fluid being produced.

Effective Gas Permeability

The effective gas permeability of each core in the presence of the residual fluid saturation was determined from a standard Klinkenberg Plot, utilizing the integrated form of Darcy's Law for the flow of gases.

$$k = \frac{T}{T_m} \cdot \frac{Z_{av}}{Z_m} \cdot \frac{P_m}{P_{av}} \cdot \frac{q\mu L}{A(P_2-P_1)} \qquad (36)$$

T = temperature of the gas in the core

T_m = temperature at which gas is measured

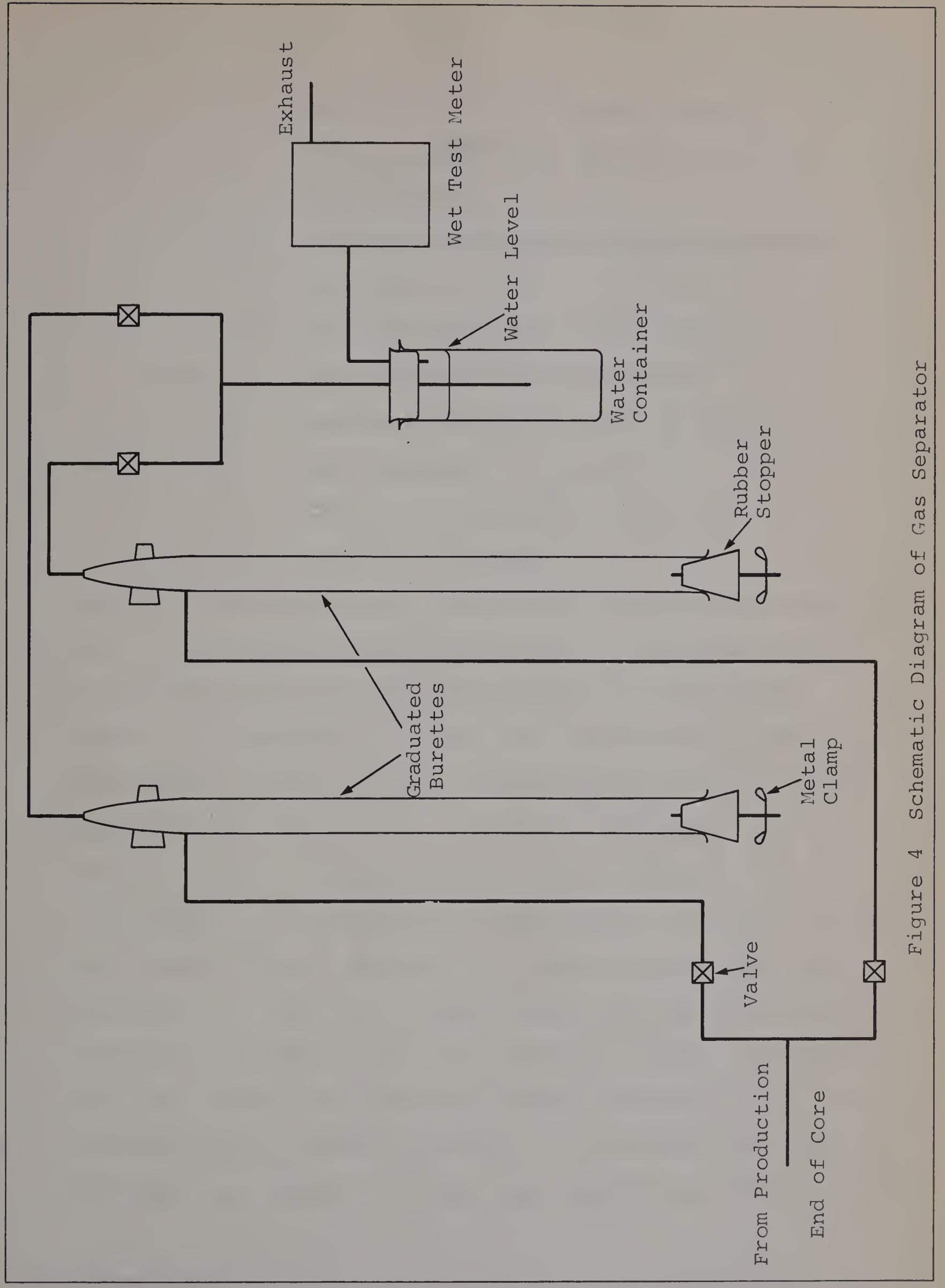

Figure 4 Schematic Diagram of Gas Separator

P_m = pressure at which gas is measured

P_{av} = average pressure in the core equal to $(P_2 + P_1)/2$

Z_{av} = average gas compressibility factor based P_{av} and T

Z_m = gas compressibility factor at P_m and T_m

(P_2-P_1) = pressure drop across the core

q = measured gas flow rate at T_m and P_m

μ = gas viscosity at P_{av} and T

A = cross-sectional area of the core

L = length of the core

However, for equation (36) to be valid, the flow must be viscous. Consequently efforts were made to determine whether or not the flow rate data obtained fell in the viscous region. The regions of viscous and visco-inertial flow were established by the method of Dranchuk and Kolada[15]. The standard back-pressure plot in Figure 5 indicates that the region of flow substantiating the use of equation (36) is very small. A re-evaluation of the theory, however, suggests that a modified back-pressure plot accounting for the dependence of Z, μ, and k on pressure would provide a more accurate criterion for establishing the turbulent region. The method now lends itself to a trial and error procedure in an attempt to establish the values of b and K in equation (12). Usually the lower flow rates of Figure 5 are used to provide an initial

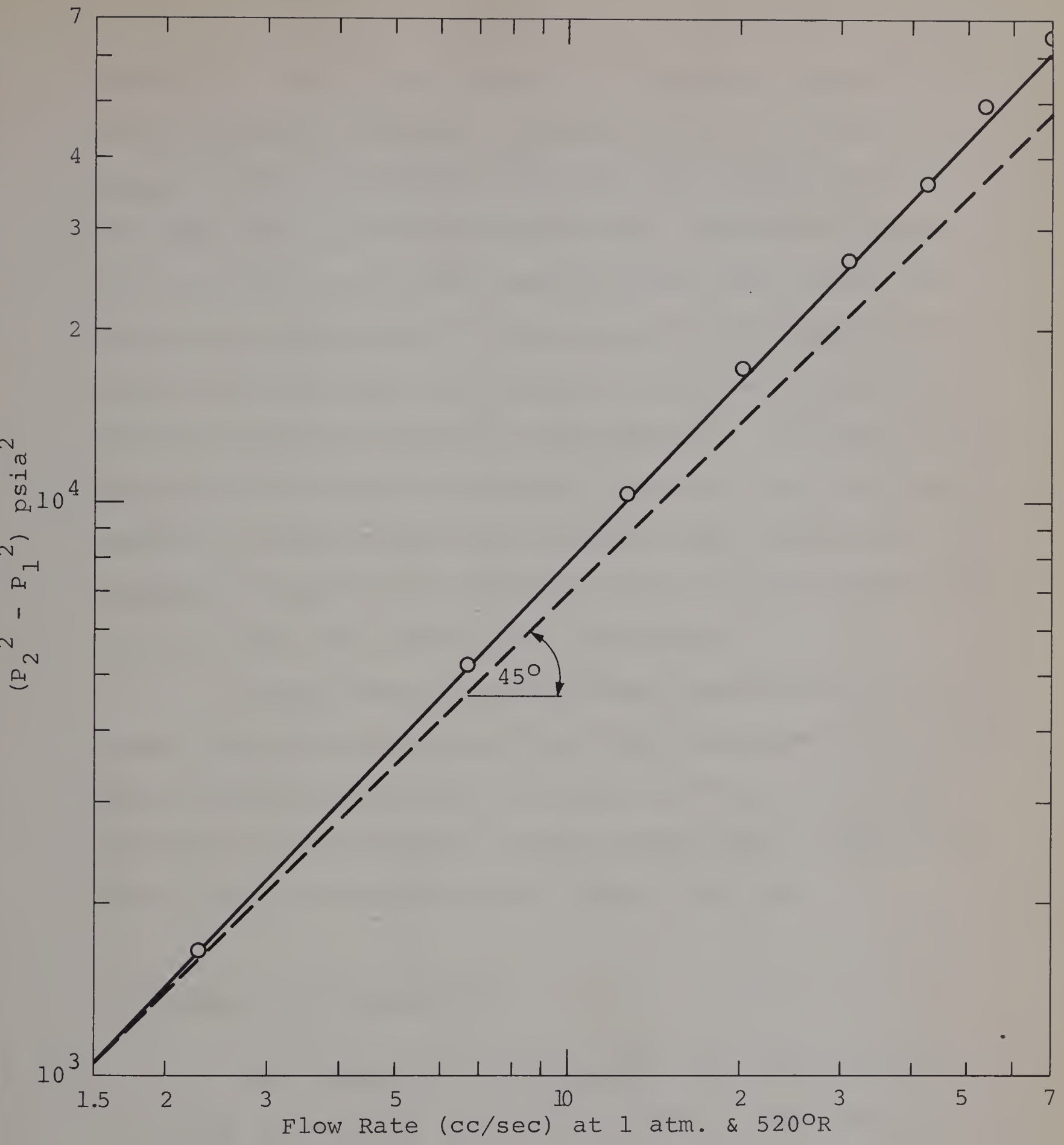

Figure 5 Back-Pressure Plot - Cut Berea Sandstone

guess for b and K (see Figure 6). The final results of the above procedure are shown in Figures 6 and 7. Note that in Figure 7 only the highest two flow rates deviate from the 45^{o} line defining the viscous region. Consequently equation (36) is valid for all but these last two flow rates. The effective permeability to gas can then be obtained by determining the value for the inverse of the mean pressure and reading the result directly from Figure 6. The above analysis was performed on the Indiana limestone, the "Cut"* Berea sandstone, and the high permeability Berea sandstone. Gas permeabilities for the remaining cores were determined from equation (36) for single point flow tests.

Stabilization pressures and temperatures at the steady state were determined for eight different flow rates using the apparatus shown in Figure 2. The rate of gas flow was measured using a triple element Model 20ER"Vol-o-Flow" meter calibrated for the range 0-290 cfh.

Calibration of Transducers

The method of calibrating a ±15 psid transducer consisted of exerting a 14.0 psi pressure differential across

---

* The significance of the adjective Cut is explained in the section entitled "Analysis of Data and Discussion of Results".

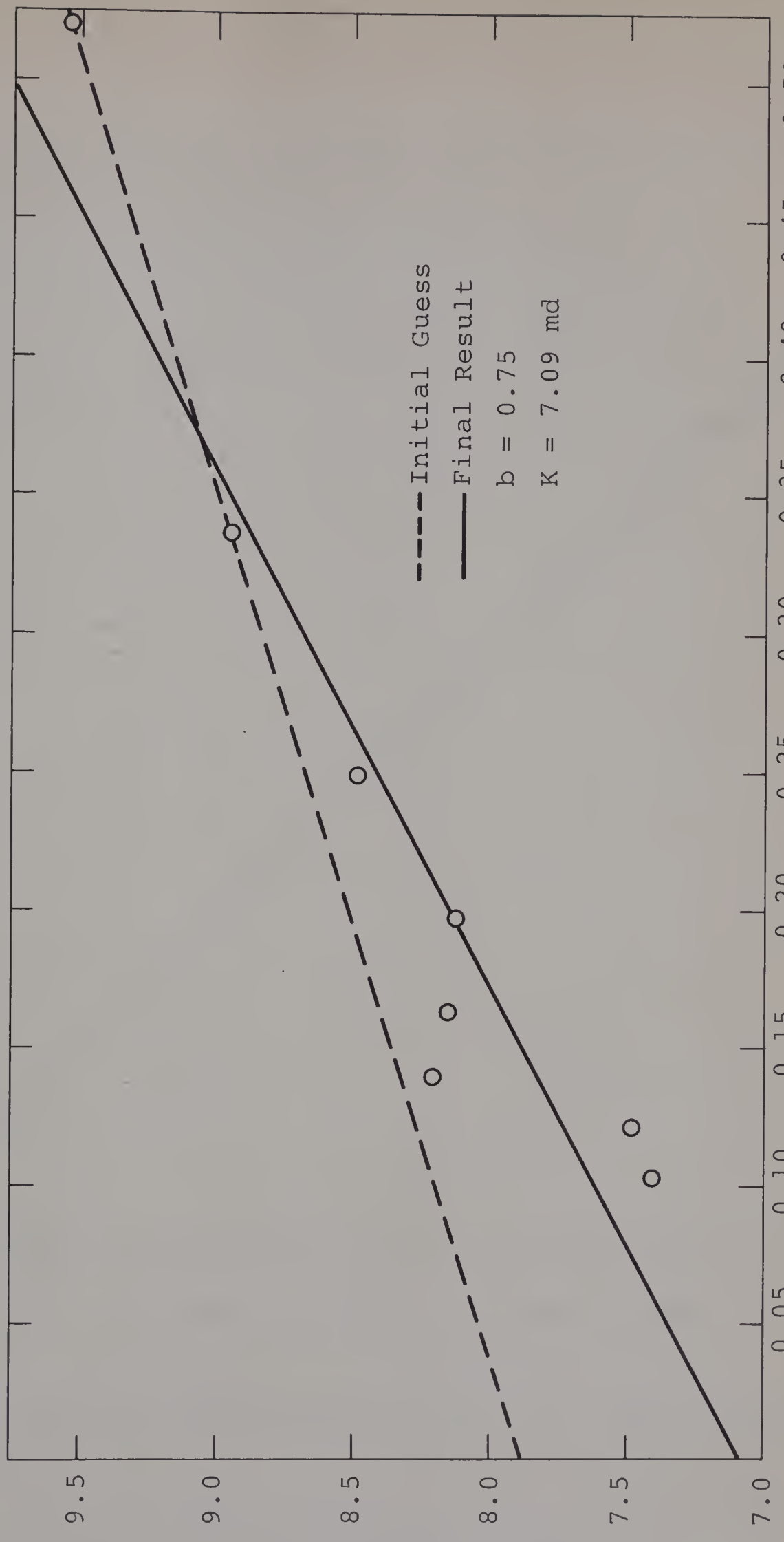

Figure 6 Klinkenberg Plot - Cut Berea Sandstone

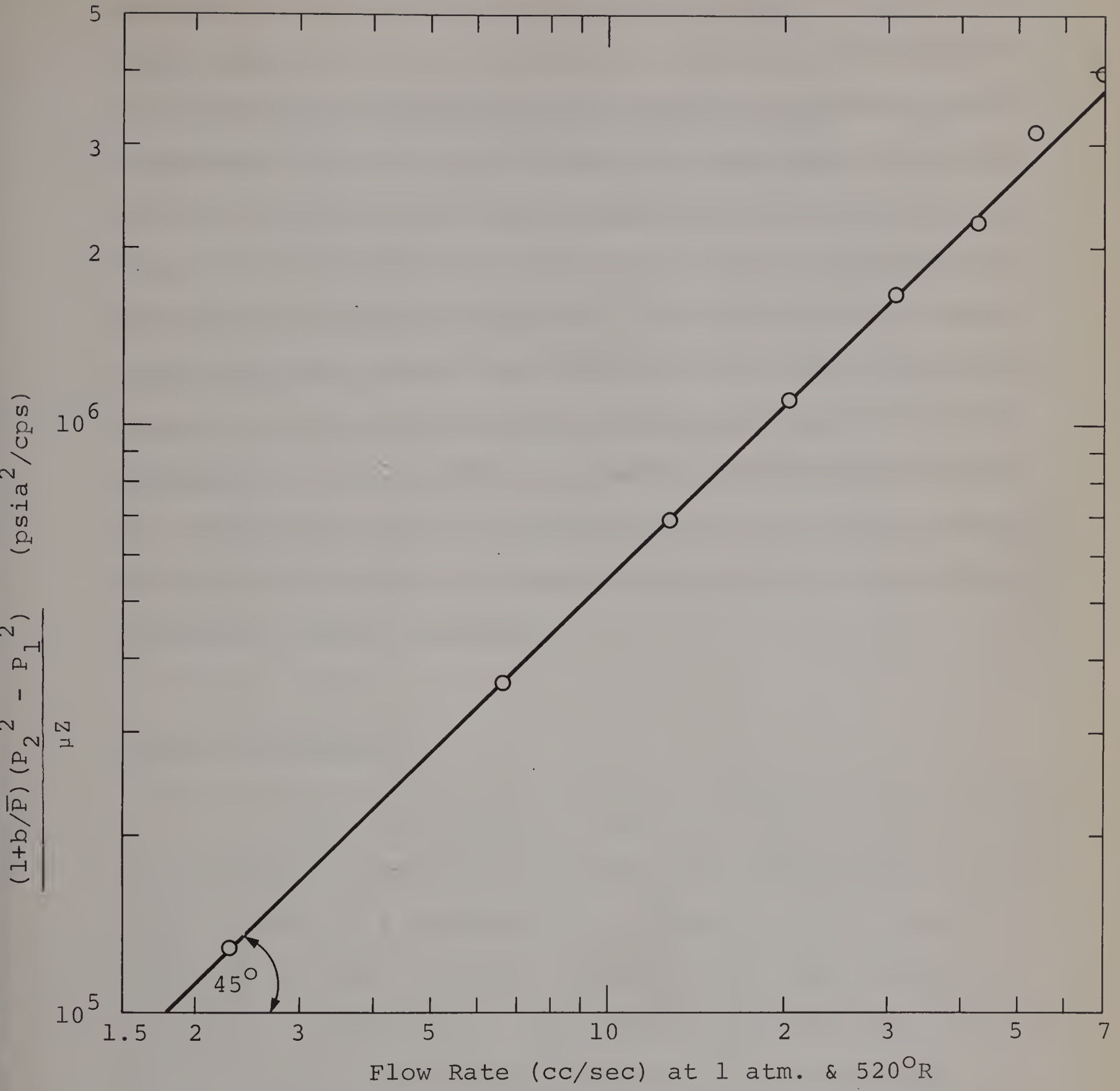

Figure 7 Modified Back-Pressure Plot - Cut Berea Sandstone

the element, and adjusting the input voltage to give a full scale deflection on the Visicorder. The input was monitored on the digital voltmeter and the result recorded for future reference. The pressure differential was then decremented by 1 psi at a time and the corresponding deflections noted. A plot of the deflection versus the pressure differential provided the final calibration. The calibration of the ±50 psid transducer varied only in that a 50.0 psi pressure differential was used to obtain a full scale deflection, and subsequent readings taken at pressure decrements of 5 psi. All transducers were calibrated against a 0-150 psig Seegers Standard Precision Test Gauge. The element of the gauge was precise to within 0.25 psig.

Testing Procedure

Since the apparatus shown in Figure 2 was located in a constant temperature cabinet, the commencement of each day's testing was preceded by a 30-minute warm up period, required for the electrical apparatus and experimental environment to stabilize. The transducers were then isolated and the inputs individually reset to give a full scale deflection for the previously mentioned pressure differentials.

For each experimental run the initial condition

$$P(x,o) = P_i \qquad (37)$$

was simulated by pressuring the core with nitrogen to some controlled level. Equilibrium conditions were indicated by an equalization of upstream and downstream pressures, and by noting a zero deflection of all galvonometers on the Visicorder. Next the Visicorder itself was adjusted for the desired paper speed and the vertical line timer set. One or two trial runs were usually sufficient to determine which settings produced the best results. The run was then initiated by simultaneously tripping open the Toggle valve and setting the paper control mechanism into motion. During the course of each run it was usually necessary to change the paper speed or the vertical line timer set or both at least once. Such changes were all duly noted to facilitate future analysis.

The condition specifying a constant pressure at the external boundary was achieved by means of the Nullmatic regulator. The sealed boundary was obtained by merely closing the valve downstream of this regulator prior to initiating a run. In order to effect an analysis of the data, the actual value of the pressure was required at one point or more in the core for all values of time. The constant upstream pressure was sufficient in the former case. However, for the sealed boundary the variation of either the upstream or downstream pressures was required as a function of time. Both were obtained by periodic observations of the two

pressure gauges and the actual time recorded from a stop watch activated at the beginning of each run. It was not possible to maintain a constant pressure at the producing boundary for the high permeability cores. Consequently, it was necessary to repeat the same run at least once, in order to accurately establish the variation in upstream and downstream pressures with time for the case of the sealed boundary. Although only one of these pressure histories was required, the second served as a check for the first. A similar history of the variation in downstream pressure with time provided a check for the constant pressure case. The actual constant terminal pressure case was obtained only for the tight cores. In such instances the pressure at the producing end stabilized at 0 psig and remained there for the duration of the run.

Because of the limitations imposed by the transducers, pressures in the range of 50 psig were used throughout the course of this investigation. The flowing gas temperature was measured with the thermocouples shown in Figure 2, and the cabinet temperature obtained from a mercury thermometer.

ANALYSIS OF DATA AND DISCUSSION OF RESULTS

Experimental Data

As previously mentioned, the Visicorder charts provided a permanent record of the galvonometer deflections as a function of time on light sensitive paper. These deflections corresponded to the pressure differentials sensed by the transducers for the respective sections of the core. To determine values of pressure it was first necessary to convert the deflections to pressure drops by means of the calibration charts obtained earlier. Thus, knowing the pressure drop from section to section within the core, the pressure distribution was obtained directly by the summation of these differentials starting at a point of known pressure. The above procedure was repeated for a number of different times and a graphical representation of the transient behavior obtained for each core. A typical set of results for the cases of a constant pressure at the external boundary and a sealed external boundary are shown in Figures 8 and 9 respectively. Similar results for the remaining cores are presented in Appendix IV. Deflections were read to within 0.1 of a division. This provided a resolution of 0.1 psid for the PM80TC transducers and a resolution of approximately 0.4 psid on the PM60TC transducer . However, because of the procedure of obtaining pressure, an error in measurement for one transducer was passed on to subsequent pressure values.

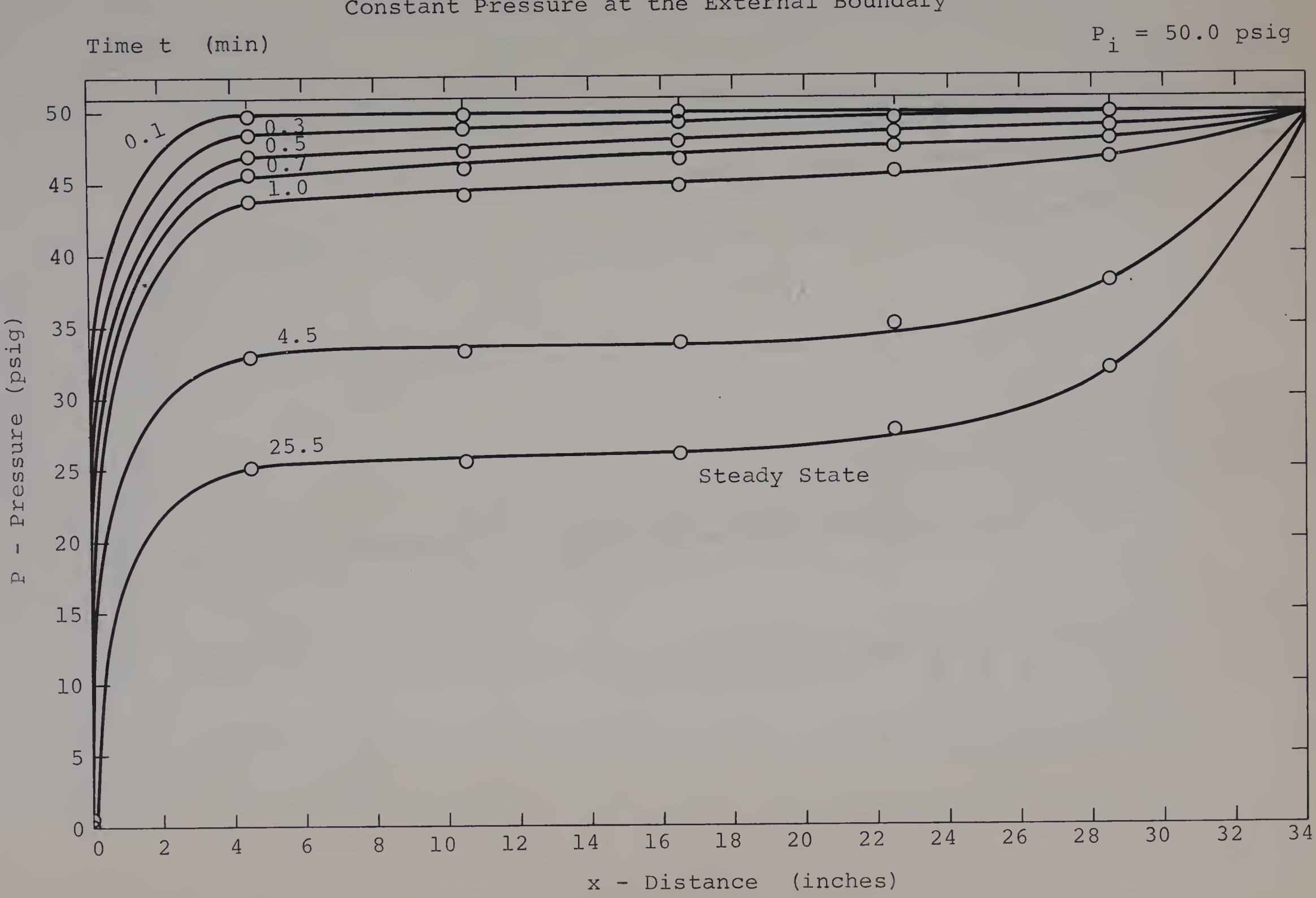

Figure 8 Transient Behavior - Berea Sandstone 1

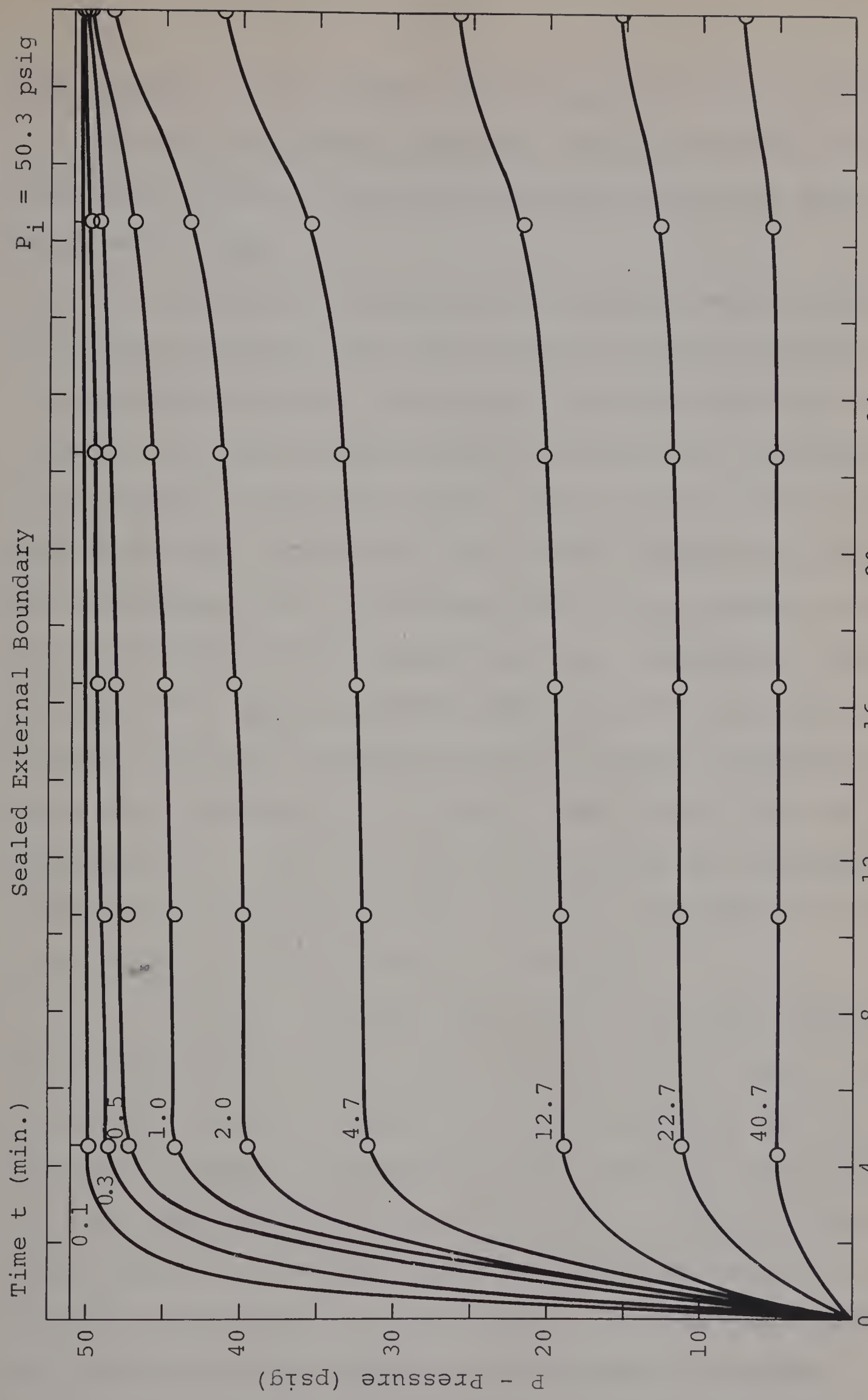

Figure 9 Transient Behavior - Be

For example, if the PM80TC transducers were all in error by 0.1 psid and the PM60TC transducer was in error by 0.4 psid, the final pressure reading determined could be in error by as much as 0.9 psi.

A further inspection of Figures 8 and 9 indicates a drastic deviation from the transient results expected for a homogeneous system. Originally this was attributed to the failure of totally eliminating the mechanical end effect due to machining of the core faces. As a result, the core casing and epoxy were cut and the core itself sheared at a distance of one pressure tap in from each end, in an attempt to once again eliminate these discontinuities. Subsequent testing of this "Cut" Berea sandstone indicated that although the overall effective permeability had increased, discontinuities were still prevalent at the ends (see Figures 29a and 29b, Appendix IV). Thus, it was concluded that the heterogeneous nature of the core was either a natural phenomenon or a direct result of damage from prior testing.

In all instances tests with a constant pressure at the external boundary were run until steady state conditions were achieved. The steady state pressure profile then provided a means for determining the effective permeability of each section of the respective cores. Where possible, flow rates at the steady state were obtained by direct measurement using the Vol-o-flow meter. However, in a number of instances an adjustment to the equipment prevented

measurements of the flow rates from being obtained. For such cases the upstream and downstream pressures were used to evaluate $(P_2^2 - P_1^2)$ and the value of the desired flow rate read from a back-pressure plot similar to Figure 5. Thus, knowing the flow rate through each section of the core and the corresponding pressure drop, the permeability distribution was determined by utilizing equation (36). The results for each core are shown in Table 1. The last column of Table 1 represents the effective gas permeability of core as determined from equation (38), which is derived for permeabilities in series.

$$k_{effective} = \frac{\sum_{i=1}^{n} L_i}{\sum_{i=1}^{n} \frac{L_i}{k_i}} \qquad (38)$$

n = number of sections

L = length of each section

k = permeability of each section

These overall core permeabilities, shown in the last column of Table 1, were then averaged with the gas permeabilities determined as described in the section titled "Experimental Procedure". This provided a suitable value for the characteristic gas permeability of each core. Other properties and characteristics of the cores tested are listed in Table 2.

Table 1

Permeability Variations in Test Cores

Core	*Section (number)	Length (in.)	Permeability (md)	Overall Core Permeability (md)
Berea Sandstone 1	1	4½	1.73	
	2	6	98.3	
	3	6	97.3	
	4	6	22.3	
	5	6	8.21	
	6	5½	1.49	4.59
Cut Berea Sandstone	1	3-7/16	2.52	
	2	3½	15.4	
	3	3½	38.8	
	4	3½	37.8	
	5	3½	86.7	
	6	3½	7.21	9.11
Berea Sandstone 2	1	3½	387	
	2	3½	484	
	3	3½	526	
	4	3½	536	
	5	3½	431	
	6	3-15/16	515	474
Series Core AUS	1	8-5/8	315	
	2	9	458	
	3	9	663	
	4	9	838	
	5	9	1039	
	6	9-3/8	962	602
Indiana Limestone	1	3-11/16	1.76	
	2	3½	5.20	
	3	3½	127	
	4	3½	253	
	5	3½	1.93	
	6	3-10/16	2.72	3.58

* Section numbers begin from the downstream end of the core.

Table 2

Properties and Characteristics of Test Cores

Core	Length (in.)	Diameter (in.)	ϕ (fraction)	S_{or} (fraction)	K (md)	$*k_g$ (md)	$**k_g$ (md)	k_g (average) (md)
Berea Sandstone 1	34	3½	0.206	0.582	5.01	4.36	4.59	4.47
Cut Berea Sandstone	20-15/16	3½	0.198	0.727***	10.6	9.09	9.11	9.10
Berea Sandstone 2	21-7/16	3½	0.228	0.544	530	489	474	481
Series Core	54	2	0.222	0.511	728	623	602	612
Indiana Limestone	21-5/16	3½	0.199	0.582	4.73	3.57	3.58	3.58

* Determine as outlined in "Experimental Procedure"

** From Table 1

*** Believed to be in error

Experimental Results

Initially the tests were designed to study the applicability of the theory developed for transient gas flow through a homogeneous linear porous system with a liquid saturation. However, all of the cores tested proved to be of a heterogeneous nature. In fact, the Series core, the only core assembled with a deliberate discontinuity, provided results more characteristic of a homogeneous system when the Alundum section was located in the upstream position. Figures 24 and 25 of Appendix IV for the Series core AUS show that there are no abrupt changes in the pressure profiles to indicate any regions of discontinuity. However, a comparison of the theoretical steady state curve for a homogeneous system with the steady state curve obtained indicates a substantial discrepancy. This is attributed to the lower permeabilities experienced in the Berea sandstone near the producing boundary. Inverting the Series core provided drastic changes in the pressure profiles. It now became apparent that a discontinuity did exist somewhere in the core, as can be seen in Figures 26 and 27 of Appendix IV. However, it was not possible to determine the exact location of the heterogeneity from the graphical results. A further inspection of the results for the Series core indicated that the presence of the Berea fracture did not noticeably influence the shape of the curves obtained in this region.

As a result it was concluded that the Berea sandstone-Alundum interface had no effect on the transient results obtained, and the discontinuity detected in this region was due entirely to the difference in permeabilities. With the exception perhaps of the Indiana limestone, no sharp or distinct breaks in the pressure profiles were discernible for the results obtained. This has been ascribed to the fact that values for the pressure are known only for specified points within the core, and drawing a curve through these points would tend to average or smooth out the effects of any discontinuities located between pressure taps, if such discontinuities actually did exist. It is suggested that one way to overcome this difficulty would be to position the pressure taps closer together in a region of known heterogeneity. One pressure tap would be located in the high permeability region while the second would be positioned a small distance away in the region of lower permeability. However, care should be taken to insure that the presence of the pressure taps would not markedly affect the transient response. Series cores with sections having greater differences in permeabilities than those studied here would provide the best results.

A comparison of Figures 25 and 27 (Appendix IV) indicates that for the sealed boundary, the Series core ADS exhausts itself much more quickly than when the Alundum section is located in the upstream position. This is to be

expected, since the flow from the high permeability Alundum for the Series core AUS is hindered by the presence of a lower permeability Berea sandstone located in the downstream position. With the Alundum section in the downstream position, the rate of flow from this region is dependent only on the back-pressure applied at the producing face. Although the time for complete exhaustion should theoretically be the same for both cases, any specified fraction of the total available gas would be recovered much more quickly from the Series core with the section of Alundum in the downstream position. Figures 25 and 30 (Appendix IV) serve to show that the sections of high permeability account for only a fraction of the total pressure drop experienced in a heterogeneous system. Note the comparatively small pressure gradients in these regions.

Substantial errors are suspected in the values measured for the variation of upstream and downstream pressures with time. The crude method in which these values were obtained leaves much to be desired, especially for the higher permeability cores where changes in pressure occurred much more rapidly. This, however, is a limitation of the apparatus used, and it is suggested that in future investigations, a measuring device be installed to automatically sense and record the variations of both the upstream and downstream pressures as a function of time. The gas entrapped in the line leading from the pressure tap to the

upstream gauge, and the free gas located in the gap created by the flange and core surface provided a second source of error, since this gas must be removed through the core in order for the gauge to detect a change in pressure.

Dimensionless Quantities

For homogeneous systems the theory states that if the parameters influencing transient behavior are expressed in dimensionless form, the value of the dimensionless pressure at the same dimensionless distance and dimensionless time should provide a single and unique answer, irrespective of the homogeneous characteristics of the core and the nature of the gas being tested. Figure 10 represents an attempt to validate this concept. A dimensionless time of 3.0 was arbitrarily chosen and the values of real time for each core determined from

$$t_D = \frac{kP_i t}{\mu \phi_e L^2} \qquad (39)$$

where ϕ_e is the effective gas porosity equal to $\phi(1-S_{or})$. The values of viscosity where evaluated at P_i from a correlation available in the literature[26]. The Visicorder charts for the sealed boundary case were then read at these values of time to obtain the pressure profiles, and hence the dimensionless pressure distribution. The definition of dimensionless pressure as presented here is valid only for the constant terminal pressure case. Since this was not achieved

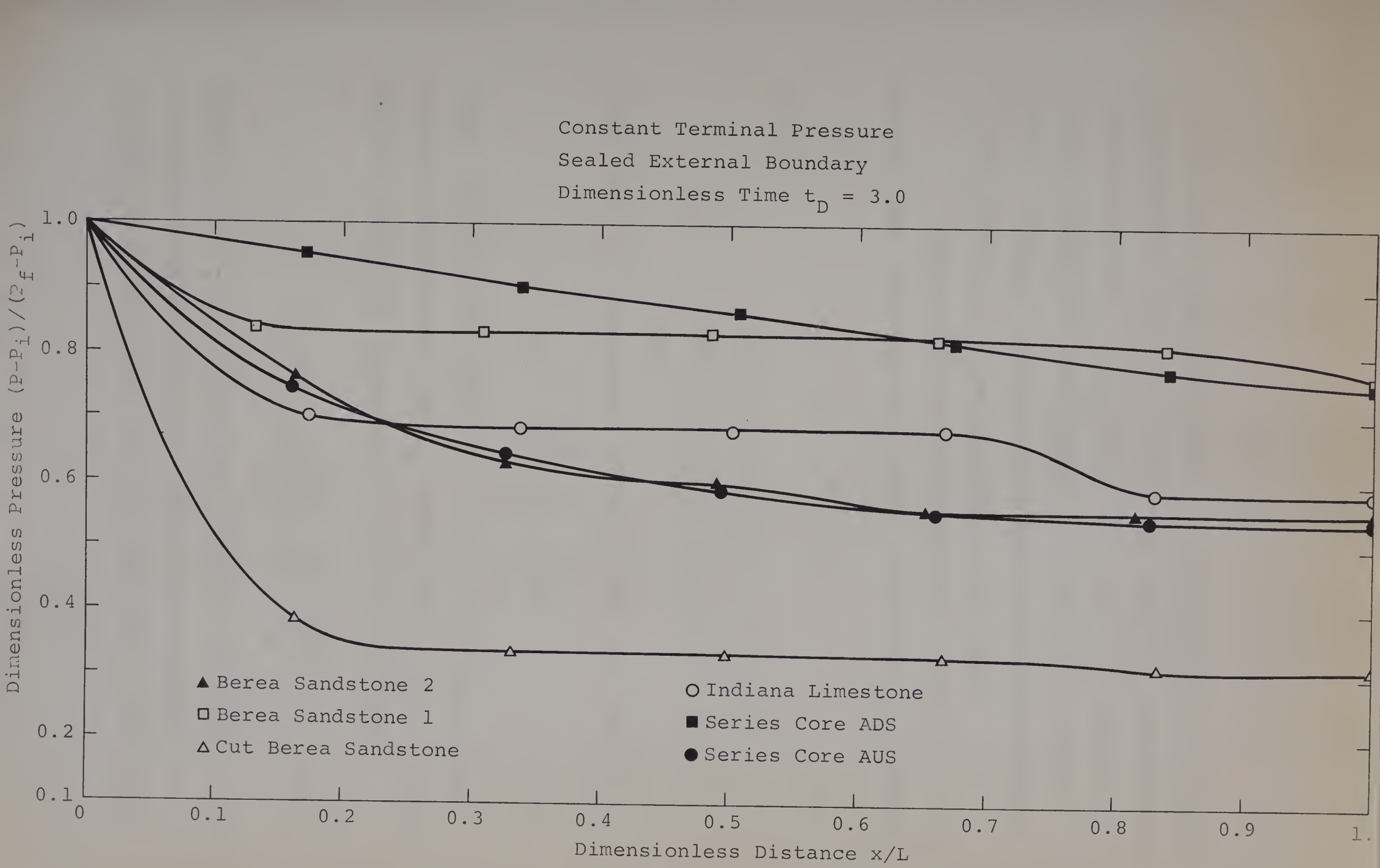

Figure 10 Correlation of Dimensionless Quantities

in the high permeability cores, it was necessary to average the downstream pressure for the time interval considered in order to obtain an appropriate value for P_f. Figure 11 further exemplifies the results of Figure 10. In this instance, however, the transient behavior for various times is presented at the same position in each core.

The cumulative molar production n_c from each core at any time t was evaluated from a simple material balance

$$n_c = n_i - n(t) \tag{40}$$

where

n_i = number of moles initially in core

$n(t)$ = number of moles remaining in core at time t

Application of the equation of state for a gas leads to

$$n_c = \frac{\phi_e LA}{RT}\left(\frac{P_i}{Z_i} - \frac{P_{av}}{Z_{av}}\right) \tag{41}$$

where subscript "i" refers to initial conditions and subscript "av" refers to average conditions at time t. Equating the results of equations (23) and (41) provides

$$Q_{t_D} = \frac{\bar{P}\, Z_f}{P_f(P_f - P_i)}\left(\frac{P_i}{Z_i} - \frac{P_{av}}{Z_{av}}\right) \tag{42}$$

where P_i and P_e are equivalent. Equation (42) was then used to evaluate the dimensionless cumulative production as a function of dimensionless time for each core. The results

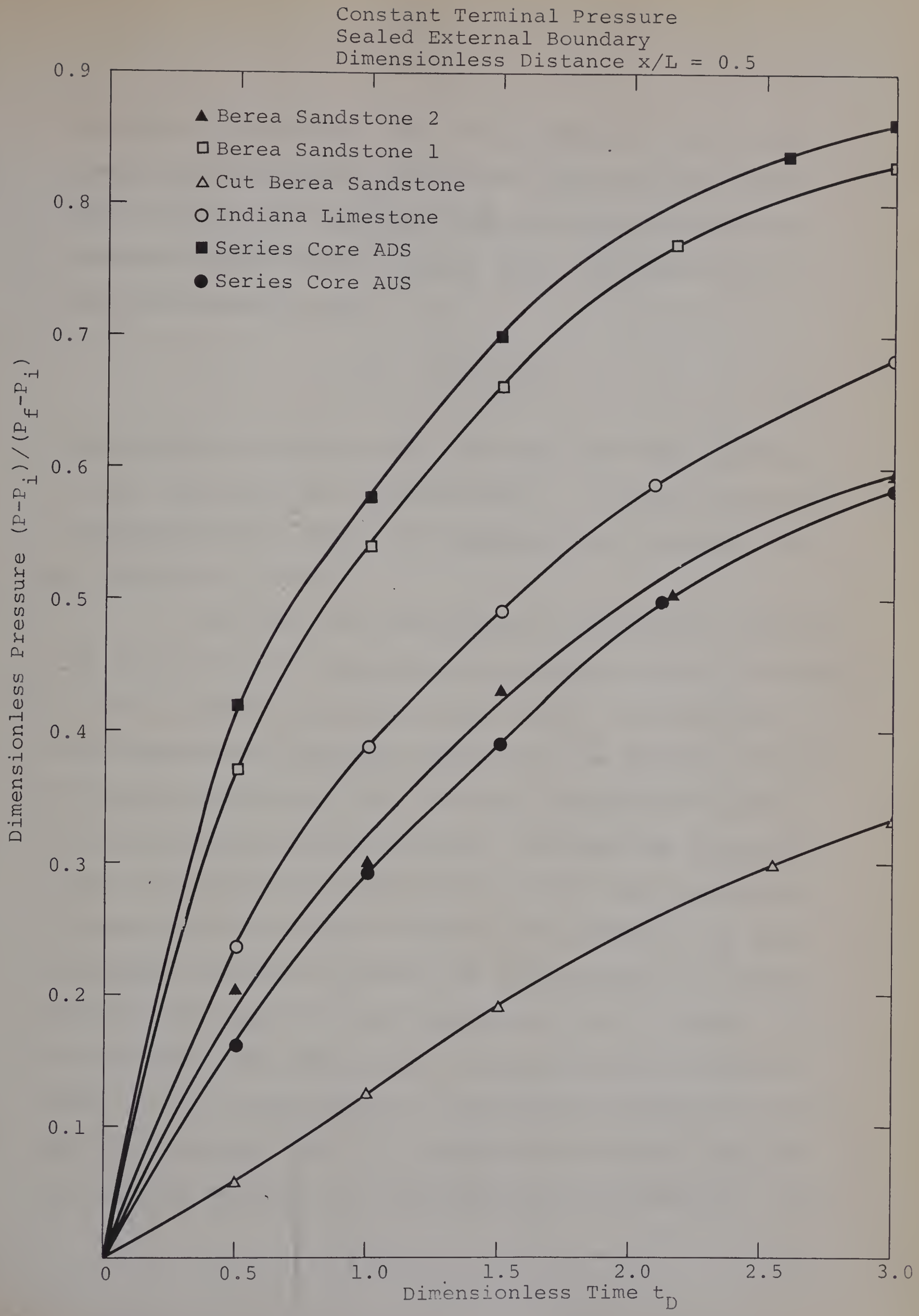

Figure 11 Correlation of Dimensionless Quantities

are shown in Figure 12. Note that although $\bar{P}$ and P_{av} represent mean pressures, the two are not numerically equal. Values for P_{av} were obtained from the transient pressure profiles for the sealed boundary case. By definition $\bar{P}$ was then evaluated from

$$\bar{P} = \frac{(P_i + P_{av})}{2} \tag{43}$$

Compressibility factors were obtained from data available in the literature for nitrogen gas[21]. Finally, corresponding dimensionless times were determined from equation (39) by replacing P_i with $\bar{P}$.

From the theory developed for homogeneous systems, the correlation of dimensionless parameters shown in Figures 10 and 11 should provide a single curve. An inspection of the dimensionless pressure profile for the Indiana limestone in Figure 10 shows why this need not necessarily be true for heterogeneous porous systems. Although the dimensionless correlation has incorporated all the basic variables influencing the transient response, no parameter has been introduced which will account for the variation of permeability from point to point within each core. However, it is this very same permeability variation which is responsible for the unique shape of the pressure profile obtained for the limestone core. To clarify this further, consider the results obtained for the Series core in Figure 11. The

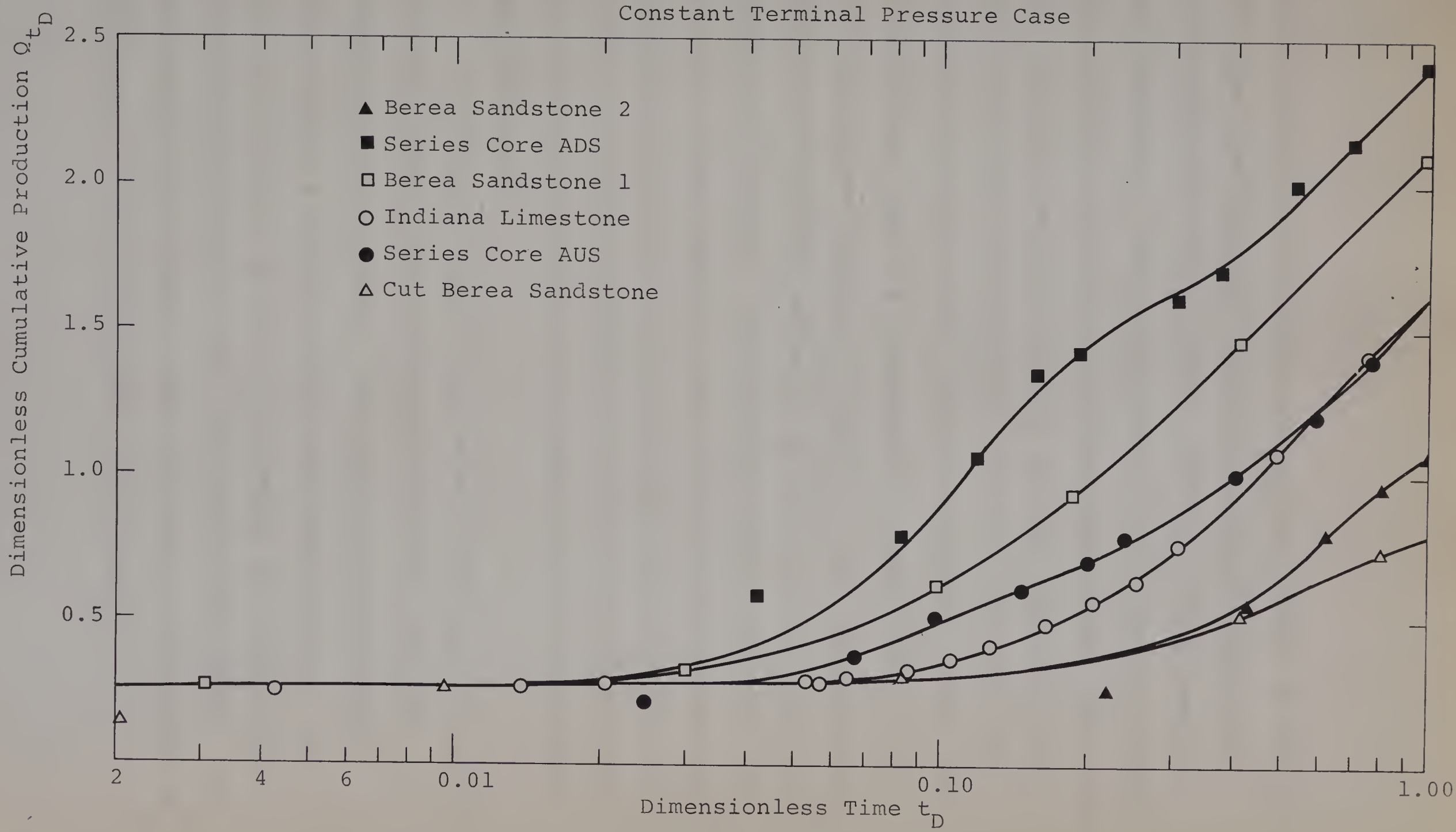

Figure 12 Dimensionless Cumulative Production

point of interest is the center of the core, which is exactly the same regardless of the position of the Alundum section. A comparison of the results for the Series core AUS and ADS indicates a large discrepancy in the values of dimensionless pressure for the same dimensionless time. Since the initial pressures were very nearly the same for both tests, it may be concluded from equation (39) that the real times under consideration are also the same. However, it has already been shown that the discrepancy in pressures for the Series core can be attributed directly to the difference in orientation of the high permeability section with respect to the producing boundary. Consequently, before the transient response of a heterogeneous system can be defined uniquely, a correlating parameter is required which will not only incorporate a variation in permeability, but will also account for the orientation of the heterogeneities with respect to a fixed reference.

The Series Core AUS and Berea Sandstone 2 in Figure 10 provided results more in keeping with those expected for a dimensionless correlation. The dimensionless pressure profiles compare favorably within experimental error. A comparison of Figures 25 and 28b (Appendix IV) shows that the pressure histories are very similar for both cores. An inspection of Table 1 reveals that this can be attributed to the similarity of the permeability distributions.

Figure 12 tests the applicability of Van Everdingen and Hurst's dimensionless cumulative production term to the experimental results obtained. As predicted by the theory, values appear to be uniquely defined in the early stages of the producing life of the cores. Very little data were available to substantiate this early production history because of the small values of real time involved, especially for the high permeability cores. The presence of large residual fluid saturations greatly reduced the effective porosity of the cores to gas. As a result the cores were exhausted more quickly than they would have been if only the gas phase was present. The predicted deviations from the single line are due to the influence of the sealed external boundaries. The irregular shapes of the curves obtained for the high permeability cores can be ascribed to the fact that these tests did not in actuality simulate the constant terminal pressure case, a prerequisite for the use of this correlation. The results for the tight cores, however, show more of a resemblance to the curves predicted by the theory. For reasons previously discussed, there is a large discrepancy in the results obtained for the Series core AUS and ADS. A comparison of the two curves, however, does serve to indicate the extent of the error that may be introduced by applying this theory to a heterogeneous system.

Radius of Drainage

Results from equations (28) and (29) were compared with values for the radius of drainages and stabilization times determined experimentally. Knowing the values of P_i and P_f, equation (27) was used to calculate the value for the pressure at the radius of drainage. The Visicorder charts then provided a means for establishing the time required for the pressure to reach this level, at the different pressure taps along the core. Appropriate values of P_f for the high permeability cores were again obtained by averaging the downstream pressure over the time interval considered. The results for the Indiana limestone are shown in Figure 13. According to equation (29) a log-log plot of stabilization time versus radius of drainage should yield a straight line with a slope of 2, if μ, ϕ, k, and $\bar{P}$ are constants. These latter restrictions are inherent in the original derivation of equation (29). For this investigation, however, the above limitations were mainly overcome by using the effective permeability of only the section of core through which the transient had traversed. Equation (38) was used to determine these effective permeabilities as the transient progressed from point to point within each core. Curve B of Figure 13 was determined in this manner.

A further inspection of equation (29) exemplifies the fact that the stabilization time is directly proportional

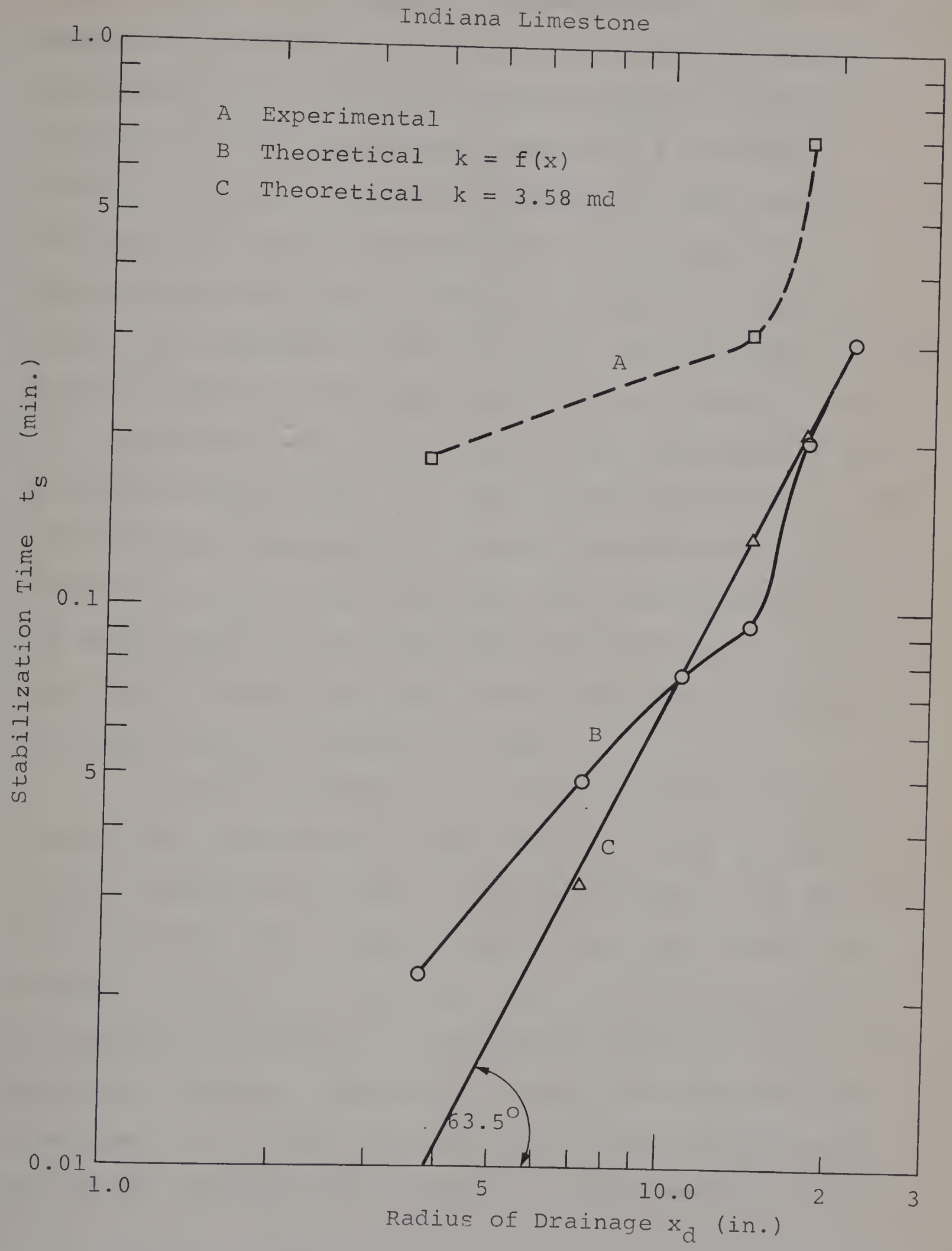

Figure 13 Radius of Drainage and Stabilization Time

to the amount of gas present, represented by ϕ, and inversely proportional to the rate at which the gas may be removed, represented by k. This relationship between the stabilization time and the porosity and permeability is tested in Figure 14 assuming a constant viscosity and mean pressure. Variations in μ and $\bar{P}$ are accounted for in Figure 15. Theoretically speaking, all values obtained for Figure 15 should fall somewhere on the 45° line. The influence of permeability alone on the stabilization time is shown in Figure 16. As expected, the stabilization times decrease for increasing permeabilities, all other factors being equal. The permeabilities obtained for Figure 16 were determined on a section by section basis for each core using equation (38). The stabilization times were determined from equation (29). Note that in all of the above cases, the porosity referred to is the effective porosity to gas.

Figure 13 shows that a large discrepancy exists between the theoretical and experimental values obtained for the stabilization times. This is believed to be due to the relatively large reaction time of the experimental apparatus to changes in pressure, and to the fact that it is not possible to obtain an instantaneous pressure drop at the producing boundary. Because the values for the stabilization time are so small, the presence of the initial excess gas in the pressure lines leading to the transducers becomes

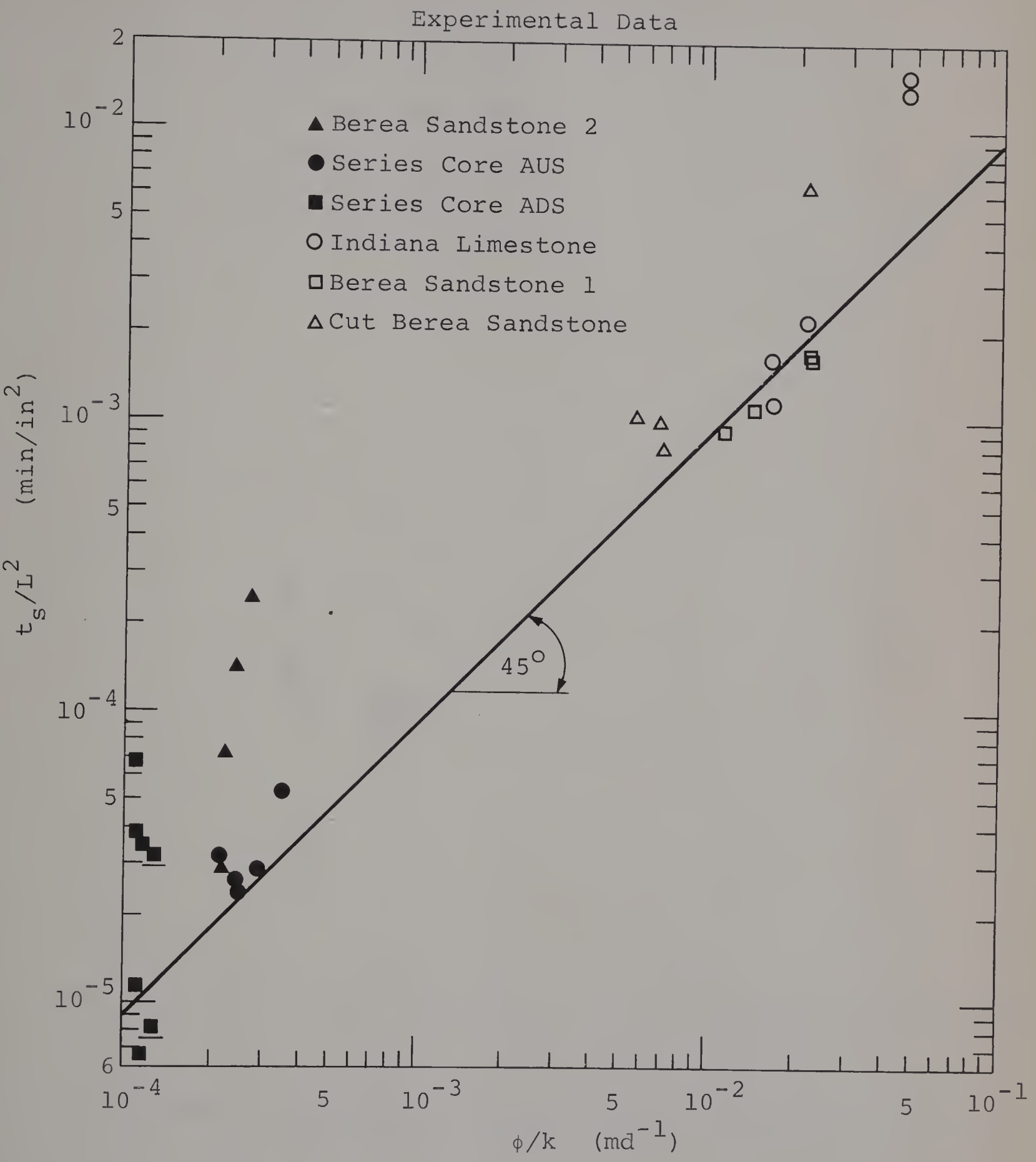

Figure 14 Influence of ϕ/k on the Radius of Drainage and Stabilization Time

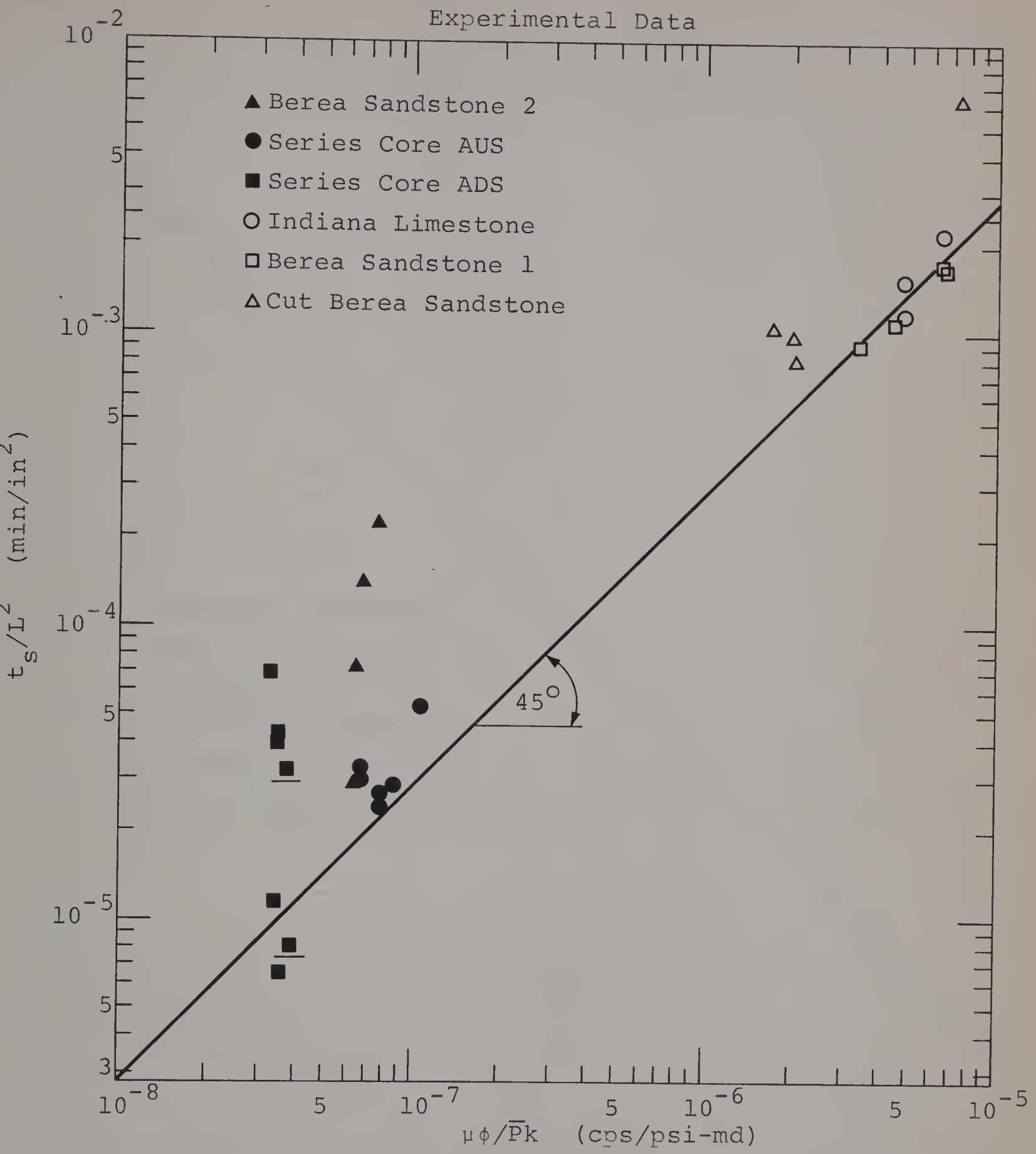

Figure 15 Influence of $\mu\phi/\bar{P}k$ on the Radius of Drainage and Stabilization Time

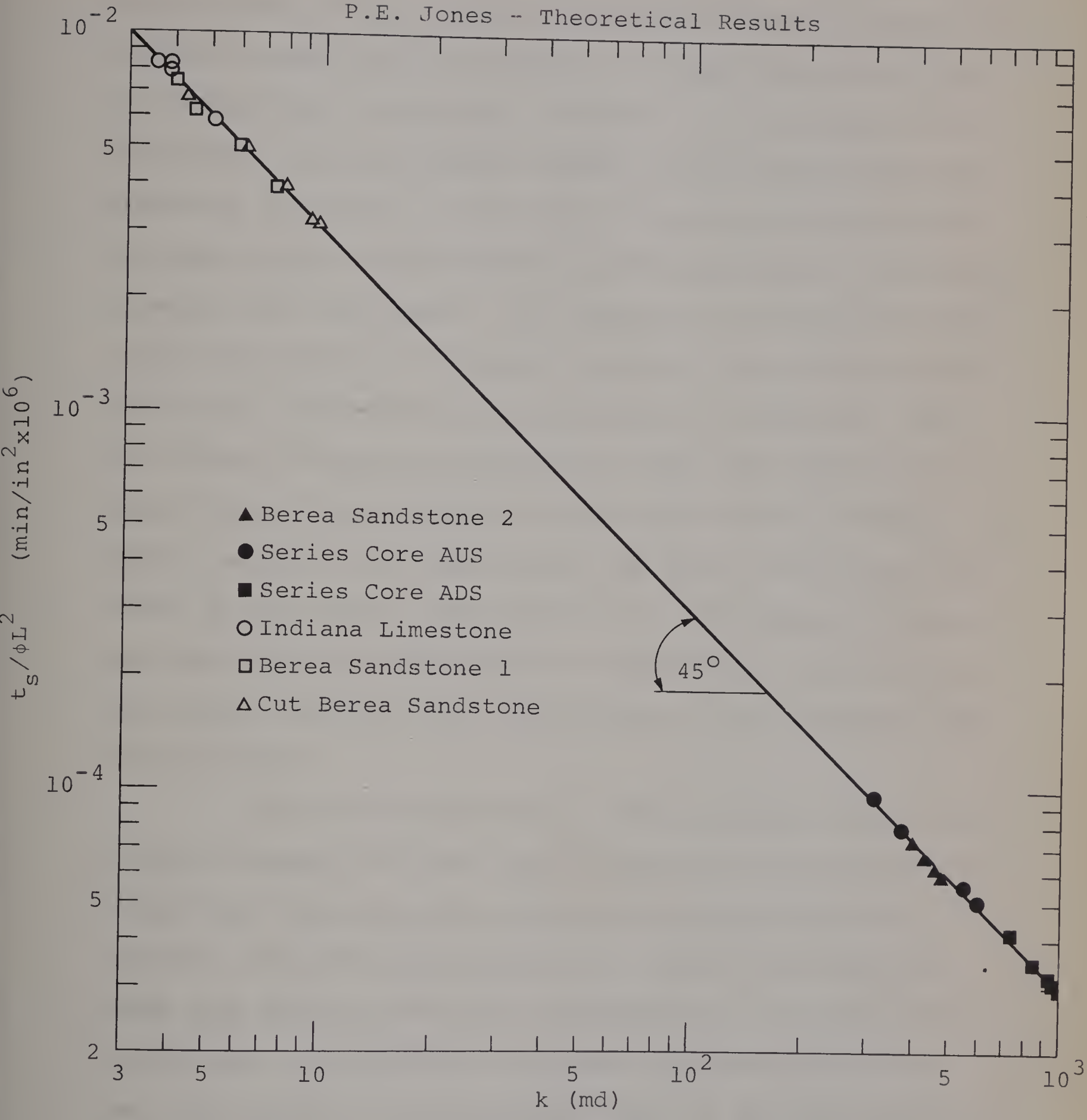

Figure 16 Influence of k on the Radius of Drainage and Stabilization Time

significant. This is especially true for the high permeability cores, since the gas entrapped in these lines must be removed through the core before a pressure differential can be detected by a transducer. Figure 17 is an example of a case where the experimental results contradicted those predicted by the theory. Note that the relative positions of the experimental curves are the direct opposite of the results expected from the theory. For reasons to be discussed later, it was not possible to obtain a value for the stabilization time at all the pressure tap locations in each core. However, enough data were available to show that although the actual values for the stabilization time did not compare, the general shape of the experimental curve was accurately predicted by the theory (see Figure 13). Consequently it was concluded that the discrepancy in experimental and theoretical results was due to the limitations of the equipment and not the theory.

The values obtained for stabilization times at the external boundary for both the homogeneous and heterogeneous systems are the same,since this calculation is based on identical effective permeabilities. Curve B in Figure 13 shows that when the effective permeability up to the radius of drainage is lower than the overall permeability of the core, the values of stabilization time for the heterogeneous system fall above the straight line. Values below the

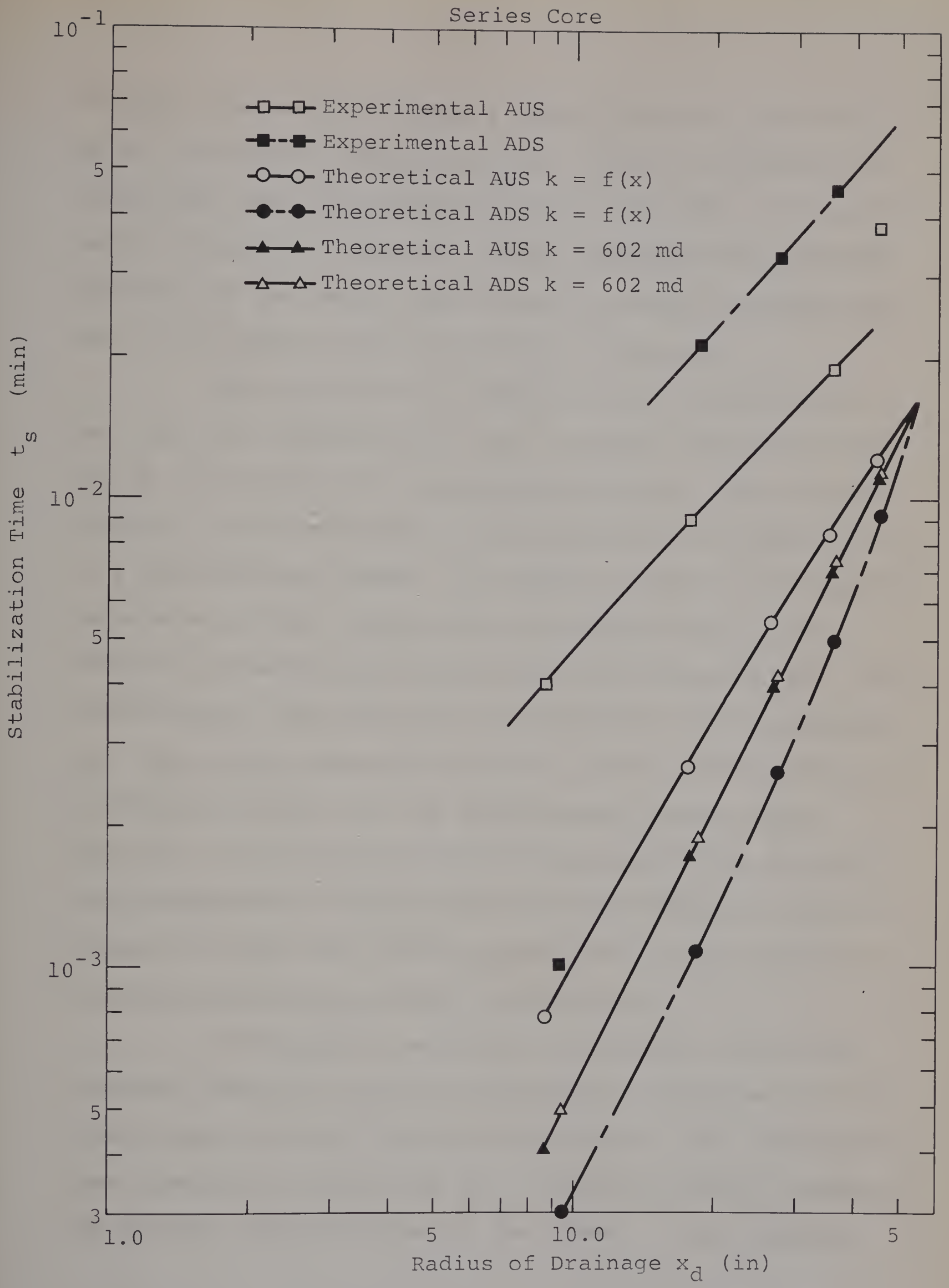

Figure 17 Radius of Drainage and Stabilization Time

straight line would indicate a higher effective permeability up to the radius of drainage, and a point of intersection would mean that the permeabilities are the same. The Series core in Figure 17 shows that in one instance the effective permeability is always higher than the overall permeability, and in the second case the opposite holds true.

The derivation of equation (29) is based on the fact that the dimensionless time is always the same at the radius of drainage for a homogeneous system. This concept, however, was not violated in the application of equation (29) to a heterogeneous system. In effect,a number of homogeneous cores were assumed having the same permeability as the effective permeabilities determined from equation (38). The stabilization times were then evaluated for these hypothetical cores at the desired locations, and the results compiled to obtain a history for the heterogeneous system being analyzed. A plot of the effective permeabilities used and the corresponding stabilization times evaluated is shown in Figure 16. Note that all the points fall on the predicted straight line having a slope of minus one.

An attempt to correlate the factors influencing transient behavior with the experimentally measured stabilization times is shown in Figures 14 and 15. The experimental data obtained in either case do not even remotely resemble the straight line predicted by the theory. This, however,

is due to the unreliability of the data and not the theory, especially in the case of the high permeability cores. The underscored data points in Figures 14 and 15 represent results for the same radius of drainage under identical circumstances. Note the large discrepancies in the values of stabilization times obtained. As can be seen, the tight cores provided the higher stabilization times and the least amount of scattering of data points. Figure 14 is valid only for the ratio of viscosity to mean pressure used in this investigation. The influence of these two variables on the stabilization time is included in Figure 15. However, since the values of viscosity and mean pressure were nearly the same for all tests and since the variation throughout the course of a run was small, the two plots are very similar.

Numerical Solution

A solution to equation (32) was effected in terms of pressure squared in an attempt to determine the influence of assuming an average pressure, $\bar{P}$, on the final results. $\bar{P}$ in this instance was defined by the finite difference expression

$$\bar{P} = \frac{1}{6}\left(P^{*}_{r+1,s+1} + P^{*}_{r,s+1} + P^{*}_{r-1,s+1} + P_{r+1,s} + P_{r,s} + P_{r-1,s}\right) \qquad (44)$$

where the asterisk denotes values from the previous iteration. Because of limitations in the experimental apparatus and the numerical solution, the influence of using $\bar{P}$ was not accurately determined.

The experimental results were expressed in terms of dimensionless parameters and a comparison made with the numerical solution. Figures 18 through 21 inclusive compare the dimensionless pressure profiles obtained experimentally with those determined numerically for the same dimensionless times. The solutions for the heterogeneous and homogeneous systems were obtained by utilizing the finite difference approximations (II-10) and (II-11) (Appendix II), respectively. Equation (39) was used to evaluate the dimensionless times.

Figures 18 and 19 for the Indiana limestone simulate the ideal case of "Constant Terminal Pressure". Because of its high permeability, the Series core, on the other hand, was subjected to a varying pressure at the producing boundary. This was simulated numerically by performing a three-point Lagrangian interpolation on the experimental data obtained for the variation of the downstream pressure with time. Consequently, as shown in Figures 20 and 21, the experimental and numerical values of pressure are identical at this point.

In all cases the length of the transient period predicted by the numerical solution varied significantly

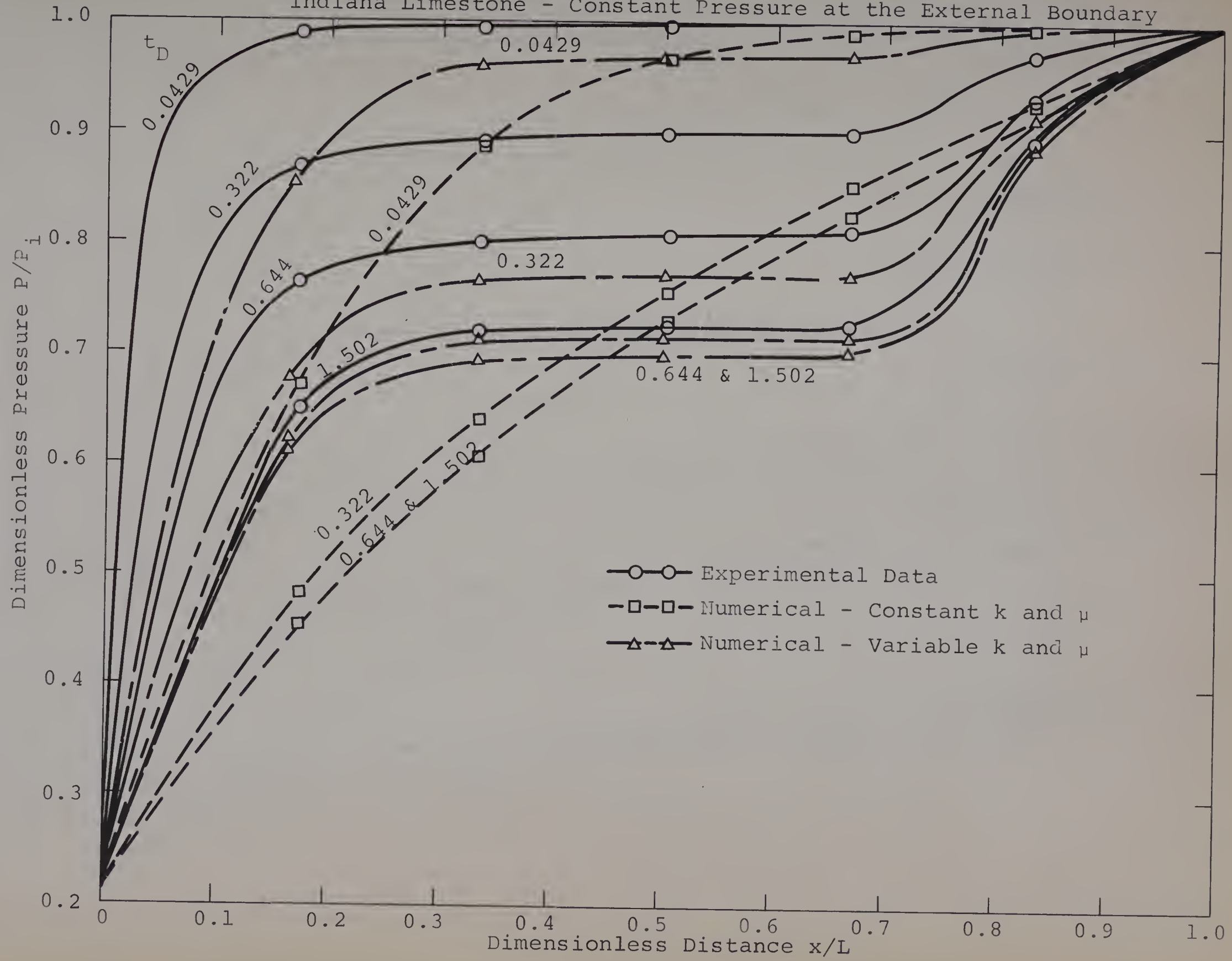

Figure 18 Comparison of Experimental and Numerical Results

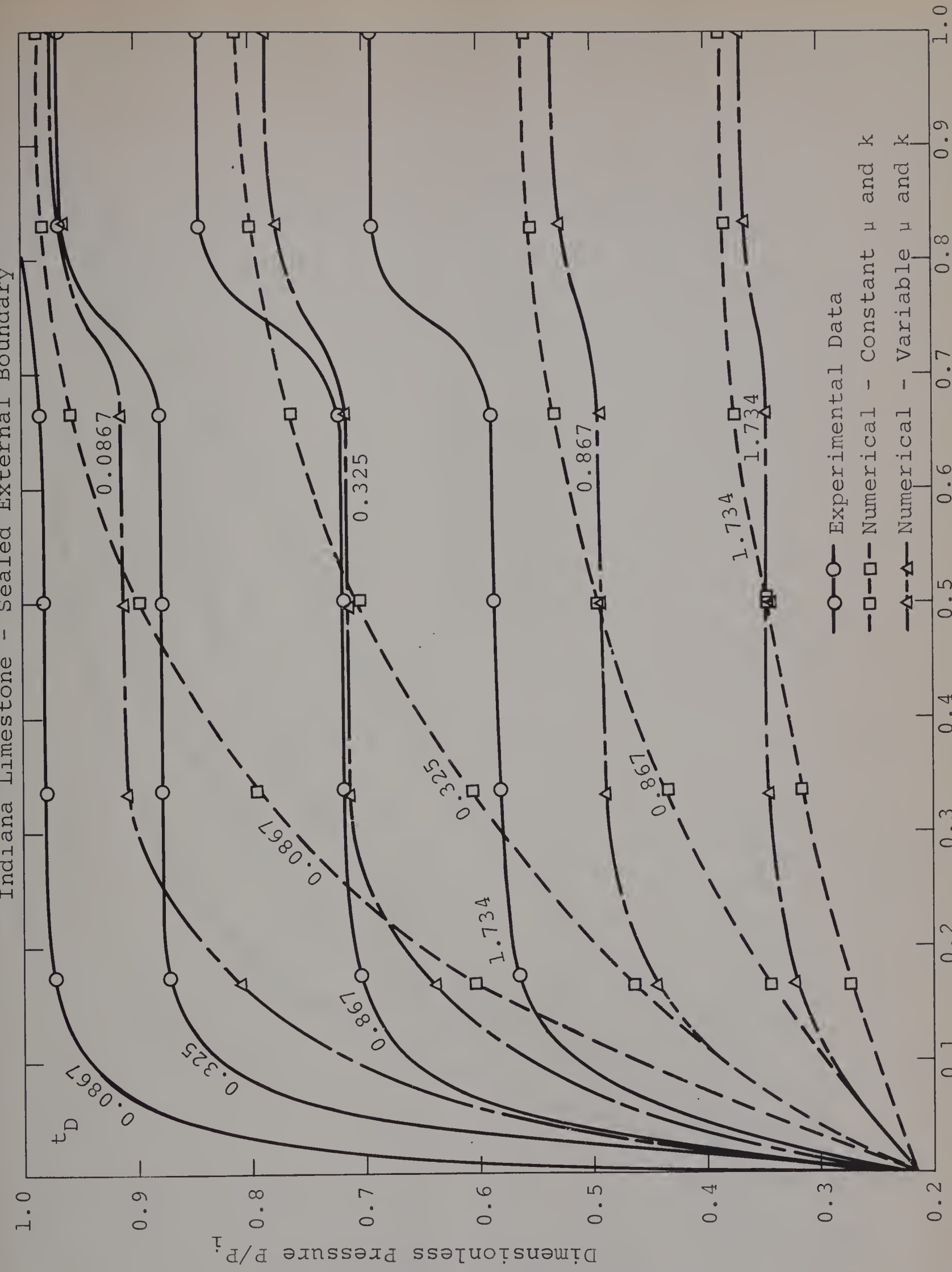

Figure 19 Comparison of Experimental and Numerical Results

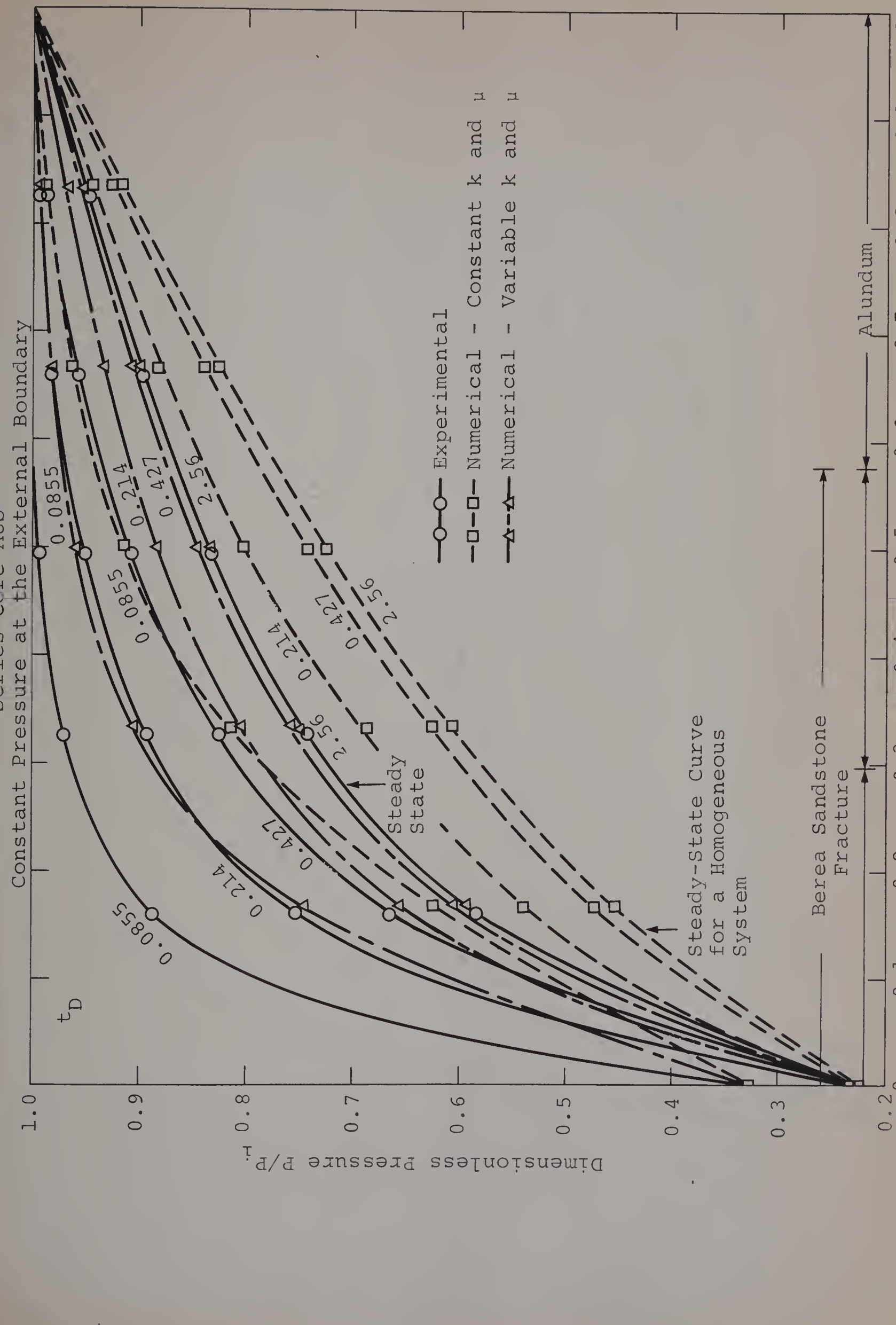

Figure 20 Comparison of Experimental and Numerical Results

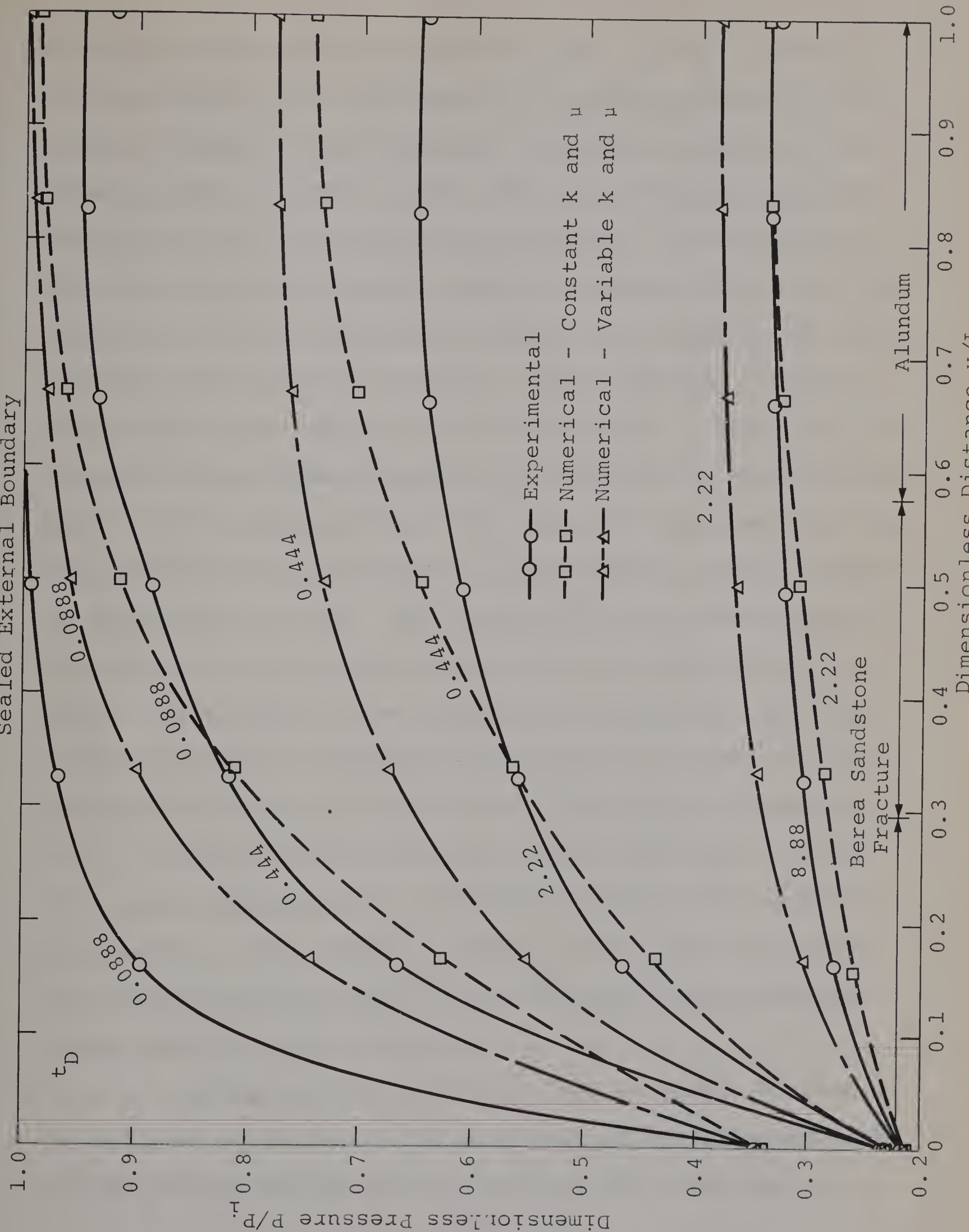

Figure 21 Comparison of Experimental and Numerical Results

from the experimental results obtained. As can be seen in Figures 18 and 20 for the case of a constant pressure at the external boundary, the numerical solution converges to the steady state in a much shorter time than would be expected on the basis of the experimental results. For the case of the sealed external boundary shown in Figures 19 and 21, the numerical solution predicts a shorter time required to effect complete exhaustion of the core. As an example, consider the dimensionless time of 1.734 in Figure 19. Note that the average dimensionless pressure, as predicted by the numerical solution, is approximately 0.35, while for the same time the experimental data provides an average dimensionless pressure of approximately 0.60. The reasons for this discrepancy in the values of time is believed to be due mainly to the inherent limitations of the experimental apparatus. For the limestone core the numerical predictions are based on the boundary condition stating that an instantaneous pressure drop is applied to the producing end at time zero. It is, of course, impossible to completely simulate this condition in practice. The numerical solution also fails to account for the finite quantities of gas entrapped in the pressure lines leading to the transducers.

The prime source of experimental error, however, is believed to be due to the machining of the pressure taps and the corresponding damage caused to the permeability in

this region. If the reduction in permeability is of a significant nature, it is feasible that substantial pressure gradients could exist across this localized region during the transient life of the core. Since the analysis of the data assumes that the pressure in the transducer lines is characteristic of the actual pressure in the core at any time, large errors could result in the subsequent interpretation of the Visicorder charts. Some evidence does exist to substantiate this hypothesis. In a number of instances negative galvonometer deflections were detected on the Visicorder charts. This would only occur if the downstream pressure were higher than the upstream pressure, which is impossible. However, if the region of core surrounding the downstream pressure tap was damaged and the corresponding upstream tap was not, it is possible that once the transient had passed through,a larger pressure could exist in the downstream transducer line than in the upstream line. This would certainly account for any negative deflections.

Neglecting the solubility of nitrogen in kerosene could also lead to errors. Thus, it is recommended that in future investigations the solubility be incorporated in the theory, or experimental evidence be provided to substantiate neglecting it altogether.

Although no agreement could be obtained on the timing of the profiles shown in Figures 18 through 21, a re-

semblance does exist in the general shape of the predicted and experimental curves. The correspondence at the steady state in Figures 18 and 20 is within experimental error and for the case of the Series core the steady state profiles are identical. It is for this reason that the discrepancy obtained for the theoretical and experimental transient results was attributed to the apparatus used and not the theory applied. Note that no attempts were made to account for the effects of slip or turbulence on the theory used to describe the transient behavior. As would be expected, there is a time correspondence between the predicted pressure profiles obtained for the homogeneous system with those obtained for the heterogeneous core.

Although the large discrepancies in the experimental and numerical results have been attributed mainly to the equipment used, it is important to note that the method of expanding equation (32) before finite differencing could lead to stability problems in the numerical solution. As a result of this procedure, the matrix of coefficients obtained is no longer symmetrical. Consequently inherent restrictions are imposed on the maximum size of Δt and Δx in order to insure stability. No attempts were made to analyze the effects of these limitations on the numerical results obtained.

Influence of the Residual Fluid Saturation

The results of this investigation were compared with the results of a similar investigation conducted by C. Fortems[17], in an attempt to determine the effects of the presence of the residual fluid saturation. A comparison was obtained for the transient pressure history at the same point in the same core with and without the presence of the second immobile phase. Both experimental and numerical results are shown for the Indiana limestone and Series core ADS in Figures 22 and 23 respectively.

It is important to note that Fortems did obtain a reasonable agreement between his numerical and experimental results for the tighter cores, especially in the later stages of the transient period where changes in pressure with time occur less rapidly (refer to Figure 22). As can be seen in Figure 23, however, his work also provided large discrepancies for the high permeability cores, for reasons previously discussed. The fact that one investigation provided some comparable results while the second provided none at all is attributed to the presence of the residual fluid saturation. Since the fluid cannot be completely displaced from the finer regions of the porous network, a reduction in effective permeability to gas is experienced. Consequently it is feasible that the kerosene would imbibe into the tight regions surrounding the machined pressure taps, and would

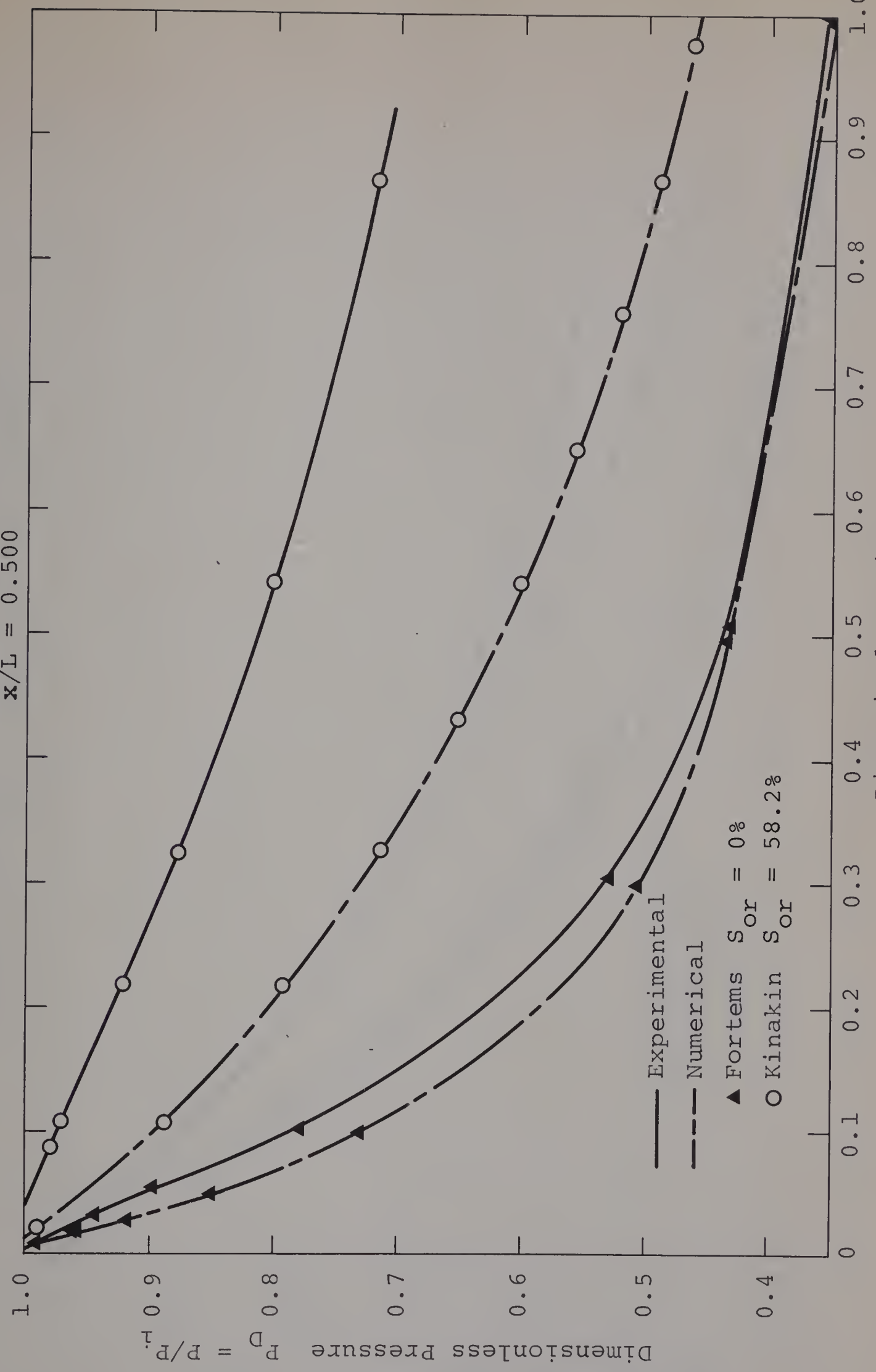

Figure 22 Influence of S_{or} on the Transient Behavior

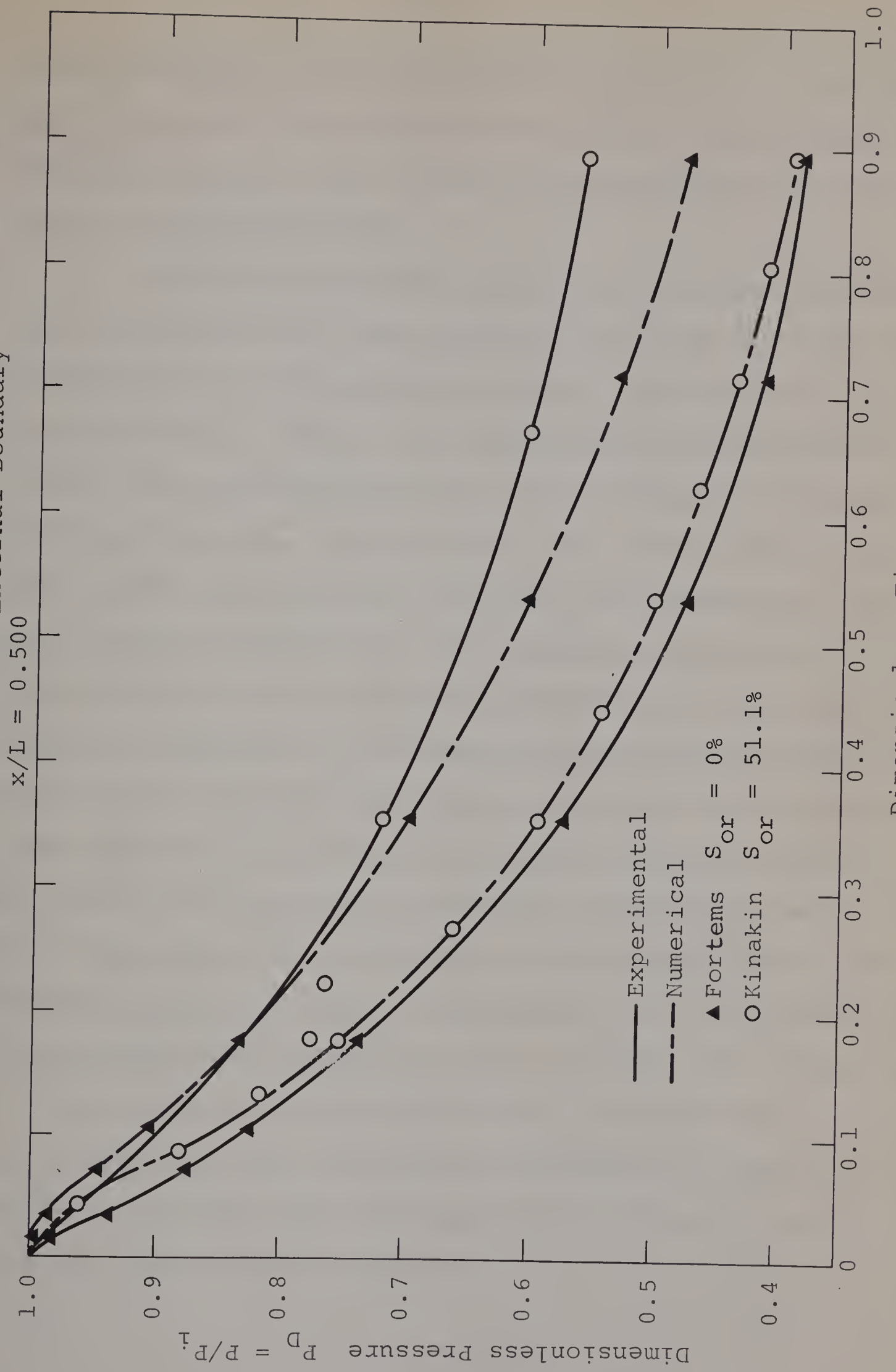

Figure 23 Influence of S_{or} on Transient Behavior

not be dispelled in the subsequent displacement by nitrogen gas. As a result the reduction in permeability in these localized regions would be further accentuated by the presence of the liquid phase.

Even more startling is the fact that no agreement could be obtained for the numerical solutions from both investigations on a dimensionless basis. Again refer to Figures 22 and 23. Since the dimensionless parameters fail to account for any heterogeneities, it is suggested that this may be a reason for the deviation. As can be seen in Figure 19 from the numerical solutions, the pressure at any point is more dependent on the surrounding permeability at this point than on the overall permeability of the core. For example,a comparison of the homogeneous and heterogeneous solutions at a dimensionless distance of 0.1667 and dimensionless time of 0.867 yields a discrepancy of approximately 25 percent in the values of pressure obtained. However, in both cases the overall effective permeability used for the core was nearly the same. Consequently, if the presence of the residual fluid saturation were to reduce the permeability of the core more in one region than in another due to saturation gradients etc., the overall permeability distribution would be altered, and a discrepancy in numerical results at any one point could be expected.

As has already been shown in Appendix I, the study of gas flow in the presence of a residual fluid saturation is a special case of multiphase flow. Consequently, a more accurate analysis of the experimental data obtained would include the concepts of total compressibility and total mobility. Since only the gaseous phase was flowing, the theory developed for single phase gas flow was sufficient to describe the actual system as far as the mobility was concerned. However, a number of approximations were required in order to establish the total compressibility of the system as the inverse of the pressure. Among these were the assumptions that the solubility of nitrogen in kerosene was negligible, and that the variation of the gas compressibility factor with pressure was small. For the range of pressures considered (0-65 psia), the approximations were valid and little error was introduced by the application of single phase gas flow theory. Note, however, that for pressures normally encountered in gas reservoirs, the effects of gas solubility, liquid compressibility, and variations in the gas compressibility factor are significant.

CONCLUSIONS AND RECOMMENDATIONS

Conclusions

1. For the cores tested the presence of the residual liquid saturation increased the discrepancy between the experimental and numerical results obtained.
2. The unsteady state gas flow theory appears to be valid for the flow of gases through porous media in the presence of a residual liquid saturation for the cores analyzed.
3. A better delineation of the properties and some modifications to the theory are required to account for the discontinuities and the sequence in which these occur, before a heterogeneous system can be accurately analyzed on a dimensionless basis.
4. Serious errors can result when applying the dimensionless cumulative production term to a heterogeneous system by using an effective overall permeability. This is especially true when the variations in permeability from point to point within the porous medium are large.
5. Although the stabilization time equation was derived for a homogeneous system, it appears to be applicable to heterogeneous porous media in the presence of a residual liquid saturation, if the effective sectional permeability up to the radius of drainage is used in the

calculations. The practical applications of this equation, however, are limited by the restrictions imposed on it through the boundary conditions. Note that equation (28) can no longer be used for heterogeneous systems, since the radius of drainage must be known in order to obtain an appropriate value for the permeability.

6. The numerical techniques developed for describing the transient flow of gas through a heterogeneous porous system appear to be valid for practical situations. Although some error may be due to the stability problems encountered in the numerical solution, the large discrepancies obtained in the experimental and numerical results may be attributed mainly to the limitations of the equipment used.
7. The internal fracture or core interface introduced by simulating two different permeabilities in series did not noticeably affect the transient response.
8. The mechanical end effects were eliminated by shearing the core faces as opposed to cutting. All discontinuities detected were thus attributed to natural heterogeneities or damage by other means.

Recommendations

1. Only long and tight cores should be used in an experimental transient analysis, since these provide the best results.
2. Automatic measuring devices should be installed at both ends of the core in order to obtain an accurate and permanent record of the pressure variation with time at these locations.

3. Attempts should be made to eliminate the effects of machining the pressure taps.
4. The effects of heterogeneities may be more accurately determined if the pressure taps are located closer together in regions of known discontinuity. Also it is suggested that future series cores be simulated with sections having a greater variation in permeability than the one analyzed here.
5. The lengths of lines leading to pressure sensing devices should be reduced to a minimum. Attempts might also be made to account for the gas entrapped in the void space created by the flange and core interface.
6. Future analyses might also incorporate the effects of the solubility of gas in the immobile liquid phase.
7. The stability problems encountered in this investigation concerning the numerical solution for equation (32) can be overcome if the matrix of coefficients obtained from the finite difference approximations is symmetrical. This can be achieved if the diffusivity equation for gas flow is finite differenced in the form expressed by equation (32). It is recommended that this procedure be followed in future investigations.
8. No attempts were made to account for the porosity variations and liquid saturation gradients within the cores. Consequently future investigations might consider variations in ϕ and S_{or}.

NOMENCLATURE

Where possible, standard letter symbols have been used as outlined by the Society of Petroleum Engineers[41]. Any deviations from this set standard have been duly noted throughout the text of this thesis.

BIBLIOGRAPHY

1. Aronofsky, J.S., Jenkins, R.: "Unsteady State Flow of Gas Through Porous Media, One-Dimensional Case", Proceedings of the First U.S. National Congress of Applied Mechanics, 1952, p. 763.

2. Aronofsky, J.S., Jenkins, R.: "A Simplified Analysis of Unsteady Radial Gas Flow", Trans. AIME, Vol. 201, 1954, p. 149.

3. Aronofsky, J.S.: "Effect of Gas Slip on Unsteady Flow of Gas Through Porous Media", Journal of Applied Physics, Vol. 25, 1954, p. 48.

4. Aronofsky, J.S., Ferris, O.D.: "Transient Flow of Non-Ideal Gases in Porous Solids - One-Dimensional Case", Journal of Applied Physics, Vol. 25, 1954, p. 1289.

5. Aronofsky, J.S., Porter, J.D.: "Unsteady Radial Flow of Gas Through Porous Media - Variable Viscosity and Compressibility", Journal of Applied Mechanics, Vol. 27, 1956, p. 128.

6. Bruce, G.H., Peaceman, D.W., Rachford, H.H. Jr., Rice, J.D.: "Calculations of Unsteady-State Gas Flow Through Porous Media", Trans. AIME, Vol. 198, 1953, p. 79.

7. Carter, R.D.: "Performance Predictions for Gas Reservoirs Considering Two-Dimensional Unsteady-State Flow", Trans. AIME, Vol. 237, 1966, p. 35.

   Discussion, Society of Petroleum Engineers Journal, Vol. 237, 1966, p. 362.

8. Chatas, A.T.: "A Practical Treatment of Nonsteady-State Flow Problems in Reservoir Systems", The Petroleum Engineer, Vol. 25, 1953, May, B42, June, B38, August, B44.

9. Chwyl, E.: "An Analytical Study of Transient Gas Flow Through Porous Media", Master's Thesis in Petroleum Engineering, University of Alberta, February, 1968.

10. Cornell, D., Katz, D.L.: "Flow of Gases Through Consolidated Porous Media", Ind. Eng. Chem., Vol. 45, 1953, p. 2145.

11. Cornell, D., Katz, D.L.: "Pressure Gradients in Natural Gas Reservoirs", Trans. AIME, Vol. 198, 1953, p.61.

12. Cornell, D.: "Applying Van Everdingen and Hurst Solutions to Natural Gas Flow Problems", World Oil, Vol. 142, February 1956, p. 134.

13. Cornell, D.: "Unsteady State Flow in Gas Reservoirs", World Oil, Vol. 144, February 1957, p. 133.

14. Craft, B.C., Hawkins, M.F.: "Applied Petroleum Reservoir Engineering", Prentice-Hall Chemical Engineering Series, 1959, Fig. 3.16, p. 132.

15. Dranchuk, P.M., Kolada, L.J.: "Interpretation of Steady Linear Visco-Inertial Gas Flow Data", Paper presented at the 18th Annual Technical Meeting of the Petroleum Society of CIM, May 24-26, 1967, Banff, Alberta.

16. Eilerts, C.K.: "Integration of Partial Differential Equation for Transient Linear Flow of Gas Condensate Fluids in Porous Structures", Society of Petroleum Engineers Journal, December 1964, p. 292.

17. Fortems, C.C.: "Unsteady State Gas Flow Through Porous Media", Master's Thesis in Petroleum Engineering, University of Alberta, April, 1968.

18. Green, L. Jr., Wilts, C.H.: "Nonsteady Flow of Gas Through a Porous Wall", Proceedings of the First U.S. National Congress of Applied Mechanics, 1952, p. 777.

19. Hetherington, C.R., MacRoberts, D.T., Huntington, R.L.: "Unsteady Flow of Gas Through Porous Media", Trans. AIME, Vol. 146, 1942, p. 166.

20. Hewitt, C.H.: "Analytical Techniques for Recognizing Water-Sensitive Reservoir Rocks", Journal of Petroleum Technology, August 1963, p. 813.

21. Hilsenrath, J., et al: "Tables of Thermal Properties of Gases", U.S. National Bureau of Standards Circular 564, 1955, Table 7.1, p. 317.

22. Hurst, W.: "Unsteady Flow of Fluids in Oil Reservoirs", Physics, Vol. 5, January, 1934, p. 20.

23. Jenkins, R., Aronofsky, J.S.: "Unsteady Radial Flow of Gas Through Porous Media", Trans. ASME, Vol. 20, 1953, p. 210.

24. Jones, P.E.: "Reservoir Limit Test on Gas Wells", Journal of Petroleum Technology, Vol. 14, June, 1962, p. 613.

25. Katz, D.L., et al: "Handbook of Natural Gas Engineering", McGraw-Hill Book Co. Inc., 1959, Chapter 10.

26. Kestin, J., Wang, H.E.: "The Viscosity of Five Gases: A Re-evaluation", Trans. ASME, Vol. 80, 1958, p. 11.

27. Klinkenberg, L.J.: "The Permeability of Porous Media to Liquids and Gases", Drilling and Production Practice, 1941, p. 200.

28. Kolada, L.J.: "Steady Linear Gas Flow Through Porous Media", Master's Thesis in Petroleum Engineering, University of Alberta, December, 1967.

29. Lapidus, L.: "Digital Computation for Chemical Engineers", McGraw-Hill Book Co. Inc., 1962, Chapter 4 and 5.

30. Mackett, R.A.: "Viscous and Visco-Inertial Gas Flow in Limestone Cores", Master's Thesis in Petroleum Engineering, University of Alberta, November,1966.

31. Martin, J.C.: "Simplified Equations of Flow in Gas Drive Reservoirs and the Theoretical Foundation of Multiphase Pressure Build-up Analysis", Trans. AIME, Vol. 216, 1959, p. 309.

32. Matthews, C.S., Russell, D.G.: "Pressure Build-up and Flow Tests in Wells", Monograph Volume 1 - Henry L.Doherty Series, Society of Petroleum Engineers of AIME.

33. Mungan, N.: "Permeability Reduction Through Changes in pH and Salinity", Journal of Petroleum Technology, December, 1965, p. 1449.

34. Muskat, M., Botset, H.G.: "Flow of Gas Through Porous Materials", Physics, Vol. 1, July, 1931, p. 27.

35. Muskat, M.: "The Flow of Compressible Fluids Through Porous Media and Some Problems in Heat Conduction", Physics, Vol. 5, March, 1934, p. 71.

36. Muskat, M., Meres, M.W.: "The Flow of Heterogeneous Fluids Through Porous Media", Physics, Vol. 7, September, 1936, p. 346.

37. Oil and Gas Journal, "Questions on Technology", Vol. 64, No. 28, July 11, 1966, p. 118.

38. Pirson, S.J.: "Oil Reservoir Engineering", McGraw-Hill Book Co. Inc., 1958, p. 79-80.

39. "Proposed Standard Computer Symbols for Petroleum Reservoir Engineering, Natural Gas Engineering and Well Logging Quantities", Journal of Petroleum Technology, May, 1967, p. 630.

40. Roberts, R.C.: "Unsteady Flow of a Gas Through a Porous Medium", Proceedings of the First U.S. National Congress of Applied Mechanics, 1952, p. 773.

41. "Standard Letter Symbols for Petroleum Reservoir Engineering, Natural Gas Engineering and Well Logging", Journal of Petroleum Technology, Vol. 17, 1965, p. 1463.

42. Trube, A.S.: "Compressibility of Undersaturated Hydrocarbon Reservoir Fluids", Trans. AIME, Vol. 210, 1957, p. 341.

43. Van Everdingen, A.F., Hurst, W.: "The Application of the Laplace Transformation to Flow Problems in Reservoirs", Trans. AIME, Vol. 186, 1949, p. 305.

44. Van Poolen, H.K.: "A Hard Look at Radius-of-Drainage and Stabilization-Time Equations", Oil and Gas Journal, Vol. 62, No. 37, September 14, 1964, p. 138.

45. Wallick, G.C., Aronofsky, J.S.: "Effect of Gas Slip on Unsteady Flow of Gas Through Porous Media - Experimental Verification", Trans. AIME, Vol. 201, 1954, p. 322, Technical Note 239.

46. Welge, H.J.: "A Simplified Method for Computing Oil Recovery by Gas or Water Drive", Trans. AIME, Vol. 195, 1952, p. 91.

APPENDIX I

THE CONCEPT OF MULTIPHASE FLOW

The equations governing the simultaneous flow of gas, oil, and water, neglecting the effects of gravity and capillary pressure, are respectively

$$\nabla\cdot\left[\left(\frac{R_s k_o}{\mu_o B_o}+\frac{R_{sw}k_w}{\mu_w B_w}+\frac{k_g}{\mu_g B_g}\right)\nabla P\right] = \phi\frac{\partial}{\partial t}\left(\frac{R_s S_o}{B_o}+\frac{R_{sw}S_w}{B_w}+\frac{S_g}{B_g}\right) \qquad (I\text{-}1)$$

$$\nabla\cdot\left(\frac{k_o}{\mu_o B_o}\nabla P\right) = \phi\frac{\partial}{\partial t}\left(\frac{S_o}{B_o}\right) \qquad (I\text{-}2)$$

$$\nabla\cdot\left(\frac{k_w}{\mu_w B_w}\nabla P\right) = \phi\frac{\partial}{\partial t}\left(\frac{S_w}{B_w}\right) \qquad (I\text{-}3)$$

In those cases where the pressure and saturation gradients are small, the vector products $\nabla P\cdot\nabla P$, $\nabla P\cdot\nabla S_o$, and $\nabla P\cdot\nabla S_w$ are small compared to ∇P, ∇S_o, and ∇S_w. For such instances Martin[31] has shown that equations (I-1) through (I-3) can be combined into the single expression

$$\nabla^2 P = \frac{\phi c_t}{\lambda}\frac{\partial P}{\partial t} \qquad (I\text{-}4)$$

where

$$c_t = -\frac{S_o}{B_o}\frac{\partial B_o}{\partial P}+\frac{S_o B_g}{B_o}\frac{\partial R_s}{\partial P}-\frac{S_w}{B_w}\frac{\partial B_w}{\partial P}$$

$$+\frac{S_w B_g}{B_w}\frac{\partial R_{sw}}{\partial P}-\frac{S_g}{B_g}\frac{\partial B_g}{\partial P} \qquad (I\text{-}5)$$

$$\lambda = \left(\frac{k_o}{\mu_o}+\frac{k_g}{\mu_g}+\frac{k_w}{\mu_w}\right) \qquad (I\text{-}6)$$

In effect c_t represents the total compressibility of the fluid and λ the total mobility.

However, for the problem being considered there is no water phase present and only the gas phase is mobile. Equation (I-6) consequently reduces to

$$\lambda = \frac{k_g}{\mu_g} \qquad \text{(I-7)}$$

and if the solubility of the gas in oil is considered negligible*, equation (I-5) reduces to

$$c_t = -\frac{S_o}{B_o}\frac{\partial B_o}{\partial P} - \frac{S_g}{B_g}\frac{\partial B_g}{\partial P} \qquad \text{(I-8)}$$

Applying the basic definition of compressibility

$$c = -\frac{1}{V}\left(\frac{\partial V}{\partial P}\right)_T \qquad \text{(I-9)}$$

equation (I-8) can be further simplified to

$$c_t = S_o c_o + S_g c_g \qquad \text{(I-10)}$$

---

* To date no experimental data exist relating the solubility of nitrogen gas in kerosene as a function of temperature and pressure. Consequently it is difficult to draw any conclusions as to the extent of the error introduced by making this assumption. An attempt was made to calculate the solubility of air in kerosene to obtain some form of a criterion for nitrogen. The results showed that the volume of gas dissolved in the kerosene could be as high as 18% of the free gas occupying the remaining pore space. However, the method of analysis[37] and the data employed are of a dubious nature, and consequently no concrete conclusions could be drawn.

It can also be shown with the aid of equation (I-9) that for the range of pressures considered in this investigation, c_g is equal to the inverse of the pressure. Consider the following set of typical values:

$$S_o = 0.55 \qquad c_o = 1.42 \times 10^{-5} \text{ psi}^{-1} \ *$$

$$S_g = 0.45 \qquad c_g = \frac{1}{P} = \frac{1}{65 \text{ psia}}$$

$$= 1.54 \times 10^{-2} \text{ psi}^{-1}$$

Therefore, $c_t = 0.55(1.42 \times 10^{-5}) + 0.45(1.54 \times 10^{-2})$

$$= 0.00781 \times 10^{-3} + 6.93 \times 10^{-3} \text{ psi}^{-1}$$

Since the compressibility of the oil is negligible compared to the compressibility of the gas, the total compressibility of the fluid can be approximated by equation (I-11) introducing very little error

$$c_t = \frac{S_g}{P} \qquad \text{(I-11)}$$

At this point it should also be mentioned that the compressibility of the porous system has been neglected in equation

---

* This value for the compressibility of kerosene was obtained by the method of Trube[42], assuming a pseudo-reduced pressure of 1.00 in order to obtain an approximate value for the pseudo-reduced compressibility. Consequently the final result itself is an approximation. It does, however, serve to illustrate the range of values to be expected.

(I-5). A typical value of c_f for a porosity of 20 percent[14] is 3.7×10^{-6} psi^{-1}. A comparison of this value with those previously mentioned indicates that the compressibility of the porous material adds very little to the net compressibility of the system.

Substituting equations (I-7) and (I-11) into equation (I-4) and replacing S_g by $(1 - S_o)$ provides

$$\nabla^2 P = \frac{\phi(1-S_o)\,\mu_g}{k_g P} \frac{\partial P}{\partial t} \qquad \text{(I-12)}$$

Now multiply both sides of equation (I-12) by 2P, assuming an average pressure $\bar{P}$ for the inverse of the compressibility, and replacing $\phi(1-S_o)$ by the effective porosity to the gas phase, equation (I-12) becomes (the subscript g is understood)

$$2P\nabla^2 P = \frac{\phi\mu}{k\bar{P}} 2P \frac{\partial P}{\partial t} \qquad \text{(I-13)}$$

Consider the mathematical relationship

$$\nabla^2 P^2 = 2\nabla P \cdot \nabla P + 2P\nabla^2 P \qquad \text{(I-14a)}$$

If now it is assumed in equation (I-14a) that $\nabla P \cdot \nabla P$ is negligible, as was done in the derivation of equation (I-4), the result is

$$\nabla^2 P^2 \simeq 2P\nabla^2 P \qquad \text{(I-14b)}$$

Substituting this relationship into equation (I-13) and simplifying provides

$$\nabla^2 P^2 = \frac{\phi\mu}{k\bar{P}} \frac{\partial P^2}{\partial t} \qquad \text{(I-15)}$$

A comparison of this equation with equation (22) of the Theory for single phase gas flow shows that the two are identical.

A P P E N D I X I I

DERIVATION OF THE FINITE DIFFERENCE APPROXIMATION

Defining

$$W(P) = \frac{1}{\mu(P)} \tag{II-1}$$

and applying the mathematical equivalent,

$$\frac{\partial W(P)}{\partial x} \equiv \frac{\partial P^2}{\partial x} \frac{dW(P)}{dP^2} \tag{II-2}$$

expansion of equation (32) of the Theory provides

$$\underline{W(P)}\ \underline{k(x)}\ \frac{\partial^2 P^2}{\partial x^2} + \underline{k(x)}\ \frac{\partial P^2}{\underline{\partial x}}\ \frac{\partial P^2}{\partial x}\ \frac{dW(P)}{\underline{dP^2}}$$

$$+\ \underline{W(P)}\ \frac{\partial P^2}{\underline{\partial x}}\ \frac{\partial}{\partial x}\ k(x) = \frac{\phi}{\overline{P}}\ \frac{\partial P^2}{\partial t} \tag{II-3}$$

The underscored terms are treated as averages in the implicit computations.

Substituting the following finite difference approximations into equation (II-3)

$$\frac{\partial P^2}{\partial t} = \frac{P^2_{r,s+1} - P^2_{r,s}}{\Delta t} \tag{II-4a}$$

$$\frac{\partial^2 P^2}{\partial x^2} = \frac{1}{2(\Delta x)^2}\left[(P^2_{r+1,s+1} - 2P^2_{r,s+1} + P^2_{r-1,s+1})\right.$$

$$\left. + (P^2_{r+1,s} - 2P^2_{r,s} + P^2_{r-1,s})\right] \tag{II-4b}$$

$$\frac{\partial P^2}{\partial x} = \frac{1}{4\Delta x}(P^2_{r+1,s+1} - P^2_{r-1,s+1} + P^2_{r+1,s} - P^2_{r-1,s}) \tag{II-4c}$$

$$\frac{\partial}{\partial x} k(x) = \frac{k_{r+\frac{1}{2}} - k_{r-\frac{1}{2}}}{\Delta x} \qquad \text{(II-4d)}$$

$$\frac{\partial P^2}{\partial x} = \frac{1}{4\Delta x} (P^{2*}_{r+1,s+1} - P^{2*}_{r-1,s+1} + P^2_{r+1,s} - P^2_{r-1,s}) \qquad \text{(II-4e)}$$

and utilizing the following definitions

$$\Delta^2_{r,s+1} = P^2_{r+1,s+1} - 2P^2_{r,s+1} + P^2_{r-1,s+1} \qquad \text{(II-5a)}$$

$$\Delta_{r,s+1} = P^2_{r+1,s+1} - P^2_{r-1,s+1} \qquad \text{(II-5b)}$$

$$\Delta^*_{r,s+1} = P^{2*}_{r+1,s+1} - P^{2*}_{r-1,s+1} \qquad \text{(II-5c)}$$

$$\Delta_{r,s} = P^2_{r+1,s} - P^2_{r-1,s} \qquad \text{(II-5d)}$$

$$\Delta = \Delta^*_{r,s+1} + \Delta_{r,s} \qquad \text{(II-5e)}$$

$$\Delta k_r = k_{r+\frac{1}{2}} - k_{r-\frac{1}{2}} \qquad \text{(II-5f)}$$

provides

$$\frac{W(P)k(x)}{2(\Delta x)^2} (\Delta^2_{r,s+1} + \Delta^2_{r,s}) + \frac{k(x)}{16(\Delta x)^2} (\Delta)(\Delta_{r,s+1} + \Delta_{r,s}) \frac{dW(P)}{dP^2} + \frac{W(P)}{4(\Delta x)^2} (\Delta)(\Delta k_r)$$

$$= \frac{\phi}{\overline{P}(\Delta t)} (P^2_{r,s+1} - P^2_{r,s}) \qquad \text{(II-6)}$$

It should be noted that equations (II-4b), (II-4c) and (II-4e) represent the implicit Crank-Nicholson[29] finite difference approximations centered at time s+½. The running variable for position is represented by r and the asterisk denotes the values of P^2 at time s+1 as determined from the previous iteration. In equation (II-6)

$$W(P) = \tfrac{1}{2}\left[W(P^*_{r,s+1}) + W(P_{r,s})\right] \qquad \text{(II-7a)}$$

$$k(x) = \tfrac{1}{2}\left(k_{r+\frac{1}{2}} + k_{r-\frac{1}{2}}\right) \qquad \text{(II-7b)}$$

$$\frac{dW(P)}{dP^2} = \tfrac{1}{2}\left[\frac{dW(P^*_{r,s+1})}{dP^2} + \frac{dW(P_{r,s})}{dP^2}\right] \qquad \text{(II-7c)}$$

$$\overline{P} = \frac{1}{6}\left(P^*_{r+1,s+1} + P^*_{r,s+1} + P^*_{r-1,s+1}\right.$$

$$\left. + P_{r+1,s} + P_{r,s} + P_{r-1,s}\right) \qquad \text{(II-7d)}$$

Define

$$D(P) = \frac{dW(P)}{dP^2} \qquad \text{(II-8a)}$$

$$\beta = \frac{\overline{P}\ W(P)\ k(x)\ \Delta t}{\phi(\Delta x)^2} \qquad \text{(II-8b)}$$

If equation (II-6) is now multiplied by $2(\Delta x)^2/k(x)W(P)(\Delta)$ and equations (II-8a) and (II-8b) utilized, the result is

$$\frac{\Delta^2_{r,s+1}}{(\Delta)} + \frac{D(P)}{8W(P)}\,\Delta_{r,s+1} - \frac{2}{(\Delta)\beta}\,P^2_{r,s+1}$$

$$= \frac{-\Delta^2_{r,s}}{(\Delta)} - \frac{D(P)}{8W(P)}\,\Delta_{r,s} - \frac{2}{(\Delta)\beta}\,P^2_{r,s} - \frac{(\Delta k_r)}{2k(x)} \qquad \text{(II-9)}$$

Expanding the subscripted Δ's and collecting like terms provides the final result

$$\left[1 + \frac{(\Delta)D(P)}{8W(P)}\right]P^2_{r+1,s+1} - 2\left(1 + \frac{1}{\beta}\right)P^2_{r,s+1}$$

$$+ \left[1 - \frac{(\Delta)D(P)}{8W(P)}\right]P^2_{r-1,s+1} = -\left[1 + \frac{(\Delta)D(P)}{8W(P)}\right]P^2_{r+1,s}$$

$$+ 2\left(1 - \frac{1}{\beta}\right)P^2_{r,s} - \left[1 - \frac{(\Delta)D(P)}{8W(P)}\right]P^2_{r-1,s} - \frac{(\Delta)(\Delta k_r)}{2k(x)} \qquad \text{(II-10)}$$

If the viscosity and permeability are constant, equation (II-10) reduces to the familiar finite difference approximation for a linear parabolic partial differential equation.

$$P^2_{r+1,s+1} - 2\left(1 + \frac{1}{\beta}\right)P^2_{r,s+1} + P^2_{r-1,s+1}$$

$$= -P^2_{r+1,s} + 2\left(1 - \frac{1}{\beta}\right)P^2_{r,s} - P^2_{r-1,s} \qquad \text{(II-11)}$$

The method of solution now lends itself to evaluating equation (II-10) for every point within the grid spacing, and solving the resulting set of linear equations simultaneously. The values for P^2 at time s+1 represent the unknowns. All the values for P^2 at time s are known and all

the coefficients in equation (II-10) can be evaluated. The values of D(P) were computed directly, as an analytical expression for viscosity as a function of pressure was available from the literature[26].

Special forms of equation (II-10) are required at both ends of the grid system, depending upon the boundary conditions applied. For cases where the pressure at the boundary is explicitly defined, either $P^2_{r-1,s+1}$ (downstream boundary) or $P^2_{r+1,s+1}$ (upstream boundary) represent known values. At a sealed external boundary

$$\frac{\partial P^2}{\partial x} = 0 \qquad \text{(II-12)}$$

To simulate equation (II-12) numerically, a fictitious boundary is assumed a distance Δx past the actual boundary. If r represents the position of the actual sealed boundary, then the conditions which prevail at r+1 are identical to those at r-1. More specifically,

$$P^2_{r+1,s+1} = P^2_{r-1,s+1} \qquad \text{(II-13a)}$$

and

$$P^2_{r+1,s} = P^2_{r-1,s} \qquad \text{(II-13b)}$$

The final solution to the resulting tri-diagonal matrix was achieved by the method of Thomas[29].

A P P E N D I X I I I

COMPUTER PROGRAM

The final solution to the problem outlined in Appendix II was achieved by means of a computer program, written in Fortran IV computer programming language, and executed on the IBM OS/360/67 model computer. The program is designed to solve equation (32) of the Theory for essentially four separate boundary conditions:

1) constant terminal pressures at both boundaries;
2) the constant terminal pressure case with a sealed external boundary;
3) a varying sandface pressure with a constant terminal pressure at the external boundary; and
4) a varying sandface pressure with a sealed external boundary.

The initial condition in all cases was

$$P(x,0) = P_i \qquad \text{(III-1)}$$

Although written primarily to accommodate variations in viscosity and permeability, the program is flexible enough to solve equation (32) for a homogeneous system and a constant viscosity, requiring only minor adjustments.

The data required is as follows:

1) initial pressure (psia)
2) residual fluid saturation (fraction)
3) porosity (fraction

4) flowing sandface pressure (psia)*

5) atmospheric pressure (psia)

6) temperature (^{o}F)

7) total length (inches)

8) incremental length (inches)

9) total time (minutes)

10) incremental time (minutes)

11) permeability distribution as a function of dimensionless distance, x/L (md)**

12) the variation of the sandface pressure (psig) as a function of time (minutes)**

13) the criterion for convergence (psi)

The choice of boundary conditions was effected by means of a positive (pressure varies) - negative (pressure is constant) coding system.

The final computer output consists of a pressure and dimensionless pressure (P/P_i) distribution for each incremental time step Δt. Also included are several statements describing the nature of the problem and the boundary conditions being applied.

---

* In all cases the constant flowing sandface pressure, where required, and atmospheric pressure were the same.

** These data are optional,and depend upon the problem being solved and the boundary conditions applied. In cases where either μ or k are considered constant, it is necessary to read in the respective values separately.

Wherever possible standard[39] mnemonic computer symbols have been used. Most deviations from this standard are self-explanatory within the program itself. Exceptions to the above, however, are listed below for further clarification.

PRSXP2 ≡ P^2

PRSREQ ≡ P_f at time t

PRSCS ≡ P_f constant

DELK2 ≡ $k_{r+\frac{1}{2}}$

DELK1 ≡ $k_{r-\frac{1}{2}}$

PRMGVT ≡ k(x/L)

B(M,N) = coefficients of the tri-diagonal matrix

D(M) = corresponding vector for B(M,N)

SUBRTC, BCC — storage locations for the positive-negative codes

PECHEK, VCHECK, TCHECK, FCHECK — codes which determine the execution of certain operations depending on their respective values

It should be noted that the computer program as presented here represents a working solution to the problems discussed. Absolutely no attempt has been made to optimize the calculations by available programming techniques.

```
      COMMON/MANE/PRSXP2(3,105),B(105,3),D(100),K
      COMMON/CALCB/SUBRTC(3),PRMG,BETA,BETAI,K
      COMMON/VISCSY/PRSVIS,TEM,VCHECK,VISC
      COMMON/FUNSUN/DELP,WOFPRS,DELPKG,FCHECK
      COMMON/PERM/PECHEK,DELLTH,DELPRM,N
      COMMON/PCLATE/PRSREQ,TIM,TCHECK
      COMMON PRS(3,105)
      INTEGER R
      DIMENSION BCC(3),PRSQ(100)
      REAL PRSI,SATLR,PCRT,PRSCS,DELTIM,DELLTH,TIMT,PORE,TEM
     1,LTH,DELPRS
      READ(5,10)(SUBRTC(I),I=1,3)
   10 FORMAT(1X,3(1X,F4.1))
      WRITE(6,10)(SUBRTC(I),I=1,3)
      READ(5,11) PRSI,SATLR,PCRT,PRSCS,TEM,LTH
   11 FORMAT(1X,F7.1,2(1X,F7.4),1X,F7.1,1X,F5.1,F7.3)
      WRITE(6,11) PRSI,SATLR,PCRT,PRSCS,TEM,LTH
      READ(5,12) DELTIM,DELLTH,TIMT
   12 FORMAT(1X,3(1X,F6.3))
      WRITE(6,12) DELTIM,DELLTH,TIMT
      READ(5,13) (BCC(I),I=1,2)
   13 FORMAT(1X,2(1X,F4.1))
      WRITE(6,13) (BCC(I),I=1,2)
      READ(5,26) DELPRS
   26 FORMAT(1X,F7.4)
      WRITE(6,26) DELPRS
      M=TIMT/DELTIM
      N=LTH/DELLTH
      TIM=0.0
      PORE=PCRT*(1.0-SATLR)
      NP2=N+2
      DO 30 R=1,NP2
      PRS(1,R)=PRSI
      PRS(2,R)=1.0
      PRS(3,R)=PRSI
      PRSXP2(1,R)=PRSI**2.0
      PRSXP2(2,R)=1.0
   30 PRSXP2(3,R)=PRSI**2.0
      BETAI=DELTIM/(PORE*DELLTH**2.0)*0.00063283
      IF(BCC(2).GT.0.0)  GO TO 111
      WRITE(6,23) PRSI
   23 FORMAT(1X,'THE PRESSURE AT THE EXTERNAL BOUNDARY IS CO',
     1'NSTANT AT  ',F7.1,'PSIA')
      GO TO 112
  111 WRITE(6,24)
   24 FORMAT(1X,'THE POROUS MEDIA IS FINITE WITH A SEALED EX',
     1'TERNAL BOUNDARY')
  112 IF(SUBRTC(1).LT.0.0) GO TO 100
      WRITE(6,14)
   14 FORMAT(1X,'THE DOWNSTREAM PRESSURE VARIES WITH TIME')
      GO TO 102
  100 WRITE(6,15) PRSCS
   15 FORMAT(1X,'THE DOWNSTREAM PRESSURE IS CONSTANT AT  ',F
     17.1,'PSIA')
```

```
102 IF(SUBRTC(2).GT.0.0) GO TO 103
    READ(5,16) PRMG
 16 FORMAT(1X,F8.2)
    WRITE(6,17) PRMG
 17 FORMAT(1X,'THE PERMEABILITY OF THE POROUS MEDIA IS CON',
   1'STANT AT  ',F8.2,'MD')
    GO TO 104
103 WRITE(6,18)
 18 FORMAT(1X,'THE PERMEABILITY OF THE POROUS MEDIA VARIES',
   1' WITH POSITION')
104 IF(SUBRTC(3).GT.0.0) GO TO 105
    READ(5,19) VISG
 19 FORMAT(1X,F8.5)
    WRITE(6,20) VISG
 20 FORMAT(1X,'THE GAS VISCOSITY IS CONSTANT AT  ',F8.5,'CP',
   1'PS')
    GO TO 106
105 WRITE(6,21)
 21 FORMAT(1X,'THE GAS VISCOSITY IS TEMPERATURE AND PRESSU',
   1'RE DEPENDENT')
    PECHEK=0.0
    VCHECK=0.0
    TCHECK=0.0
106 DO 200 KS=1,M
    TIM=TIM+DELTIM
400 IF(BCC(1).LT.0.0) GO TO 107
    CALL TERPCL
    PRSXP2(2,1)=(PRSREG+PRSCS)**2.0
    GO TO 108
107 PRSXP2(2,1)=PRSCS**2.0
108 R=2
    PRSXP2(1,1)=PRSXP2(2,1)
    CALL SUBETA
    CONSTP=1.+DELP
    CONSTM=1.-DELP
    B(1,2)=-2.0*(1.+1./BETA)
    B(1,3)=CONSTP
    D(1)=-PRSXP2(1,3)*CONSTP+2.*(1.-1./BETA)*PRSXP2(1,2)-P
   1RSXP2(1,1)*CONSTM-PRSXP2(2,1)*CONSTM-DELPRM
    IF(BCC(2).LT.0.0) GO TO 109
    R=N+1
    PRS(1,R+1)=PRS(1,R-1)
    PRS(3,R+1)=PRS(3,R-1)
    PRSXP2(1,R+1)=PRSXP2(1,R-1)
    PRSXP2(3,R+1)=PRSXP2(3,R-1)
    CALL SUBETA
    B(N,1)=2.
    B(N,2)=-2.*(1.+1./BETA)
    D(N)=-2.*PRSXP2(1,R-1)+2.*(1.-1./BETA)*PRSXP2(1,R)
    K=N
    GO TO 110
109 R=N
    PRSXP2(2,N+1)=PRS1**2.0
    CALL SUBETA
```

```
      R=N-1
      CONSTP=1.+DELP
      CONSTM=1.-DELP
      B(R,1)=CONSTM
      B(R,2)=-2.*(1.+1./BETA)
      D(R)=-PRSXP2(1,R+2)*CONSTP+2.*(1.-1./BETA)*PRSXP2(1,R+
     11)-PRSXP2(1,R)*CONSTM-PRSXP2(2,R+2)*CONSTP-DELPRM
      K=N-1
  110 DO 199 R=3,K
      CALL SUBETA
      CONSTP=1.+DELP
      CONSTM=1.-DELP
      B(R-1,1)=CONSTM
      B(R-1,2)=-2.*(1.+1./BETA)
      B(R-1,3)=CONSTP
  199 D(R-1)=-PRSXP2(1,R+1)*CONSTP+2.*(1.-1./BETA)*PRSXP2(1,
     1R)-PRSXP2(1,R-1)*CONSTM-DELPRM
      CALL THOMAS
      NP1=N+1
      DO 198 I=1,NP1
  198 PRS(2,I)=SQRT(PRSXP2(2,I))
      DO 195 I=1,NP1
      IF(ABS(PRS(2,I)-PRS(3,1)).LE.DELPRS) GO TO 197
  401 DO 194 J=1,NP1
      PRSXP2(3,J)=PRSXP2(2,J)
  194 PRS(3,J)=PRS(2,J)
      IF(I.EQ.NP1) GO TO 113
      GO TO 400
  197 IF(I.EQ.NP1) GO TO 401
  195 CONTINUE
  113 DO 193 J=1,NP1
      PRS(1,J)=PRS(2,J)
  193 PRSXP2(1,J)=PRSXP2(2,J)
      WRITE(6,25) TIM
   25 FORMAT(1H0,'THE CUMULATIVE TIME IS ',F6.3,'MINUTES')
      WRITE(6,27) (PRS(1,I),I=1,NP1)
   27 FORMAT(1X,14F9.2)
      DO 192 I=1,NP1
  192 PRSQ(I)=PRS(1,I)/PRSI
      WRITE(6,22)(PRSQ(I),I=1,NP1)
   22 FORMAT(1X,14F8.5)
  200 CONTINUE
      STOP
      END
```

```
      SUBROUTINE SUBETA
      INTEGER R
      COMMON/CALCB/SUBRTC(3),PRMG,BLTA,BETAI,R
      COMMON/FUNSUN/DELP,WOFPRS,DELPKG,FCHECK
      COMMON PRS(3,105)
      PRSAV=1./6.*(PRS(1,R-1)+PRS(1,R)+PRS(1,R+1)+PRS(3,R-1)
     1+PRS(3,R)+PRS(3,R+1))
      IF(SUBRTC(2).LT.0.0) GO TO 10
      CALL FUNPRS
   10 IF(SUBRTC(3).LT.0.0) GO TO 20
      CALL PRMBLY
   20 BETA=BETAI*PRMG*PRSAV*WOFPRS
      RETURN
      END
```

```
      SUBROUTINE THOMAS
      COMMON/MANE/PRSXP2(3,105),B(105,3),D(100),K
      DIMENSION W(100),Q(100),G(100)
      W(1)=B(1,2)
      DO 10 I=2,K
   10 W(I)=B(I,2)-B(I,1)*B(I-1,3)/W(I-1)
      KM1=K-1
      DO 40 I=1,KM1
   40 Q(I)=B(I,3)/W(I)
      G(1)=D(1)/W(1)
      DO 20 I=2,K
   20 G(I)=(D(I)-B(I,1)*G(I-1))/W(I)
      PRSXP2(2,K+1)=G(K)
      KM=0
      KD=K-1
      DO 30 I=1,KD
      KM=KM+1
      KN=KM-1
   30 PRSXP2(2,K+1-KM)=G(K-KM)-Q(K-KM)*PRSXP2(2,K+1-KN)
      NP1=13
      RETURN
      END
```

```
      SUBROUTINE PRMBLY
      COMMON/PERM/PECHEK,DELLTH,DELPRM,N
      COMMON/CALCB/SUBSTC(3),PRMG,BETA,BETAI,R
      COMMON/FUNSUN/DELP,WOFPRS,DELPKG,FCHECK
      REAL LTHQ(100),PRMGVT(100)
      INTEGER NI,N,R
      IF(PECHEK.GT.0.1) GO TO 12
      READ(5,25) NI
   25 FORMAT(1X,I3)
      WRITE(6,25) NI
      READ(5,26) (LTHQ(I),I=1,NI)
   26 FORMAT(1X,18F7.4)
      WRITE(6,26) (LTHQ(I),I=1,NI)
      READ(5,27) (PRMGVT(I),I=1,NI)
   27 FORMAT(1X,18F6.2)
      WRITE(6,27)(PRMGVT(I),I=1,NI)
      PECHEK=1.0
   12 PCHECK=FLOAT(R-1)/FLOAT(N)
      PCHECK=PCHECK-0.5/FLOAT(N)
      DO 18 I=1,NI
      IF(PCHECK.LE.LTHQ(I)) GO TO 13
   18 CONTINUE
   13 DELK1=PRMGVT(I)
      ICP=I
      PCHECK=PCHECK+1.0/FLOAT(N)
      DO 14 I=1,NI
      IF(PCHECK.LE.LTHQ(I)) GO TO 15
   14 CONTINUE
   15 DELK2=PRMGVT(I)
      JCP=I
      PRMG=(DELK1+DELK2)/2.
      IF(FCHECK.LT.0.5) GO TO 16
      IF(ICP.EQ.JCP) GO TO 16
      DELPRM=(DELK2-DELK1)/(2.*PRMG)*DELPKG
      GO TO 17
   16 DELPRM=0.
   17 RETURN
      END
```

```
      SUBROUTINE FUNPRS
      COMMON/MANE/PRSXP2(3,105),B(105,3),D(100),K
      COMMON/VISCSY/PRSVIS,TEM,VCHECK,VISG
      COMMON/FUNSUN/DELP,WOFPRS,DELPKG,FCHECK
      COMMON/CALCB/SUBRTC(3),PRMG,BETA,BETA1,R
      COMMON PRS(3,105)
      INTEGER R
      DIMENSION W(3)
   13 DO 10 I=1,3,2
      PRSVIS=PRS(I,R)
      CALL VISCOS
   10 W(I)=1./VISG
      WOFPRS=0.5*(W(1)+W(3))
      FCHECK=0.0
      DELP=0.
      IF((PRSXP2(1,R-1)+.01).GE.PRSXP2(1,R+1).AND.(PRSXP2(1,
     1R+1)+.01).GE.PRSXP2(1,R-1)) GO TO 12
      DELP=DELP+PRSXP2(1,R+1)-PRSXP2(1,R-1)
      FCHECK=1.0
   12 IF((PRSXP2(3,R-1)+.01).GE.PRSXP2(3,R+1).AND.(PRSXP2(3,
     1R+1)+.01).GE.PRSXP2(3,R-1)) GO TO 20
      DELP=DELP+PRSXP2(3,R+1)-PRSXP2(3,R-1)
      FCHECK=1.0
      DOFPRS=0.
      DO 11 I=1,3,2
      PRSATM=PRS(I,R)/14.696
   11 DOFPRS=DOFPRS-0.5*W(I)**2./PRSATM*889.E-05*(8.958E-04+
     1 1.224E-06*(PRSATM-1.)+1.1991E-07*(PRSATM-1.)**2.)/(14.
     2696)**2.
      DELPKG=DELP
      DELP=DELP*DOFPRS/(8.*WOFPRS)
      GO TO 21
   20 DELP=0.
   21 RETURN
      END
```

```
      SUBROUTINE VISCOS
      COMMON/VISCSY/PRSVIS,TEM,VCHECK,VISG
      IF(VCHECK.GT.0.1) GO TO 10
      TEM=5./9.*(TEM-32.)
      DELTEM=TEM-25.
      TEMCF=DELTEM*4.55E-05
      VCHECK=1.0
   10 PRSATM=PRSVIS/14.696
      VISGI=(100.0+(PRSATM-1.0)*(0.08958+(PRSATM-1.0)*(0.000
     10612+0.3997E-05*(PRSATM-1.0))))*1.778E-04
      VISG=VISGI+TEMCF
      RETURN
      END
```

```
      SUBROUTINE TERPOL
      COMMON/POLATE/ANSWER,XR,ICHECK
      DIMENSION XV(30),YV(30),X(5),Y(5),COEFF(5)
      INTEGER NX,NY,NC
      IF(ICHECK.GT.0.1) GO TO 80
      READ(5,10) NX,NY,NC
   10 FORMAT(2X,3I4)
      WRITE(6,10) NX,NY,NC
      READ(5,11) (XV(I),I=1,NX)
   11 FORMAT(1X,11F7.4)
      WRITE(6,11) (XV(I),I=1,NX)
      READ(5,12) (YV(I),I=1,NY)
   12 FORMAT(1X,11F7.2)
      WRITE(6,12) (YV(I),I=1,NY)
      ICHECK=1.0
   80 DO 30 I=2,NX
      IF(XR.GT.XV(I)) GO TO 30
      IF(I.GE.NC) GO TO 70
      IM2=I-2
      DO 29 J=1,3
      X(J)=XV(IM2+J)
   29 Y(J)=YV(IM2+J)
      GO TO 40
   30 CONTINUE
   40 DO 50 I=1,3
      PROD=1.0
      DO 49 K=1,3
      IF(I.EQ.K) GO TO 49
      PROD=PROD*(XR-X(K))/(X(I)-X(K))
   49 CONTINUE
   50 COEFF(I)=PROD
      ANSWER=0.0
      DO 60 I=1,3
      IF(Y(I).LT.1.0E-06) GO TO 60
      ANSWER=ANSWER+COEFF(I)*Y(I)
   60 CONTINUE
      GO TO 90
   70 ANSWER=YV(NC)
   90 RETURN
      END
```

APPENDIX IV

GRAPHICAL RESULTS

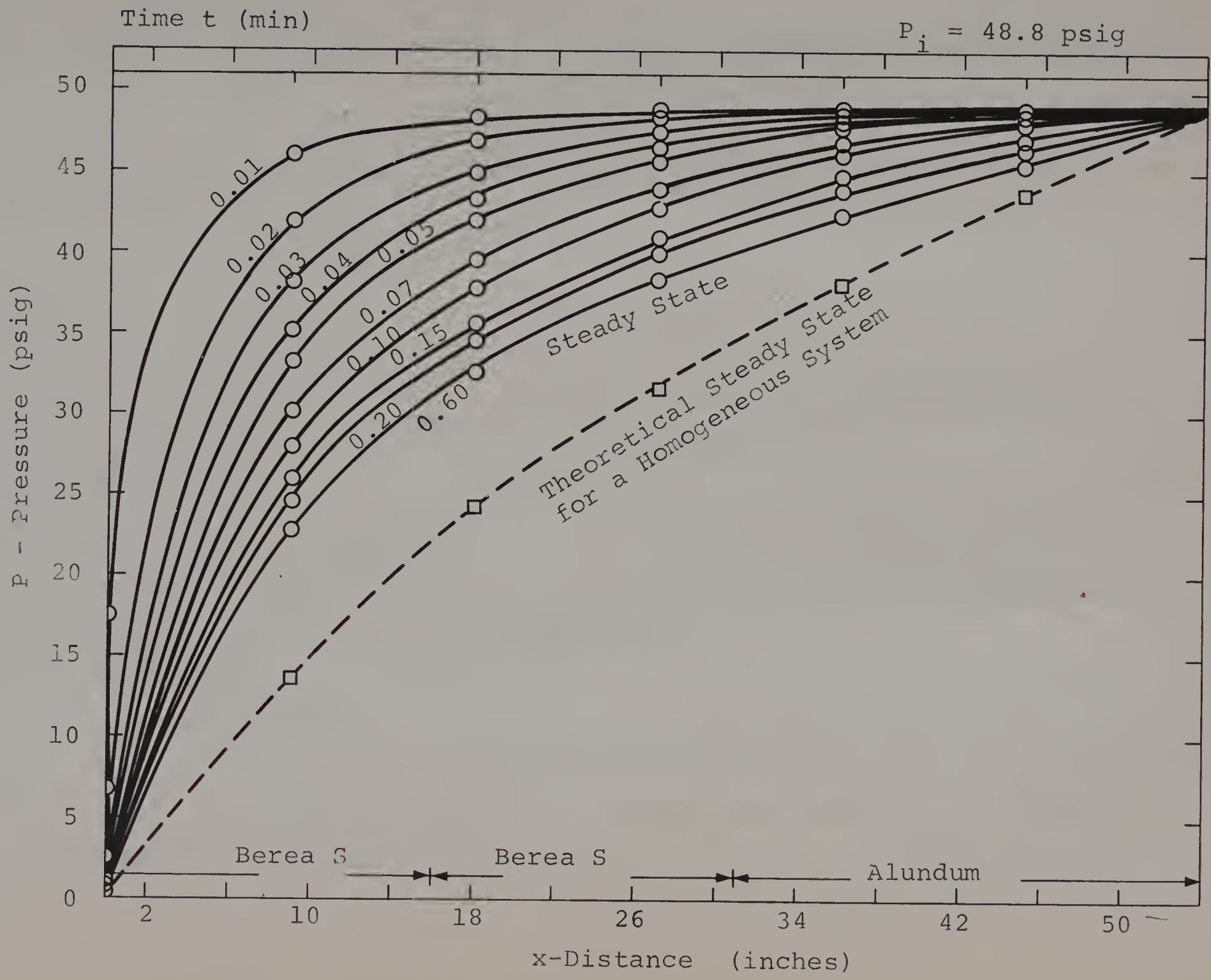

Figure 24 Transient Behavior - Series Core AUS

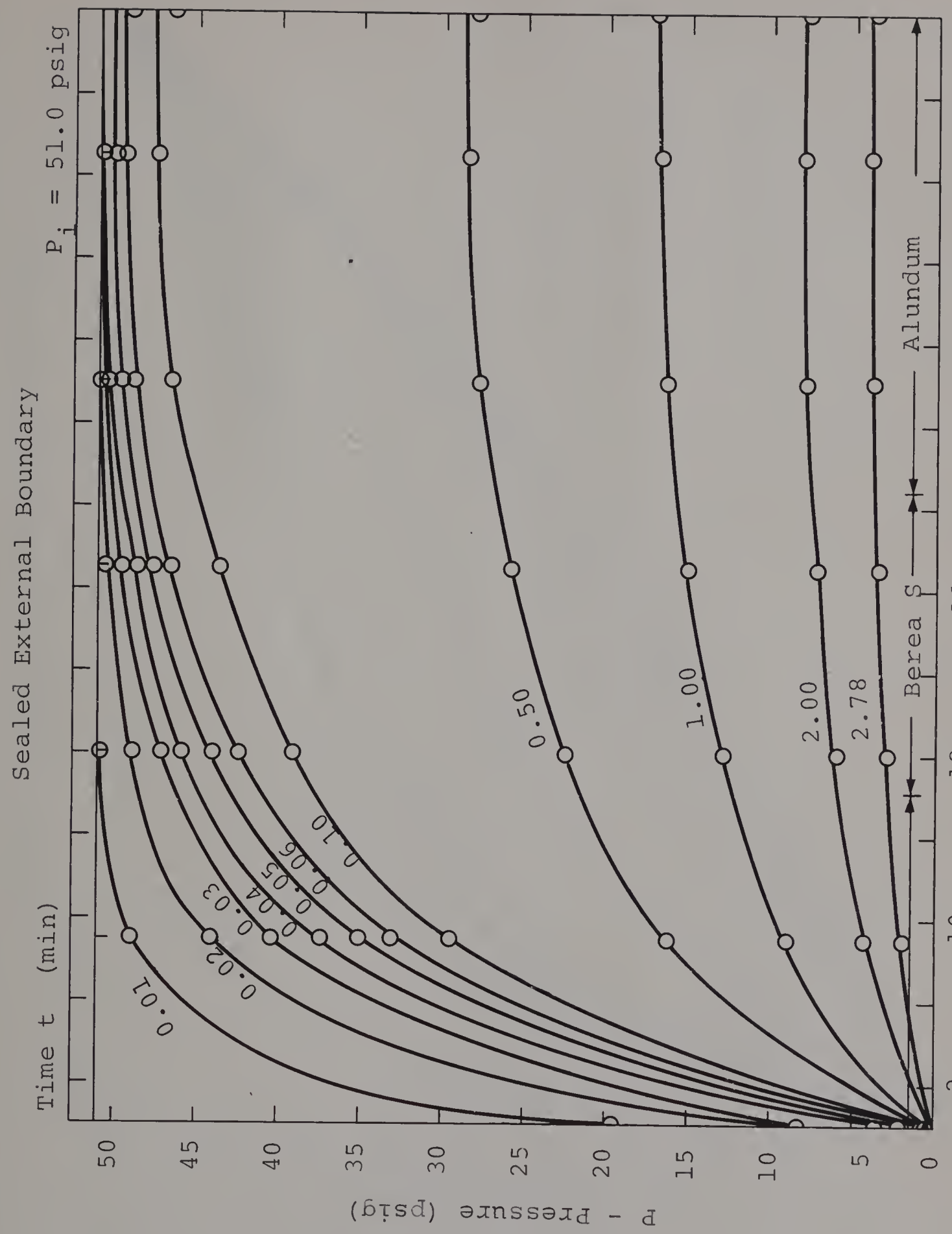

Figure 25 Transient Behavior - Series Core AUS

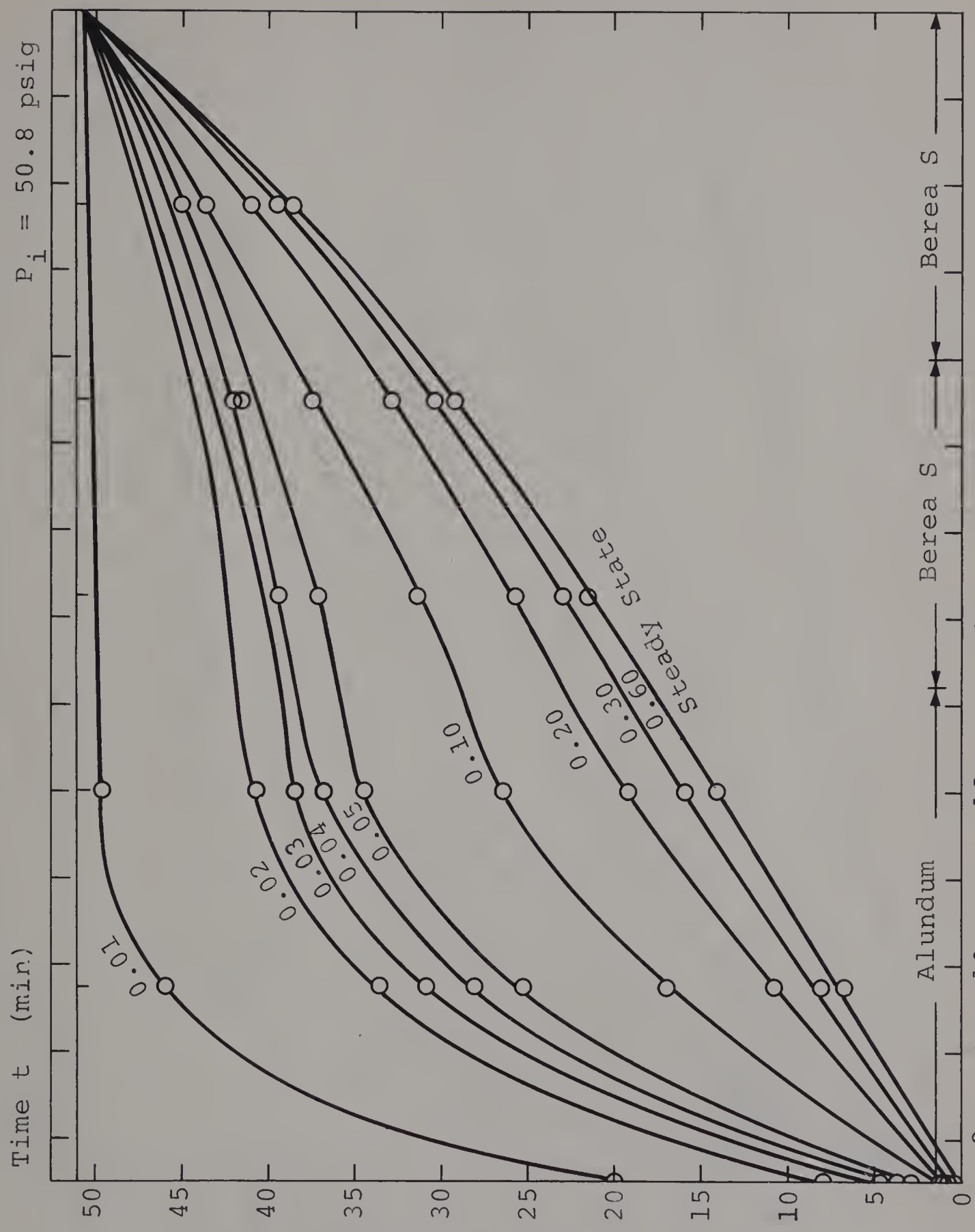

Figure 26 Transient Behavior - Series Core ADS

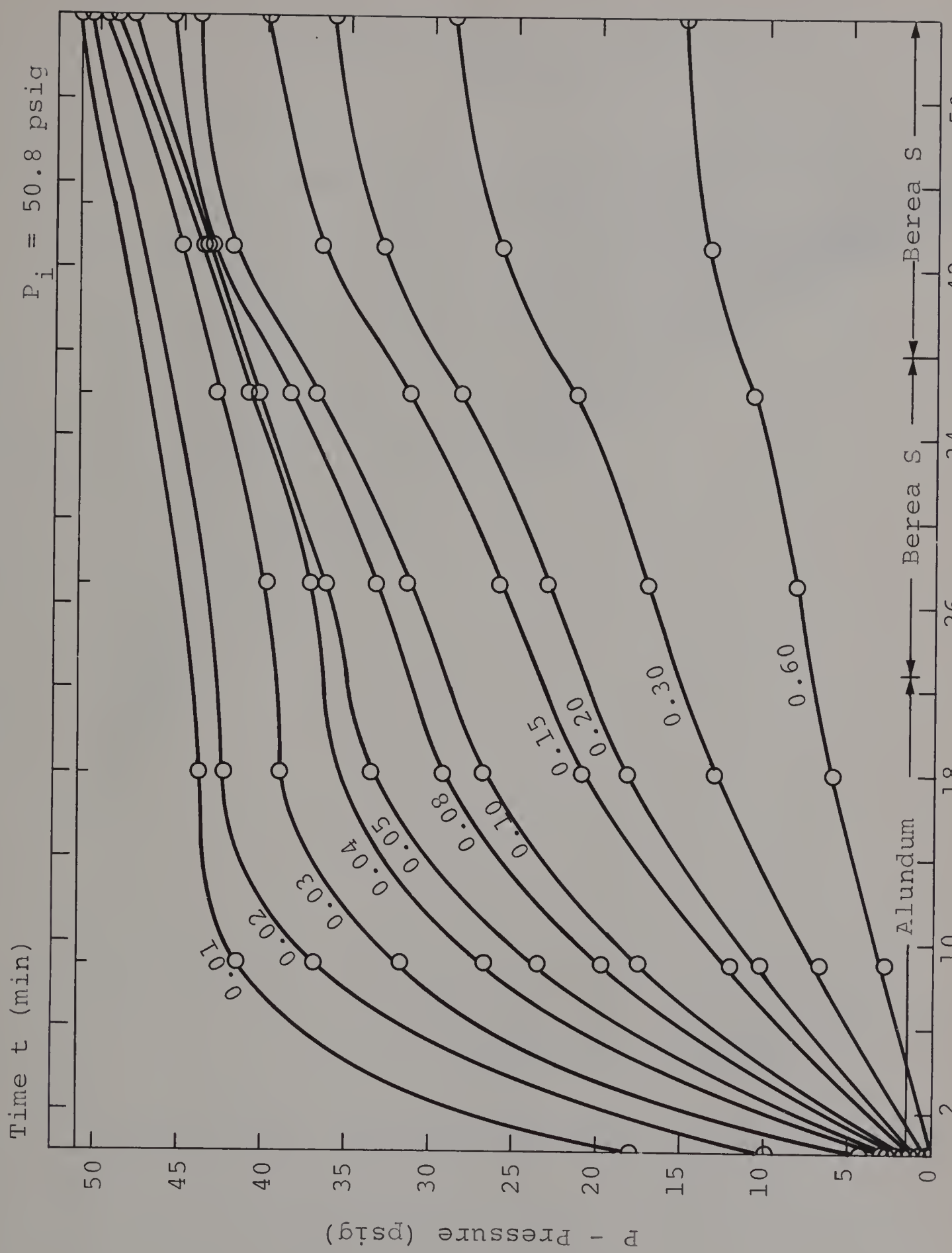

Figure 27 Transient Behavior - Series Core ADS

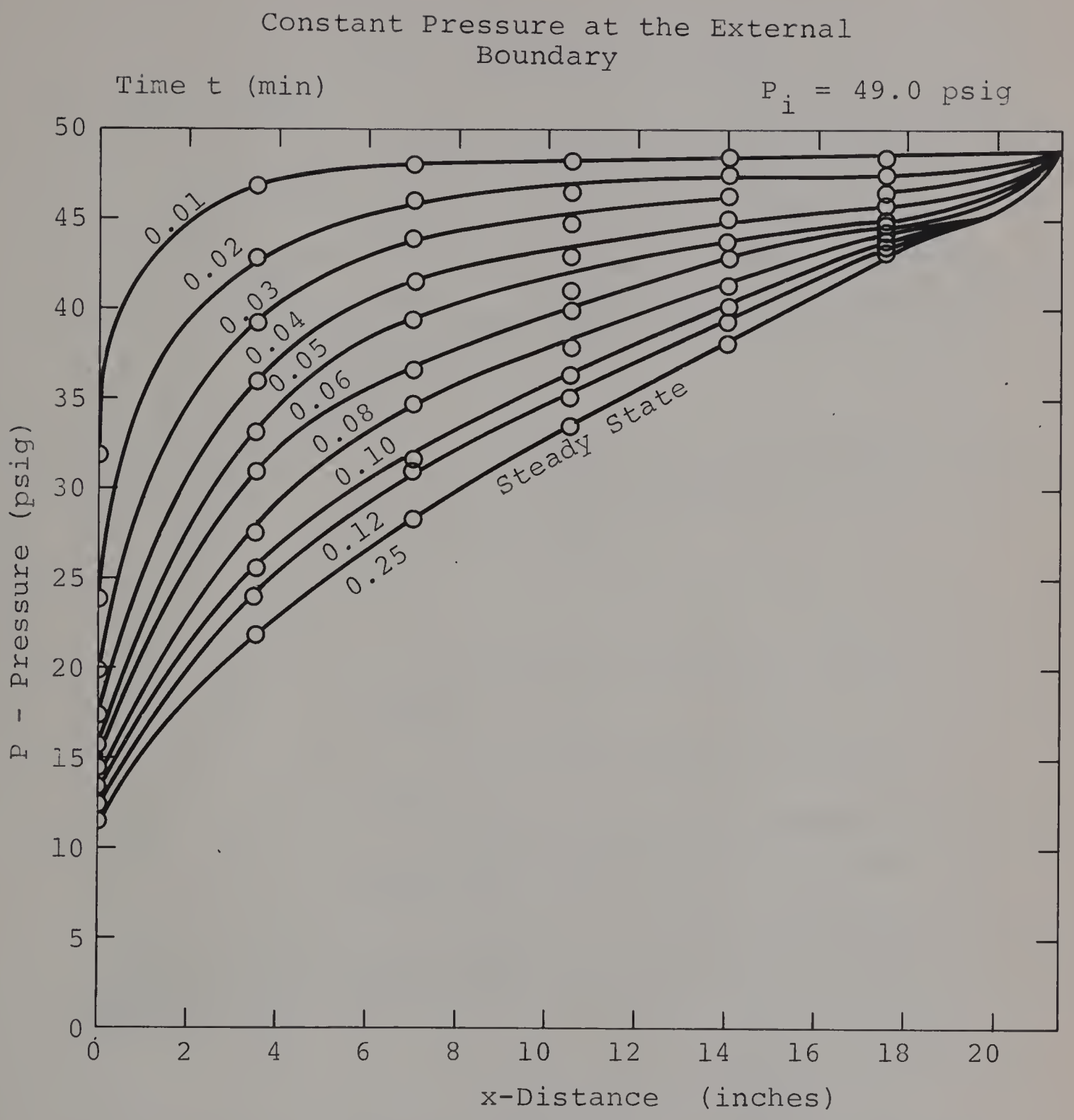

Figure 28a Transient Behavior - Berea Sandstone 2

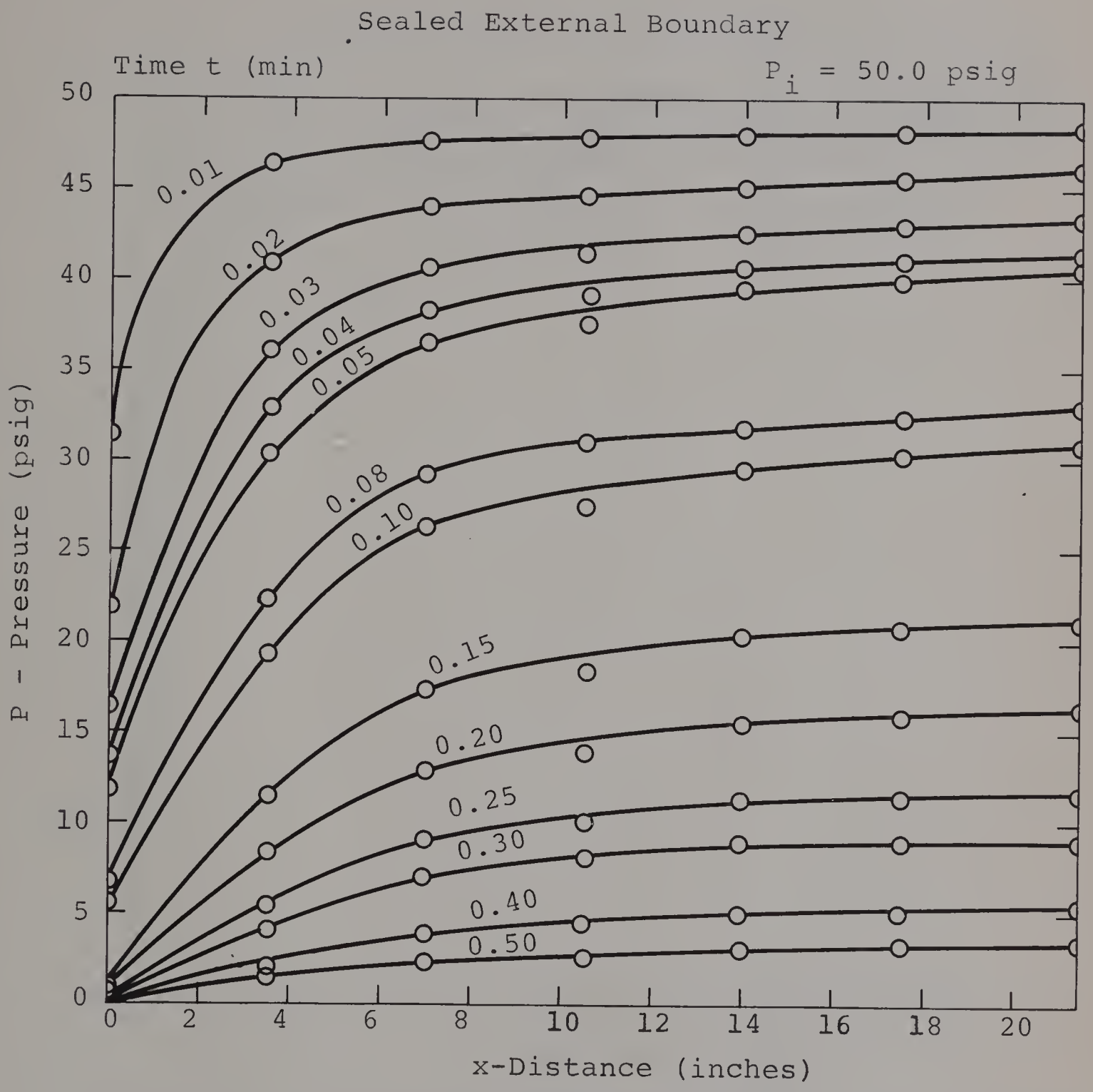

Figure 28b Transient Behavior - Berea Sandstone 2

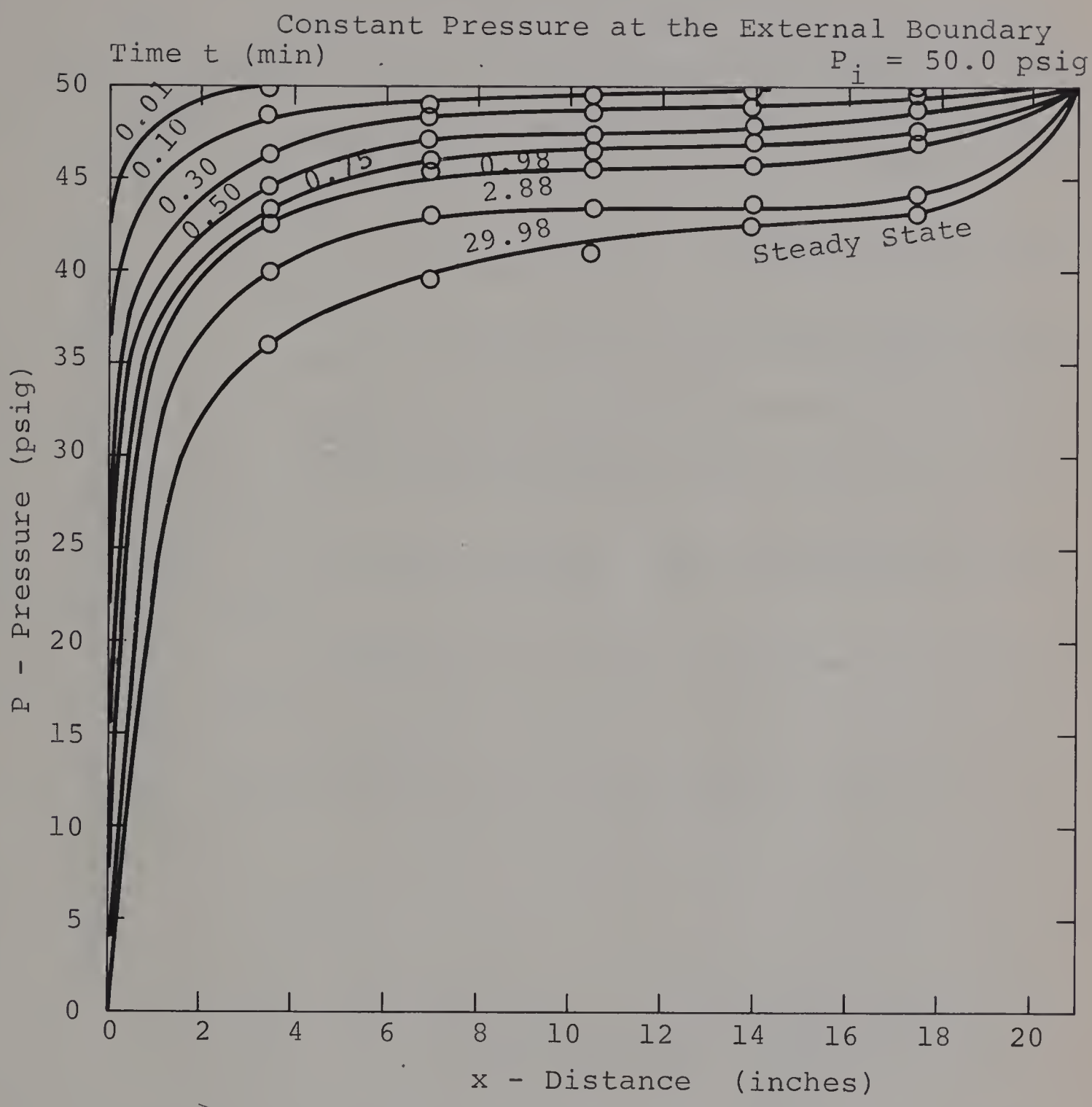

Figure 29a Transient Behavior - Cut Berea Sandstone

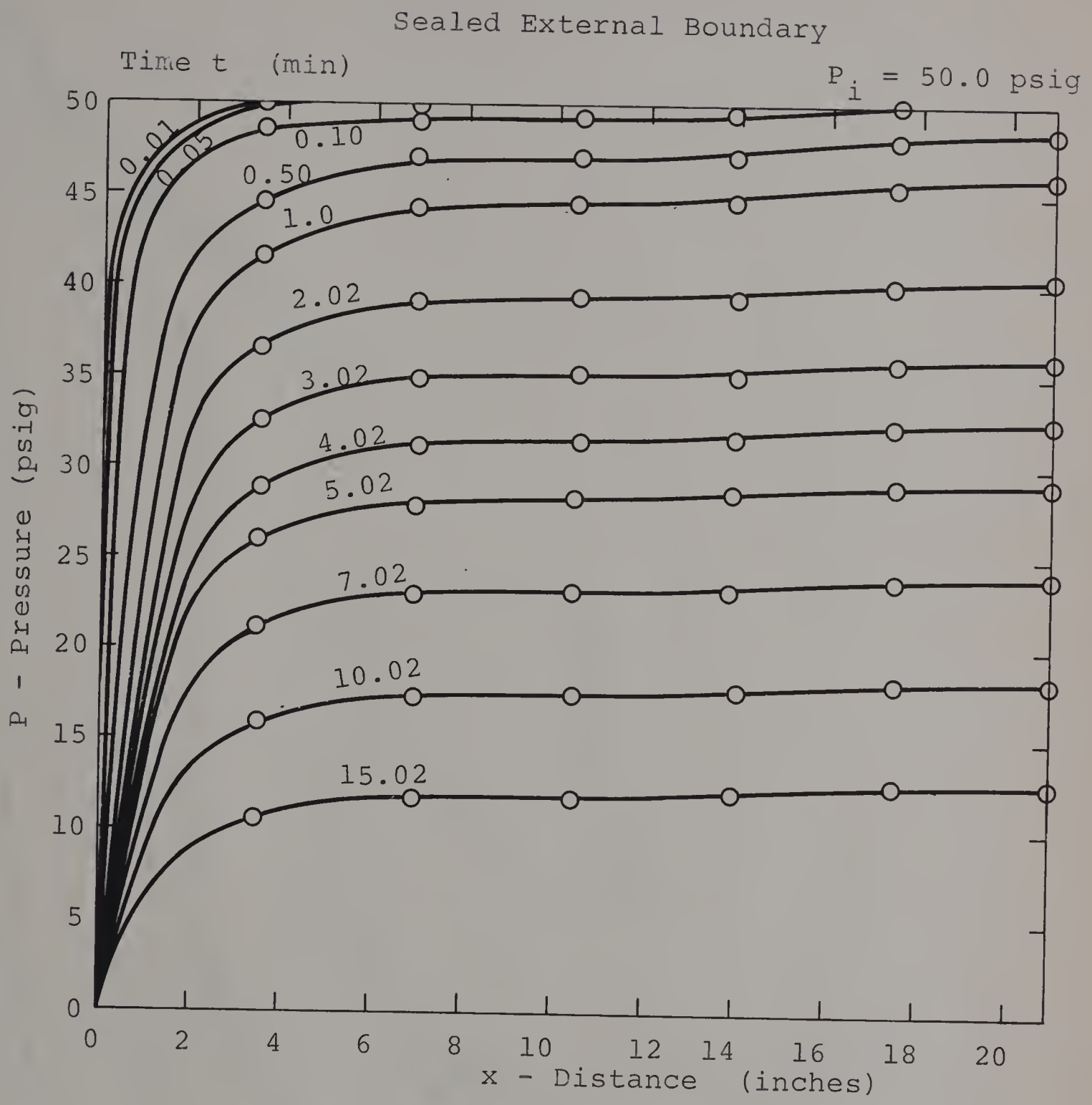

Figure 29b Transient Behavior - Cut Berea Sandstone

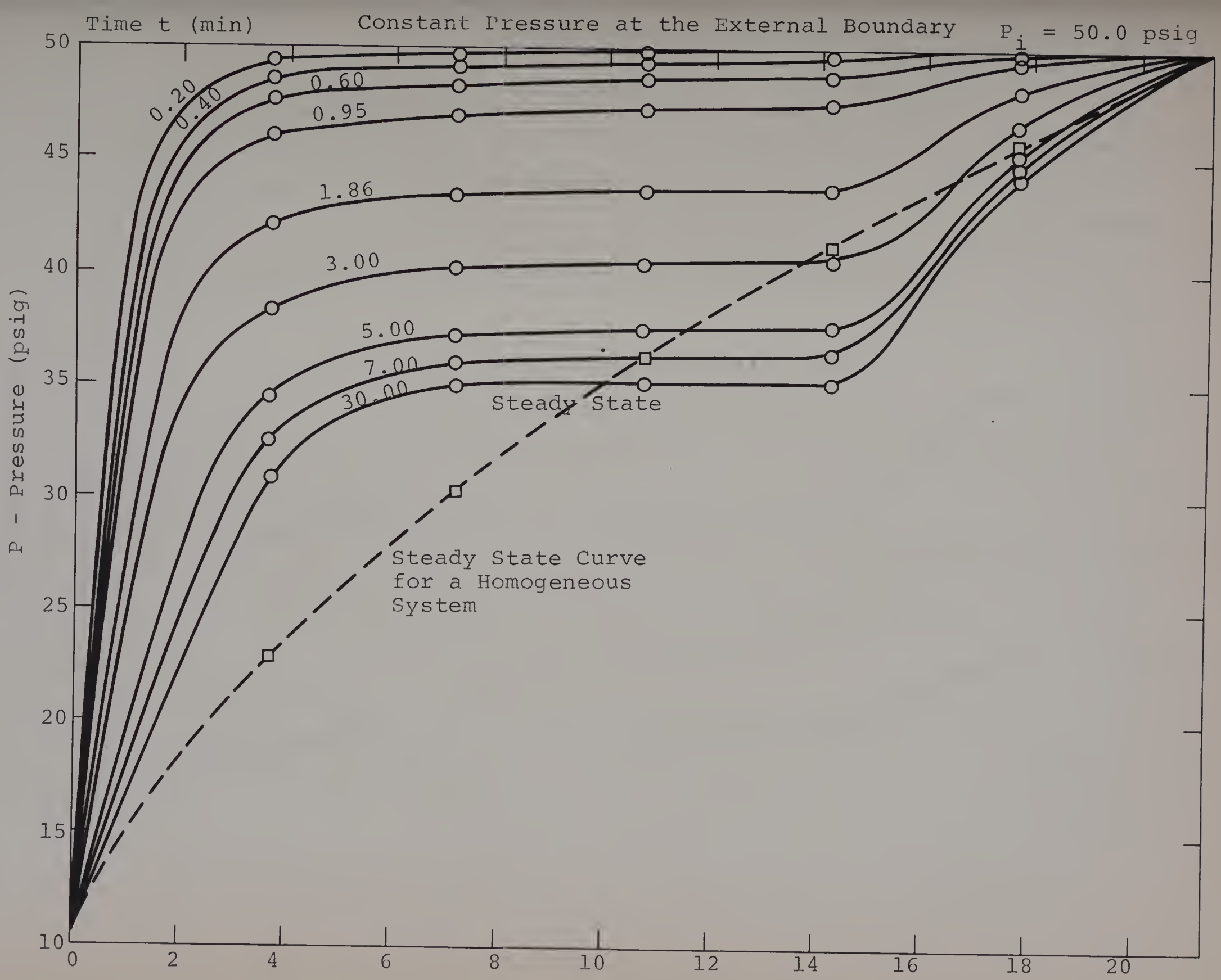

Figure 30 Transient Behavior - Indiana Limestone

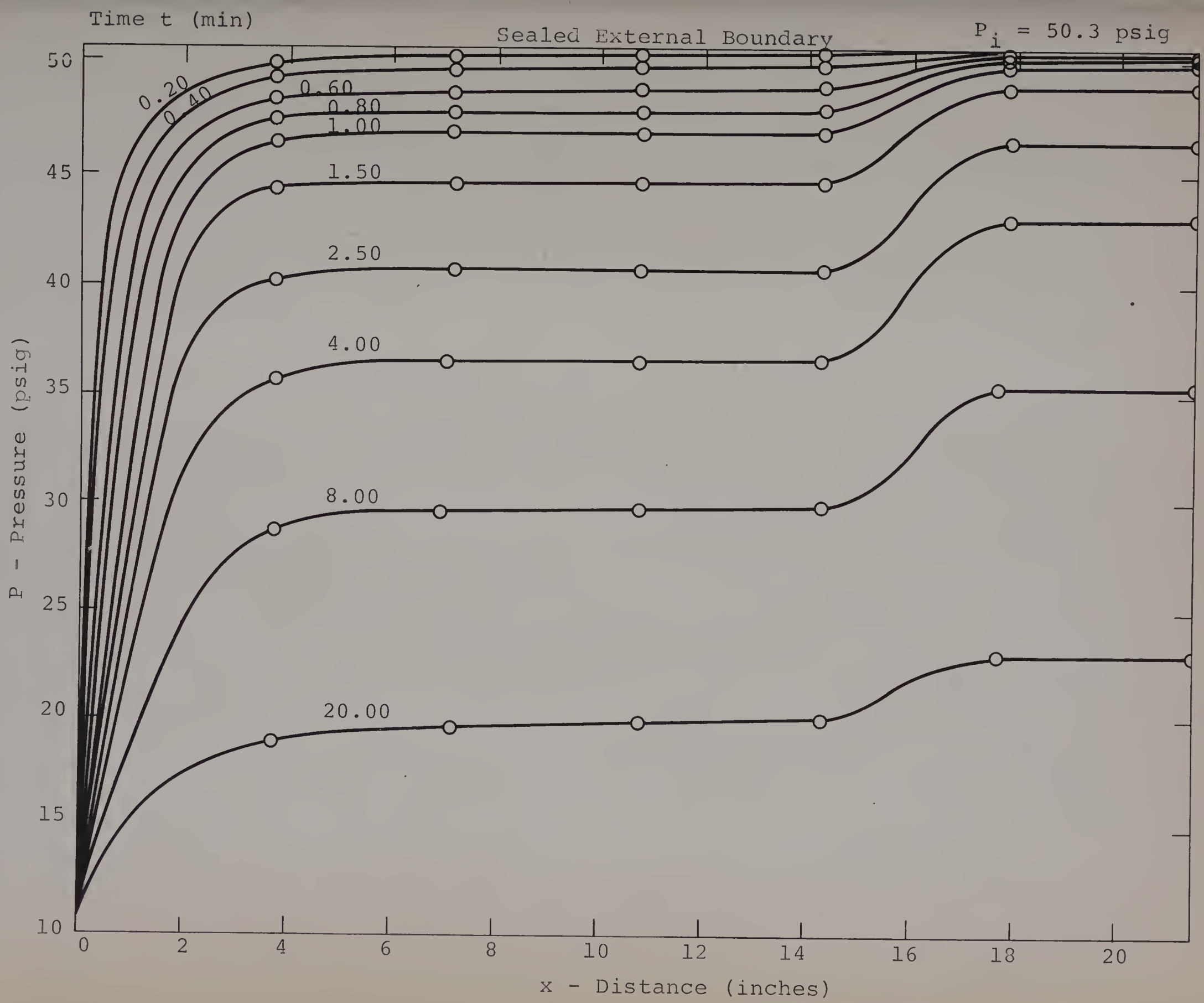

Figure 31 Transient Behavior - Indiana Limestone

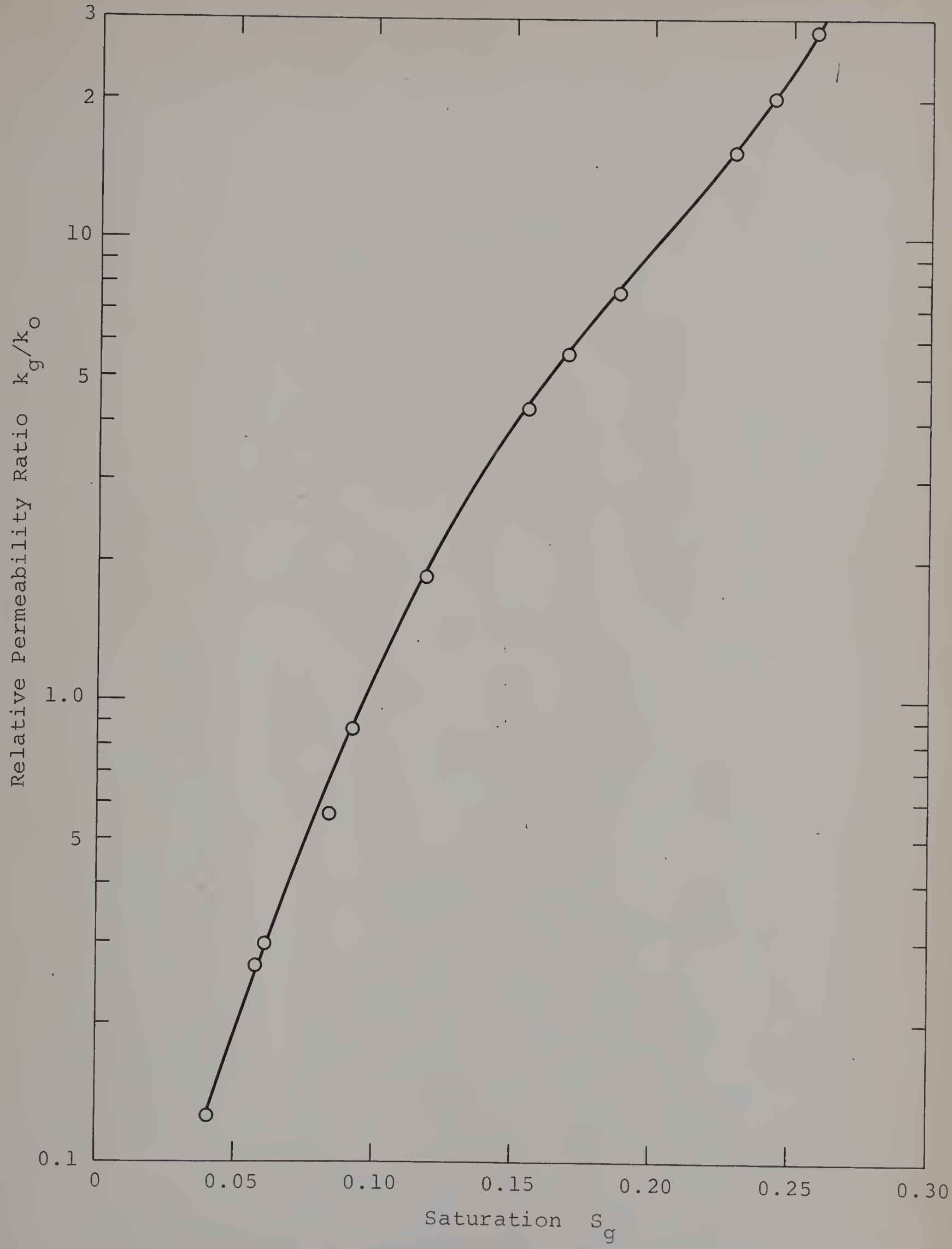

Figure 32 Relative Permeability Ratio - Berea Sandstone 1